

Guidelines for Detection, Analysis, and Treatment of Materials-Related Distress in Concrete Pavements Volume 3: Case Studies Using the Guidelines

PUBLICATION NO. FHWA-RD-01-165

AUGUST 2002



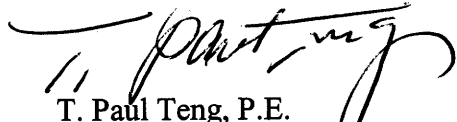
U.S. Department of Transportation
Federal Highway Administration

Research, Development, and Technology
Turner-Fairbank Highway Research Center
6300 Georgetown Pike
McLean, VA 22101-2296

FOREWORD

This report presents several example case studies of the application of a set of guidelines developed for the evaluation of materials-related distress (MRD) in concrete pavements. The performance of concrete pavements can be adversely affected by the concrete's inability to resist the environment in which it is placed. This lack of durability can occur even when the structural design of the pavement is adequate. The distresses that result from this lack of durability are referred to herein as MRD. The guidelines developed cover three major areas of MRD: field distress surveys, pavement sampling, and sample handling; laboratory testing, data analysis, and interpretation; and treatment, rehabilitation, and prevention of MRD. This report is Volume 3 of a three-volume set and documents the application of the guidelines to several concrete pavements. Volume 1 is the Final Report, which documents the work conducted in the study. Volume 2 is the Guidelines for the Detection, Analysis, and Treatment of Materials-Related Distress in Concrete Pavements, and documents the guidelines developed and their use.

These guidelines were prepared with the practitioner in mind, and therefore this report will be of interest to those involved in evaluating concrete distress and performance, as well as those involved in the design and construction of concrete pavements. Sufficient copies are being distributed to provide 10 copies to each FHWA Resource Center, 5 copies to each FHWA Division, and 5 copies to each State highway agency. Direct distribution is being made to the FHWA Division Offices. Additional copies may be purchased from the National Technical Information Service (NTIS), 5285 Port Royal Road, Springfield, Virginia 22161.



T. Paul Teng, P.E.
Director, Office of Infrastructure
Research and Development

NOTICE

This document is disseminated under the sponsorship of the Department of Transportation in the interest of information exchange. The United States Government assumes no liability for its contents or use thereof. This report does not constitute a standard, specification, or regulation.

The United States Government does not endorse products or manufacturers. Trade and manufacturer's names appear in this report only because they are considered essential to the object of the document.

1. Report No. FHWA-RD-01-165	2. Government Accession No.	3. Recipient's Catalog No.	
4. Title and Subtitle GUIDELINES FOR DETECTION, ANALYSIS, AND TREATMENT OF MATERIALS-RELATED DISTRESS IN CONCRETE PAVEMENTS - Volume 3: Case Studies Using the Guidelines		5. Report Date August 2002	
		6. Performing Organization Code	
7. Author(s) L. L. Sutter, K. R. Peterson, T. J. Van Dam, K. D. Smith, M. J. Wade		8. Performing Organization Report No.	
9. Performing Organization Name and Address Michigan Technological University Department of Civil and Environmental Engineering 1400 Townsend Drive Houghton, MI 49931		10. Work Unit No. (TRAIS)	
		11. Contract or Grant No. DTFH61-96-C-00073	
12. Sponsoring Agency Name and Address Federal Highway Administration, Research Technology and Development; 6300 Georgetown Pike McLean, Virginia 22101-2296		13. Type of Report and Period Covered Final Report 1996-2002	
		14. Sponsoring Agency Code HCP30-B	
15. Supplementary Notes: FHWA Contracting Officer's Technical Representative (COTR): Dr. Stephen W. Forster Special thanks are given to the following highway agencies for their assistance in the conduct of this study: Minnesota, California, Iowa, South Dakota, and North Carolina.			
16. Abstract <p>The performance of concrete pavements can be adversely affected by the concrete's inability to resist the environment in which it is placed. This lack of durability can occur even when the structural design of the pavement is adequate. The distresses that result from this lack of durability are referred to herein as materials-related distress (MRD). This report documents the investigation of MRD in concrete pavements and the development of a set of systematic guidelines for the evaluation of MRD. The guidelines developed cover three major areas of MRD: field distress surveys, pavement sampling, and sample handling; laboratory testing, data analysis, and interpretation; and treatment, rehabilitation, and prevention.</p> <p>This report is Volume 3 of a three-volume set, and documents the results of the use of the guidelines on in-service concrete pavements. The other two reports are:</p> <p>FHWA-RD-01- 163, Volume 1: Final Report FHWA-RD-01- 164, Volume 2: Guidelines Description and Use</p>			
17. Key Word concrete materials; concrete pavements; concrete durability; concrete distress; concrete evaluation; petrographic examination; concrete mixture design.		18. Distribution Statement No restrictions. This document is available through the National Technical Information Service; Springfield, Virginia 22161.	
19. Security Classif. (of this report) Unclassified	20. Security Classif. (of this page) Unclassified	21. No. of Pages 127	22. Price

SI* (MODERN METRIC) CONVERSION FACTORS

APPROXIMATE CONVERSIONS TO SI UNITS

APPROXIMATE CONVERSIONS FROM SI UNITS

Symbol	When You Know	Multiply By	To Find	Symbol	When You Know	Multiply By	To Find	Symbol
LENGTH								
in	inches	25.4	millimeters	mm	millimeters	0.039	inches	in
ft	feet	0.305	meters	m	meters	3.28	feet	ft
yd	yards	0.914	meters	m	meters	1.09	yards	yd
mi	miles	1.61	kilometers	km	kilometers	0.621	miles	mi
AREA								
in ²	square inches	645.2	square millimeters	mm ²	square millimeters	0.0016	square inches	in ²
ft ²	square feet	0.093	square meters	m ²	square meters	10.764	square feet	ft ²
yd ²	square yards	0.836	square meters	m ²	square meters	1.195	square yards	yd ²
ac	acres	0.405	hectares	ha	hectares	2.47	acres	ac
mi ²	square miles	2.59	square kilometers	km ²	square kilometers	0.386	square miles	mi ²
VOLUME								
fl oz	fluid ounces	29.57	milliliters	mL	milliliters	0.034	fluid ounces	fl oz
gal	gallons	3.785	liters	L	liters	0.264	gallons	gal
ft ³	cubic feet	0.028	cubic meters	m ³	cubic meters	35.71	cubic feet	ft ³
yd ³	cubic yards	0.765	cubic meters	m ³	cubic meters	1.307	cubic yards	yd ³
NOTE: Volumes greater than 1000 l shall be shown in m ³ .								
MASS								
oz	ounces	28.35	grams	g	grams	0.035	ounces	oz
lb	pounds	0.454	kilograms	kg	kilograms	2.202	pounds	lb
T	short tons (2000 lb)	0.907	megagrams (or "metric ton")	Mg (or "t")	megagrams (or "metric ton")	1.103	short tons (2000 lb)	T
TEMPERATURE (exact)								
°F	Fahrenheit temperature	5(F-32)/9 or (F-32)/1.8	Celsius temperature	°C	Celsius temperature	1.8C + 32	Fahrenheit temperature	°F
ILLUMINATION								
fc	foot-candles	10.76	lux	lx	lux	0.0929	foot-candles	fc
fl	foot-Lamberts	3.426	candela/m ²	cd/m ²	candela/m ²	0.2919	foot-Lamberts	fl
FORCE and PRESSURE or STRESS								
lbf	poundforce	4.45	newtons	N	newtons	0.225	poundforce	lbf
lbf/in ²	poundforce per square inch	6.89	kilopascals	kPa	kilopascals	0.145	poundforce per square inch	lbf/in ²

FORCE and PRESSURE or STRESS

* SI is the symbol for the International System of Units. Appropriate rounding should be made to comply with Section 4 of ASTM E380.

TABLE OF CONTENTS

<u>Chapter</u>	<u>Page</u>
CHAPTER 1. INTRODUCTION	1
CHAPTER 2. PRIMARY CASE STUDIES	5
2.1 I-90 NEAR SPEARFISH, SOUTH DAKOTA (SD-090-019).....	5
<i>Project Description</i>	5
<i>Field Evaluation</i>	6
MRD Field Characterization	6
<i>Laboratory Analysis</i>	10
Core Selection/Visual Inspection	10
Stereo Optical Microscopy	11
Staining Tests	13
Petrographic Optical Microscopy.....	16
Scanning Electron Microscopy (SEM)	19
Chemical Laboratory Tests	21
<i>Interpretation and Diagnosis</i>	21
<i>Recommended Treatment/Rehabilitation Alternatives</i>	22
<i>Recommended Prevention Strategies</i>	28
2.2 TH 65 IN MORA, MINNESOTA (MN-065-064)	29
<i>Project Description</i>	29
<i>Distress Survey Results</i>	30
MRD Field Characterization	31
<i>Laboratory Analysis</i>	33
Core Selection/Visual Inspection	33
Stereo Optical Microscopy/Staining Tests	34
Petrographic Optical Microscopy.....	36
Scanning Electron Microscopy (SEM)	46
<i>Interpretation and Diagnosis</i>	48
<i>Recommended Treatment/Rehabilitation Alternatives</i>	55
<i>Recommended Prevention Strategies</i>	56
2.3 NEAR RALEIGH, NORTH CAROLINA (NC-440-015)	56
<i>Project Description</i>	56
<i>Distress Survey Results</i>	56
MRD Field Characterization	59
<i>Laboratory Analysis</i>	61
Core Selection/Visual Inspection	61
Stereo Optical Microscopy	61
Staining Tests	63
Petrographic Optical Microscopy.....	63
Scanning Electron Microscopy	65
<i>Interpretation and Diagnosis</i>	66
<i>Recommended Treatment/Rehabilitation Alternatives</i>	73
<i>Recommended Prevention Strategies</i>	74

TABLE OF CONTENTS

<u>Chapter</u>	<u>Page</u>
2.4 SR 58 NEAR BORON, CALIFORNIA (CA-058-141)	74
<i>Project Description</i>	74
<i>Distress Survey Results</i>	75
MRD Field Characterization	76
<i>Laboratory Analysis</i>	77
Core Selection/Visual Inspection	77
Stereo Optical Microscopy	79
Staining Tests	79
Petrographic Optical Microscopy	80
Scanning Electron Microscopy	80
<i>Interpretation and Diagnosis</i>	84
<i>Recommended Treatment/Rehabilitation Alternatives</i>	84
<i>Recommended Prevention Strategies</i>	90
CHAPTER 3. SECONDARY CASE STUDIES	93
3.1 NEAR MOJAVE, CALIFORNIA (CA-014-011)	93
<i>Project Description</i>	93
<i>Distress Survey Results</i>	94
MRD Field Characterization	95
<i>Laboratory Analysis</i>	96
Core selection/Visual Inspection	96
Stereo Optical Microscopy	96
Staining Tests	99
<i>Interpretation and Diagnosis</i>	99
3.2 SR 2 NEAR IOWA-NEBRASKA BORDER (IA-002-002)	102
<i>Project Description</i>	102
<i>Distress Survey Results</i>	103
MRD Field Characterization	104
<i>Laboratory Analysis</i>	104
Core Selection/Visual Inspection	104
Stereo Optical Microscopy	104
Petrographic Optical Microscopy	109
<i>Interpretation and Diagnosis</i>	110
CHAPTER 4. CONCLUSIONS	119
CHAPTER 5. REFERENCES	121

LIST OF FIGURES

<u>Figure</u>	<u>Page</u>
3-1. General location of projects included in study	3
3-2. Typical distress manifestation observed on SD-090-019-002.....	9
3-3. Typical distress manifestation observed on SD-090-019, Sections 1 and 2.....	9
3-4. Typical distress manifestation observed on SD-090-019-002.....	10
3-5. Core specimens from SD-090-019.	11
3-6. Stereo optical micrographs of typical cracking pattern associated with porous siltstone aggregate SD-090-019.....	12
3-7. Stereo optical micrograph showing gel deposits in SD-090-019 aggregates.	12
3-8. Slab 1B stained with sodium cobaltinitrite/rhodamine B from SD-090-019-001.	13
3-9. Slab 1B stained with sodium cobaltinitrite/rhodamine B from SD-090-019-001.	14
3-10. Slab 2B stained with sodium cobaltinitrite/rhodamine B from SD-090-019-002.	15
3-11. Stereo optical micrographs of air voids filled with sulfate minerals stained with potassium permanganate (note differences due to polishing).	16
3-12. Core SD-090-019-001B, thin-section micrographs of same rhyolite aggregate that was stained with sodium cobaltinitrite.	17
3-13. Core SD-090-019-001B, thin-section micrographs of same volcanic aggregate that was stained with sodium cobaltinitrite.	18
3-14. Ettringite (a) and hydrocalumite (b) infilling in void and crack, respectively..	19
3-15. Ternary diagram showing the probable range of composition for the hydrocalumite deposits analyzed from SD-090-019.	21
3-16. Flowchart for assessing the likelihood of MRD causing the observed distress in the pavement as applied to the Spearfish, South Dakota site.	23
3-17. Flowchart for assessing general concrete properties based on visual examination as applied to the Spearfish, South Dakota site.	24
3-18. Flowchart for assessing the condition of the concrete paste as applied to the Spearfish, South Dakota site.	25
3-19. Flowchart for assessing the condition of the concrete aggregates as applied to the Spearfish, South Dakota site.....	26
3-20. Flowchart for identifying infilling materials in cracks and voids as applied to the Spearfish, South Dakota site.....	27
3-21. Typical distress manifestations observed at MN-065-064.	33
3-22. Cores evaluated for MN-065-064.	35
3-23. Stereo optical micrographs showing sulfate minerals filling air voids.....	36
3-24. Histogram of 16 fluorescence measurements from calibration thin section composed of quartz sand in a dyed epoxy matrix.....	38
3-25. Histogram of 30 fluorescence measurements from 0.38 w/c standard.	39
3-26. Histogram of 30 fluorescence measurements from 0.41 w/c standard.	39
3-27. Histogram of 30 fluorescence measurements from 0.42 w/c standard.	40
3-28. Histogram of 30 fluorescence measurements from 0.52 w/c standard.	40
3-29. Histogram of 30 fluorescence measurements from 0.56 w/c standard.	41
3-30. Histogram of 30 fluorescence measurements from 0.74 w/c standard.	41
3-31. Histogram of 30 fluorescence measurements from 0.80 w/c standard.	42

LIST OF FIGURES (CONTINUED)

Figure	Page
3-32. Average cement paste fluorescence measurements versus w/c. Error bars represent one standard deviation.	43
3-33. Histogram of fluorescence measurements from 1950 concrete from mid-panel of the left-turn lane of site MN-065-064-001.	43
3-34. Histogram of fluorescence measurements from 1990 concrete from mid-panel of the traffic lane of site MN-065-064-001.	44
3-35. Distribution of the w/c values from the 1950 concrete from mid-panel of the left-turn lane of site MN-065-064-001.	44
3-36. Distribution of the w/c values from the 1990 concrete from mid-panel of the traffic lane of site MN-065-064-001.	45
3-37. The w/c values versus depth from the 1950 concrete from mid-panel of the left-turn lane of site MN-065-064-001.	45
3-38. The w/c values versus depth from the 1990 concrete from mid-panel of the traffic lane of site MN-065-064-001.	46
3-39. Typical SEM micrograph and x-ray analysis for ettringite infilling air void.	47
3-40. Typical SEM micrograph and x-ray analysis for hydrocalumite infilling air void.	47
3-41. Flowchart for assessing the likelihood of MRD causing the observed distress in the pavement as applied to MN-065-064.	50
3-42. Flowchart for assessing general concrete properties based on visual examination as applied to MN-065-064.	51
3-43. Flowchart for assessing the condition of the concrete paste as applied to MN-065-064. ...	52
3-44. Flowchart for assessing the condition of the concrete aggregates as applied to MN-065-064.	53
3-45. Flowchart for identifying infilling materials in cracks and voids as applied to MN-065-064.	54
3-46. Typical cracking pattern at NC-444-015. Note distress over entire slab length with spalling occurring at joints.	60
3-47. Cores and specimens evaluated from NC-440-015.	61
3-48. Stereo optical micrographs of ASR gel and reactive coarse aggregate from NC-440-015.	62
3-49. Typical stereo optical micrographs of stained concrete. Note that the broad banding occurs from the montage process to create a single image.	63
3-50. Petrographic micrographs from spall obtained from NC-440-015 showing ettringite filled entrained air voids. Ettringite growths are unusually dense.	64
3-51. Petrographic micrograph of a tan to red coating observed on some of the fine aggregates that appears to undergo ASR from spall obtained from NC-440-015.	64
3-52. Petrographic micrograph of ettringite and "ASR gel blob" from spall obtained from NC-440-015.	64
3-53. Petrographic micrograph of ettringite intermixed with ASR gel.	65
3-54. Petrographic micrograph of ASR gel in crack within coarse aggregate.	65
3-55. SEM micrograph of ettringite filling air voids and crack.	66
3-56. SEM micrograph of ettringite and ASR reaction product.	66
3-57. Typical spectra for ettringite and ASR reaction product.	67
3-58. Flowchart for assessing the likelihood of MRD causing the observed distress in the pavement as applied to NC-440-015.	68

LIST OF FIGURES (CONTINUED)

Figure	Page
3-59. Flowchart for assessing general concrete properties based on visual examination as applied to NC-440-015.	69
3-60. Flowchart for assessing the condition of the concrete paste as applied to NC-440-015. ...	70
3-61. Flowchart for assessing the condition of the concrete aggregates as applied to NC-440-015.	71
3-62. Flowchart for identifying infilling materials in cracks and voids as applied to NC-440-015.	72
3-63. Typical conditions at CA-058-141.	78
3-64. Photographs of core specimens analyzed from CA-058-141.	78
3-65. Stereo optical micrographs showing staining observed in core CA-058-141-001C.	80
3-66. Petrographic micrograph of core CA-058-141-001E.	81
3-67. Petrographic micrograph of core CA-058-141-001E.	82
3-68. SEM spectra and micrograph from CA-058-141.	83
3-69. Flowchart for assessing the likelihood of MRD causing the observed distress in the pavement as applied to CA-058-141.	85
3-70. Flowchart for assessing general concrete properties based on visual examination as applied to CA-058-141.	86
3-71. Flowchart for assessing the condition of the concrete paste as applied to CA-058-141. ...	87
3-72. Flowchart for assessing the condition of the concrete aggregates as applied to CA-058-141.	88
3-73. Flowchart for identifying infilling materials in cracks and voids as applied to CA-058-141.	89
3-74. Typical conditions at CA-014-011.	95
3-75. Map cracking pattern on core CA-014-011-001E, emphasized by wetting down the surface.	96
3-76. Inverse image of polished cross section of core CA-014-011-001E.	97
3-77. Same area of core CA-058-011-001E as shown in figure 3-78.	98
3-78. Results of staining test applied to core CA-058-011-001E.	99
3-79. Phenolphthalein stained polished slab, showing carbonation along plastic shrinkage crack.	100
3-80. Flowchart for assessing the likelihood of MRD causing the observed distress in the pavement as applied to CA-014-011.	101
3-81. Site conditions at IA-002-002.	107
3-82. Closeup view of longitudinal hairline cracks.	107
3-83. Polished slab from core IA-002-002-001A.	108
3-84. Stereo micrograph showing air void structure of IA-002-002-001A.	109
3-85. Reactive fine aggregate particle with alkali-silica gel filled air voids as viewed in thin section.	110
3-86. Flowchart for assessing the likelihood of MRD causing the observed distress in the pavement as applied to IA-002-002.	112
3-87. Flowchart for assessing general concrete properties based on visual examination as applied to IA-002-002.	113

LIST OF FIGURES (CONTINUED)

<u>Figure</u>	<u>Page</u>
3-88. Flowchart for assessing the condition of the concrete paste as applied to IA-0020002.....	114
3-89. Flowchart for assessing the condition of the concrete aggregates as applied to IA-002-002.	115
3-90. Flowchart for identifying infilling materials in cracks and voids as applied to IA-002-002.	116

LIST OF TABLES

<u>Table</u>	<u>Page</u>
3-1. Primary and secondary test sites included in study.....	2
3-2. Summary of design features for SD-090-019.	5
3-3. Summary of pavement condition surveys for SD-090-019-001.	7
3-4. Summary of pavement condition surveys for SD-090-019-002.	8
3-5. Summary of MRD characterization for SD-090-019.....	8
3-6. Results of ASTM C 457 for concrete from SD-090-019.	12
3-7. Summary of 10 analyses from ettringite deposits, compared to a calculated composition for dehydrated ettringite.	20
3-8. Summary of 13 analyses from hydrocalumite deposits.	20
3-9. Identified diagnostic features along with their associated MRD type and significance as related to SD-090-019.	28
3-10. Summary of design features for MN-065-064.	30
3-11. Summary of pavement condition surveys for MN-065-064-001.	31
3-12. Summary of pavement condition surveys for MN-065-064-002.	32
3-13. Summary of MRD characterization for MN-065-064.....	33
3-14. Results of ASTM C 457 on concrete from MN-065-064-001.	34
3-15. Quantitative results from single spectrum collected from ettringite deposit, compared to a calculated composition for dehydrated ettringite.	48
3-16. Summary of 10 analyses and theoretical composition of hydrocalumite deposits.	49
3-17. Diagnostic features identified along with their associated MRD type and significance as related to MN-065-064.	55
3-18. Summary of design features for NC-440-015.	57
3-19. Summary of pavement condition surveys for NC-440-015-001.....	58
3-20. Summary of pavement condition surveys for NC-440-015-002.....	59
3-21. Summary of MRD characterization for NC-440-015.	60
3-22. Results of ASTM C 457 on concrete from NC-440-015.	62
3-23. Diagnostic features identified along with their associated MRD type and significance as related to NC-440-015.	73
3-24. Summary of design features for CA-058-141.	75
3-25. Summary of pavement condition surveys for CA-058-141-001.....	76
3-26. Summary of MRD characterization for CA-058-141.	77
3-27. Results of ASTM C 457 on concrete from CA-058-141.	79
3-28. Summary of 12 analyses of ASR gel deposit shown in figure 3-68.	83
3-29. Diagnostic features identified along with their associated MRD type and significance as related to this pavement.	90
3-30. Summary of design features for CA-014-011.	93
3-31. Summary of pavement condition surveys for CA-014-011-001.....	94
3-32. Summary of MRD characterization for CA-014-011.	95
3-33. Diagnostic features identified along with their associated MRD type and significance as related to CA-014-001.	102
3-34. Summary of design features for IA-002-002.	103
3-35. Summary of pavement condition surveys for IA-002-002-001.	105
3-36. Summary of pavement condition surveys for IA-002-002-002.	106

LIST OF TABLES (CONTINUED)

<u>Table</u>	<u>Page</u>
3-37. Summary of MRD characterization for IA-002-002.....	106
3-38. Air-void characteristics of core IA-002-002-001A as determined by ASTM C457.....	108
3-39. Diagnostic features identified along with their associated MRD type and significance as related to this pavement.....	117

CHAPTER 1. INTRODUCTION

The objective of this research, conducted under FHWA Contract DTFH61-96-C-00073, was to develop guidelines to provide pavement engineers and field and laboratory personnel with a systematic procedure for the identification, evaluation, treatment, and prevention of materials-related distresses (MRD) in portland cement concrete (PCC) pavements.

This report, *Volume 3: Case Studies Using the Guidelines*, presents the six case studies that were conducted as part of this study. The other two reports are:

- *Volume 1: Final Report*
- *Volume 2: Guidelines Description and Use*

Each of these in-service concrete pavements appeared to be exhibiting MRD, and were subjected to a coordinated series of field-testing and laboratory evaluation activities. In this way, the usefulness and applicability of the guidelines were evaluated under actual field conditions, thereby providing feedback on what areas of the guidelines worked well and what areas required modification or refinement. The results of these case studies were directly used to establish the final version of the guidelines as published in *Volume 2: Guidelines Description and Use*.

In this volume, the field and laboratory testing activities that were conducted under this project are presented. A general summary of the data collection and analysis procedures conducted on each pavement case study is provided. This is followed by a summary of the condition survey, field sampling, and laboratory analysis results obtained for each of the case studies, leading up to the identification of the most likely MRD type present in the pavement. Finally, remediation strategies for each pavement examined are presented.

The case studies have already been briefly introduced in *Volume 1: Final Report*. As described, two sets of test sites were established:

- **Primary Test Sites**—Four test sites exhibiting MRD that are located in each Strategic Highway Research Program (SHRP) Long-Term Pavement Performance (LTPP) climatic region. Each of these pavement test sites are subjected to the full battery of field and laboratory tests.
- **Secondary Test Sites**—Two test sites exhibiting MRD that provide an alternative site in a particular climatic region. These pavement test sites are subjected to the same level of field testing as the primary sites, but are subjected to less intensive laboratory testing.

The primary and secondary test sites included in the study are summarized in table 3-1. Again, the primary test sites represent each of the four SHRP LTPP climatic regions, and also include a range of other factors including age, pavement design, and type of distress manifestation. The secondary sites are included to provide additional sections for assessing the guidelines. The general location of these projects is shown in figure 3-1.

The case studies included in the study were subjected to a detailed field condition survey, and core samples were retrieved from prescribed locations for laboratory testing and evaluation. All

of these activities were performed in accordance with the systematic procedures outlined in the guidelines.

Chapter 2 of this volume presents the primary case studies and chapter 3 presents the secondary case studies. Chapter 4 provides a brief conclusion. Due to the vast amount of data collected in the course of this study, it is not practical to present it all in printed format. Thus a web-based appendix is used to provide this detailed information.

Table 3-1. Primary and secondary test sites included in study.

State	Highway/City	Climatic Region	Pavement Design	Year Built
<i>Primary Sites</i>				
California	SR 58, Boron	Dry-Nonfreeze	230 mm JPCP 4.0-5.8-5.5-3.7-m joint spacing No dowels	1971
Minnesota	TH 65, Mora	Wet-Freeze	200 mm JPCP 4.0-4.6-5.2-04.6-m joint spacing No dowels	1989
North Carolina	I-440, Raleigh	Wet-Nonfreeze	200 mm JPCP 7.6-7.0-5.8-5.5 m joint spacing 32-mm dowels	1982
South Dakota	I-90, Spearfish	Dry-Freeze	200 mm JPCP 12.3-m joint spacing 25-mm dowels	1968
<i>Secondary Sites</i>				
California	SR 14, Mojave	Dry-Nonfreeze	215 mm JPCP 3.7-4.0-5.8-5.5-m joint spacing No dowels	1972
Iowa	SR 2, Nebraska City	Wet-Freeze	240 mm JPCP 6.1-m joint spacing 32-mm dowels	1986

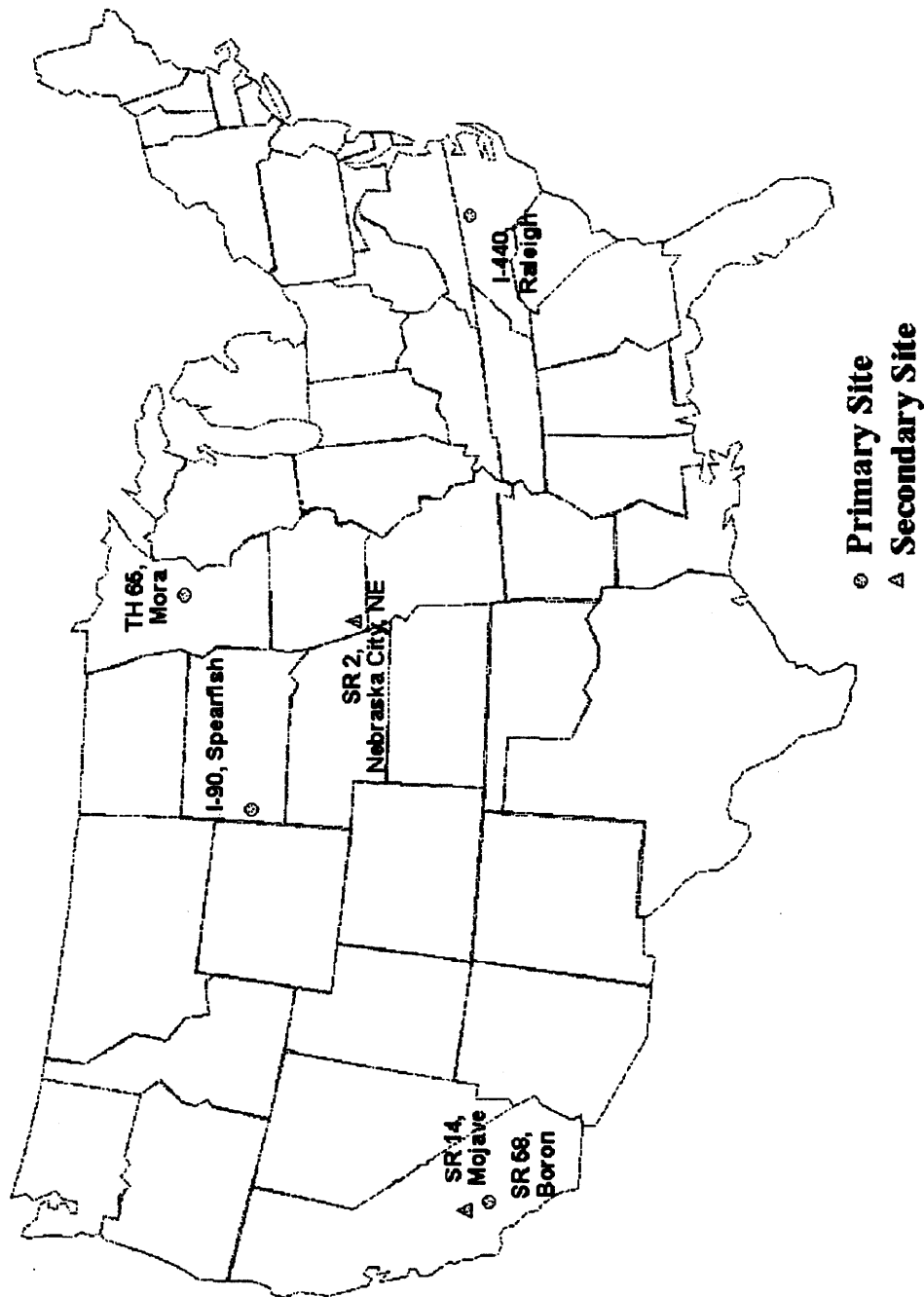


Figure 3-1. General location of projects included in study.

CHAPTER 2. PRIMARY CASE STUDIES

2.1 I-90 NEAR SPEARFISH, SOUTH DAKOTA (SD-090-019)

Project Description

The South Dakota Department of Transportation (SDDOT) provided this project as a pavement with a history of durability problems. In particular, the pavement is experiencing surface or map cracking over the entire pavement surface. This project represents the primary case study site in the dry-freeze climatic region. The area receives approximately 400 mm of precipitation each year and has a freezing index of 684 °C-days.

This 14-km-long project is located on I-90 near Spearfish, South Dakota and extends from milepost 19.8 to milepost 28.5 in both directions. Table 3-2 provides a summary of the specific design features for this project.

Table 3-2. Summary of design features for SD-090-019.

Category	Design Feature	Description
General Information	Project limits	MP 19.8 – 28.5
	Highway type	Divided
	Number of lanes	4
	Direction	Eastbound/westbound
	Construction date	1968
	Cumulative ESALs	~2,250,000
Pavement Cross Section	Pavement type	JRCP
	PCC slab thickness	200 mm
	Base	75-mm lime-treated gravel
	Subbase	150-mm lime-treated subgrade
	Subgrade type	Red clay
Transverse Joint	Joint spacing	12.3 m
	Joint skew	None
	Load transfer	25-mm dowels
	Sealant type	Silicone
Longitudinal Joint	Load transfer	
	Sealant type	Hot-pour
Outer Shoulder	Surface type	AC
	Width	3.0 m
Inner Shoulder	Surface type	AC
	Width	1.2 m
Climatic Conditions	Region	Dry-freeze
	Annual precipitation*	400 mm
	Freezing index*	684 °C-days

* Climatic data are for Rapid City, South Dakota.

The project is a four-lane divided highway, and the same design was placed in both the eastbound and westbound lanes. It is a jointed reinforced concrete pavement (JRCP) containing wire mesh reinforcement. The joints are spaced at 12.3-m intervals and contain 25-mm dowel bars. The longitudinal centerline joint is sealed with a hot-pour asphalt sealant, whereas the transverse joints are sealed with a silicone sealant. The pavement structure consists of a 200-mm JRCP, a 75-mm lime-treated gravel base, and a 150-mm lime-treated subgrade. The subgrade is a red clayey soil. There are no provisions for subsurface drainage. The inside and outside shoulders are AC-surfaced and are 1.2 and 3.0 m wide, respectively.

Field Evaluation

After an initial investigation, the survey team selected two sections—one each in the inside and outside traffic lanes—to be surveyed in order to evaluate the differences between lanes. Section 001 is located in the eastbound, inside traffic lane beginning at milepost 23.1. This section was constructed in a cut section of approximately 10 m. Section 002 is also located in the eastbound direction but in the outside traffic lane and begins at milepost 24.5. This section was constructed on approximately 3 m of fill material.

A summary of the distress survey results is provided in tables 3-3 and 3-4 for Sections 001 and 002, respectively. Overall, Section 001 appears to be in better structural condition than Section 002, as would be expected due to the lower traffic volumes on the inside traffic lane. Section 001 contains some low-severity transverse cracks, which are expected to occur on JRCP. Spalling occurs at 6 of the 14 transverse joints but only 1 has progressed to medium severity. The spalling appears to be due to the progression of MRD. Three small rigid patches, each of which is located along a transverse joint, are also present. Faulting is virtually nonexistent, averaging 0.6 and 0.7 mm measured at distances of 0.30 and 0.75 m from the slab edge.

Section 002 exhibits more distress and greater deterioration. Although low-severity transverse cracks are expected on JRCP, there are considerably more cracks as compared to Section 001. In addition, Section 002 also exhibits two medium-severity cracks and two high-severity cracks. Faulting is also much more significant, averaging 3.7 and 4.2 mm at 0.30 and 0.75 m from the slab edge. Another distress that is more significant on Section 002 is patching. A high-severity flexible patch is observed, as are 10 low-severity and 2 moderate-severity rigid patches. Some of the rigid patches are full-depth patches at transverse joints, indicating that the joints were likely badly deteriorated at one time. Five of the 14 transverse joints exhibit spalling, including 2 that have progressed to moderate severity.

MRD Field Characterization

During the field surveys, the attributes of the MRD were characterized. Although a definitive diagnosis cannot be made in the field, it is important to evaluate the attributes of the MRD as well as the effect these distresses have on pavement performance. A summary of the MRD characterization for both sections is provided in table 3-5. Figures 3-2 through 3-4 show some the typical conditions observed on the two test sections.

Table 3-3. Summary of pavement condition surveys for SD-090-019-001.

	Distress Type	Distress Measure	Severity Level			Comments
			Low	Moderate	High	
Cracking	Corner Breaks	number	1	0	0	
	Longitudinal Cracking	linear meters	0.0	0.0	0.0	
	Transverse Cracking	number of cracks	12	0	0	
		linear meters	14.7	0.0	0.0	
		percent of slabs	0			
Transverse Joints	Sealant		good condition			silicone sealant
	Spalling	number	5	1	0	
		linear meters	1.4	0.4	0	
	Faulting	millimeters	0.6			measured at 0.30 m
		millimeters	0.7			measured at 0.75 m
	Width	millimeters	23.6			
Long. Joints	Sealant		fair condition			hot-pour sealant
	Spalling	linear meters	0.0	0.0	0.0	
	Shoulder Dropoff	millimeters	17.8			
	Map Cracking	number of slabs	13			all slabs affected
Surface Conditions		square meters	588.3			entire area
	Scaling	number of slabs	0			
		square meters	0.0			
	Polished Aggregate	square meters	0.0			
	Popouts	number/sq. meter	0.0			
	Blowups	number	0			
	Flexible Patches	number	0	0	0	
Other		square meters	0.0	0.0	0.0	
	Rigid Patches	number	3	0	0	
		square meters	0.4	0.0	0.0	
	Pumping/Bleeding	number	0			
		linear meters	0.0			

Table 3-4. Summary of pavement condition surveys for SD-090-019-002.

Distress Type		Distress Measure	Severity Level			Comments
			Low	Moderate	High	
Cracking	Corner Breaks	number	1	0	0	
	Longitudinal Cracking	linear meters	0.0	0.0	0.0	
	Transverse Cracking	number of cracks	44	2	2	
		linear meters	60.9	7.4	7.4	
		percent of slabs	31			
Transverse Joints	Sealant		good condition			silicone sealant
	Spalling	number	3	2	0	
		linear meters	1.1	1.9	0.0	
	Faulting	millimeters	3.7			measured at 0.30 m
		millimeters	4.2			measured at 0.75 m
Long. Joints	Width	millimeters	17.2			
	Sealant		fair condition			hot-pour sealant
	Spalling	linear meters	0.0	0.0	0.0	
	Shoulder Dropoff	millimeters	23.6			
Surface Conditions	Map Cracking	number of slabs	13			all slabs affected
		square meters	579.0			entire area
	Scaling	number of slabs	0			
		square meters	0.0			
	Polished Aggregate	square meters	0.0			
	Popouts	number/sq. meter	0.0			
Other	Blowups	number	0			
	Flexible Patches	number	0	0	1	
		square meters	0.0	0.0	0.5	
	Rigid Patches	number	10	2	0	
		square meters	15.4	3.8	0.0	
	Pumping/Bleeding	number	0			
		linear meters	0.0			

Table 3-5. Summary of MRD characterization for SD-090-019.

Description		Section 001	Section 002	Comments
Cracking	Location	Entire slab	Entire slab	More significant at slab corners
	Orientation/shape	Criss cross	Corners: semi-circle Center: transverse	
	Extent	Entire slab	Entire slab	
	Crack size	Hairline	Hairline	
Staining	Location	Joints/cracks	Joints/cracks	
	Color	Brownish gray	Dark gray	
Exudate	Present	None	Yes	Corners only
	Color	n/a	Dark gray/white	
	Extent	n/a	Low	
Scaling	Location	None	None	
	Area of surface	n/a	n/a	
	Depth	n/a	n/a	
Vibrator Trails	Visible	None	None	
	Discolored	n/a	n/a	
	Distressed	n/a	n/a	
	Change in texture	n/a	n/a	

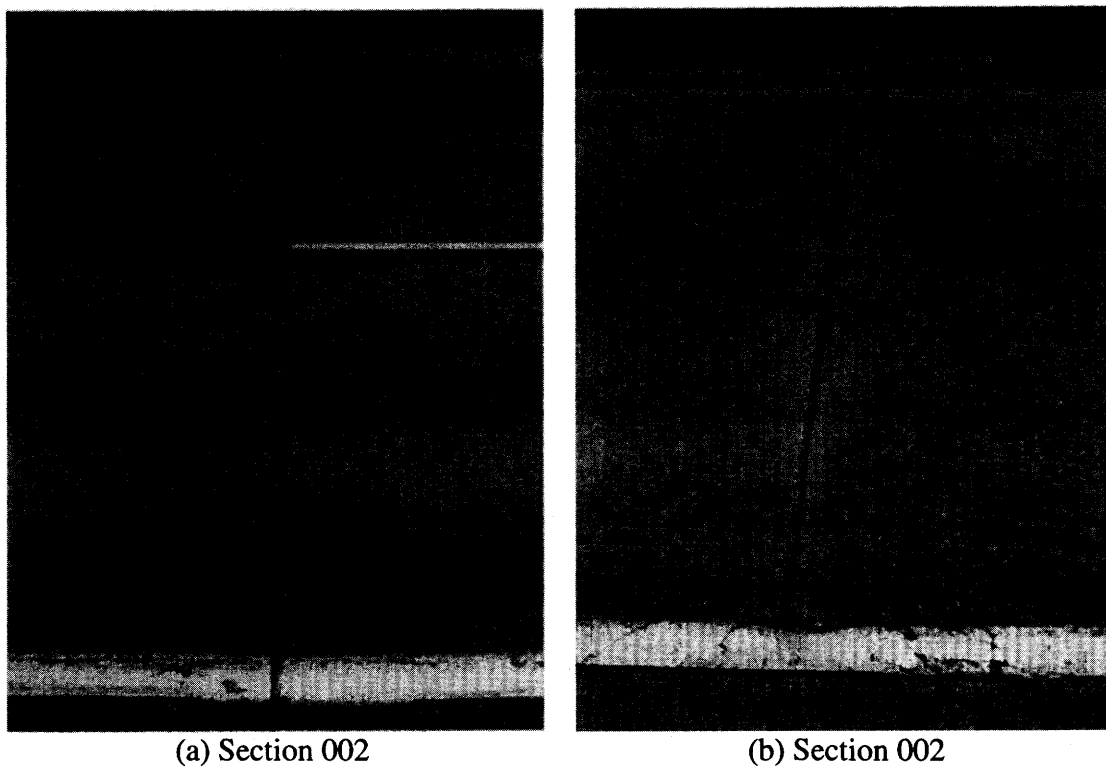


Figure 3-2. Typical distress manifestation observed on SD-090-019-002.

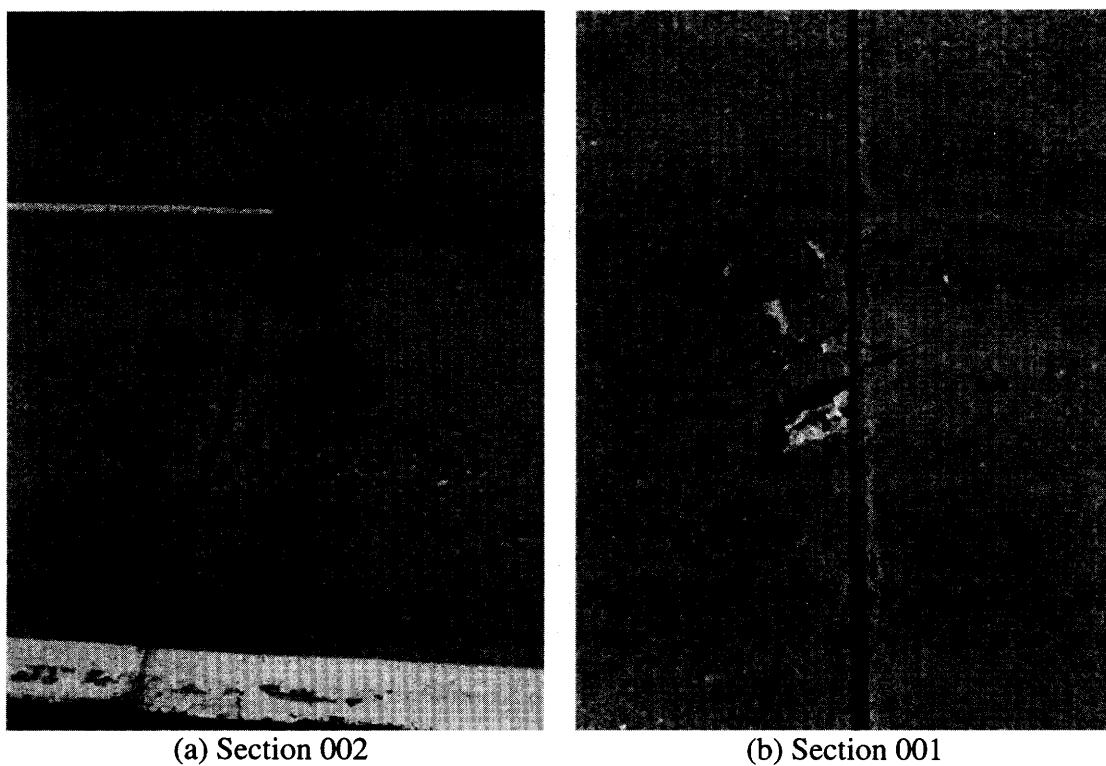


Figure 3-3. Typical distress manifestation observed on SD-090-019, Sections 1 and 2.

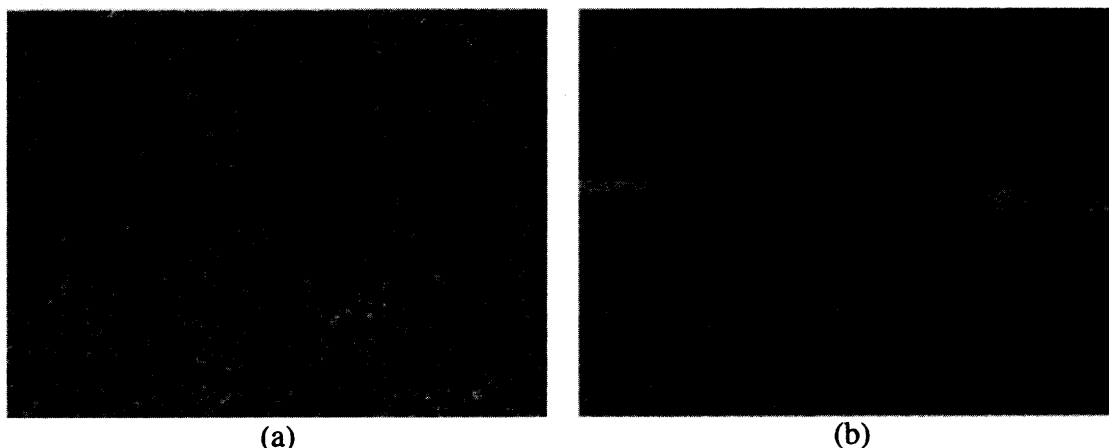


Figure 3-4. Typical distress manifestation observed on SD-090-019-002.

On both pavement sections, map cracking was observed throughout the entire area. On Section 001, the cracks appear to be confined to the upper 50 mm at the pavement surface. The majority of cracks run perpendicular to the centerline, but there are some cracks that run parallel to the centerline. The combination of cracks forms a criss-cross pattern on the surface. Although the cracking pattern is similar on Section 002, the transverse cracks on Section 001 are more pronounced and some are opened at the surface.

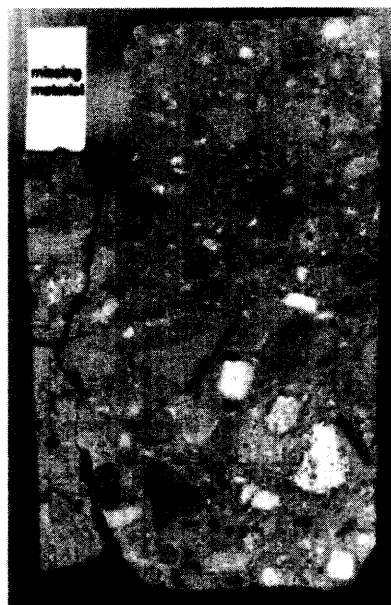
On Section 001, the area around the joints is discolored, showing a brownish-gray staining. However, the cracking pattern around the joints is similar to the slab interior. The MRD has progressed at a few of the slab corners and spalling has occurred. There is no exudate from the cracks on this section.

Section 002 exhibits a different cracking pattern along the joints. The cracking and staining form a semi-circular pattern, widening at the slab corners. A dark gray staining is observed around both the longitudinal and transverse joints. Unlike Section 001, exudate is observed at some cracks, particularly cracks located near a joint. The exudate is either a dark gray or white substance.

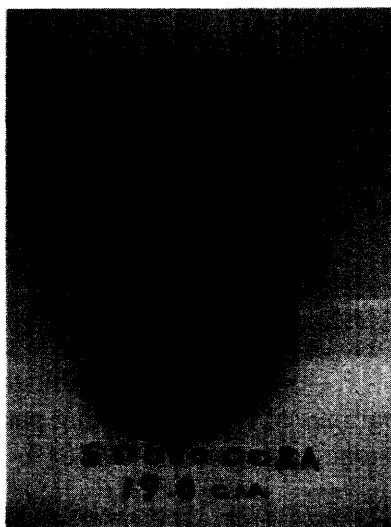
Laboratory Analysis

Core Selection/Visual Inspection

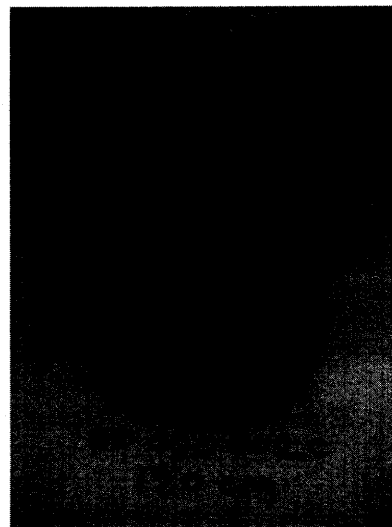
Based upon the field survey, distress was detected at joints and near slab corners. Photos of typical distresses are shown in figure 3-5. To look at concrete from more than one slab, Cores B and D were selected from Section 001 and Cores A, B, and C were selected from Section 002. All cores were cut to produce slabs for examination with stains.



(a) Section 001, Core B



(b) Section 002, Core A



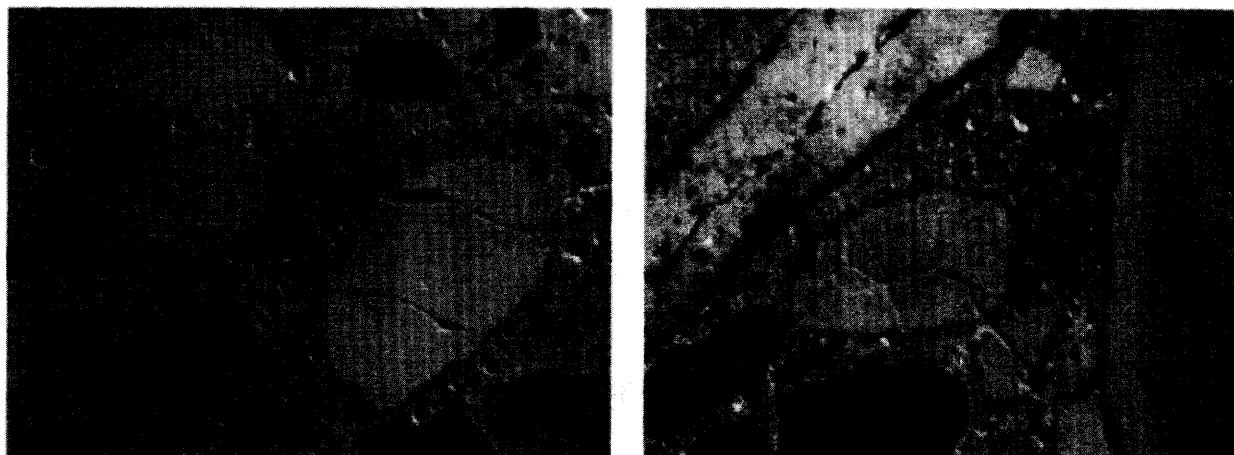
(c) Section 002, Core C

Figure 3-5. Core specimens from SD-090-019.

Mix proportions were estimated by inspecting the cores visually before and after slicing. In this case, detailed construction records were unavailable to verify the mix design. The concrete was well consolidated with no apparent segregation or parallelism of the aggregates. No scaling or sub-parallel cracking was apparent on these sites. The embedded steel was at a sufficient depth to prevent corrosion and no entrapped water voids were seen under aggregates or embedded steel. Surface cracking was apparent that was not related to plastic shrinkage cracking.

Stereo Optical Microscopy

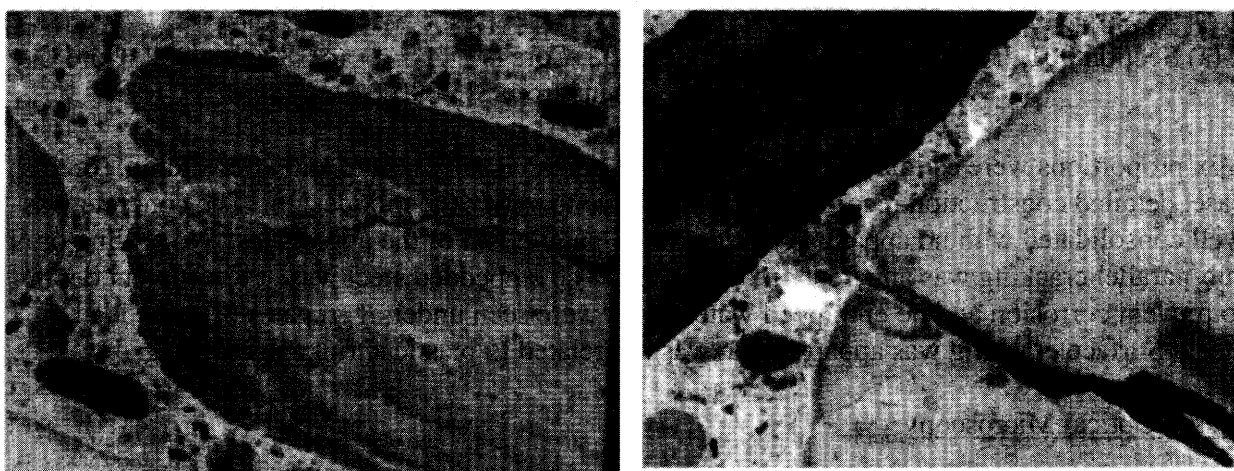
The stereo optical microscope was used to first examine polished slabs cut from each core to assess the general condition of the concrete. Typical micrographs of interesting features are presented in figures 3-6 and 3-7. The aggregate type was determined to be a natural gravel with a varied lithology including limestone, siltstone, dolomite, and rhyolite as the main rock types for the coarse aggregate. Many of the rhyolite particles had small feldspar inclusions. The fine aggregates contained the same rock types seen in the coarse aggregate in addition to shale, sandstone quartzite, and granite. Cracks passing through the paste also passed through aggregates. Reaction rims were visible along with secondary infilling in cracks and air voids. A yellow to white "soft" crumbly siltstone constituent of the coarse aggregate natural gravel is frequently cracked, with the cracks extending into the surrounding cement paste, and occasional white deposits in cracks. Aggregate particles that were volcanics or rhyolites appear to be reactive.



(a) Siltstone aggregate

(b) Siltstone and rhyolite aggregate

Figure 3-6. Stereo optical micrographs of typical cracking pattern associated with porous siltstone aggregate SD-090-019.



(a) Metamorphic aggregate

(b) Siltstone aggregate

Figure 3-7. Stereo optical micrograph showing gel deposits in SD-090-019 aggregates.

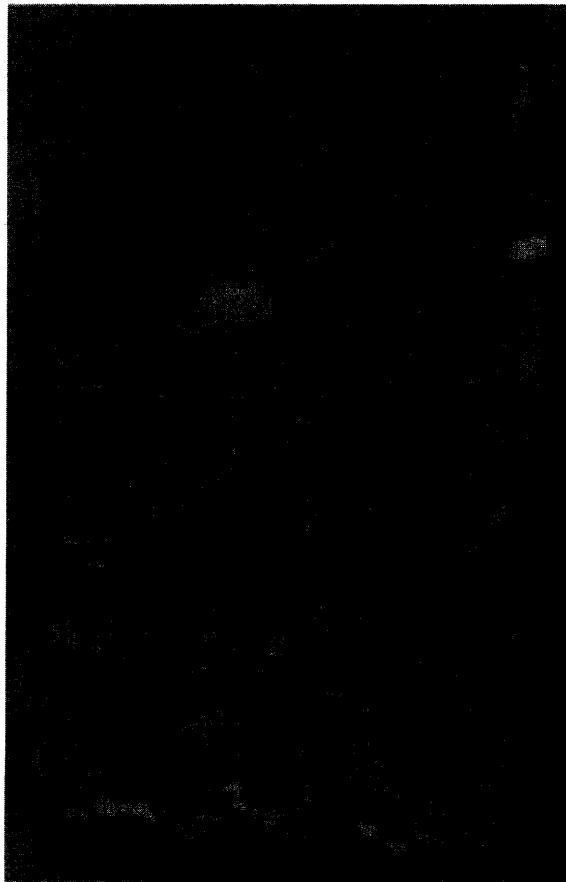
The stereo microscope was also used to perform a modified point count in accordance with ASTM C 457. As part of the modified point count, the volume fractions of paste and aggregate were also determined to confirm mix volumetrics. The results of this analysis are given in table 3-6.

Table 3-6. Results of ASTM C 457 for concrete from SD-090-019.

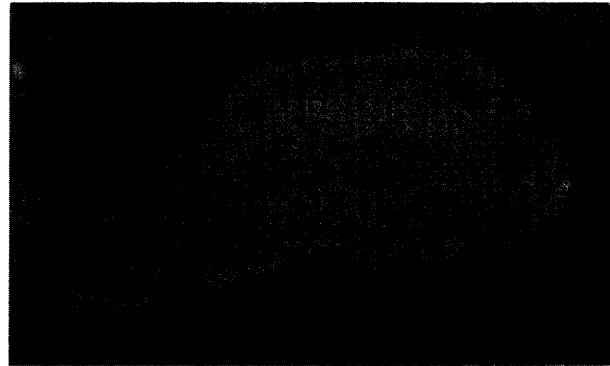
Core	Original		Existing		Volume Percent		
	Air Content (vol. %)	Spacing Factor (mm)	Air Content (vol. %)	Spacing Factor (mm)	Paste (vol. %)	Coarse Aggregate (vol. %)	Fine Aggregate (vol. %)
Site 1 Core A	6.0	0.1274	6.0	0.1375	25.6	47.9	20.5
Site 1 Core D	5.7	0.1073	5.7	0.1047	26.4	52.0	15.9
Site 2 Core C	5.5	0.1089	5.4	0.1114	27.16	41.5	25.8

Staining Tests

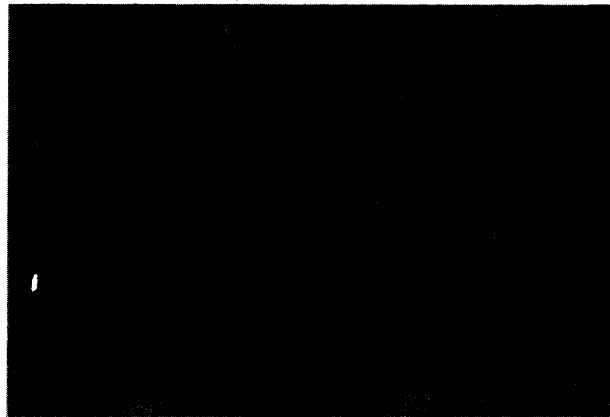
The sodium cobaltinitrite/rhodamine B staining tests were applied and a number of aggregates were identified as being susceptible to alkali-silica reactivity (ASR). The phenolphthalein staining method was used to determine the depth of carbonation on freshly cut surfaces. Slabs cut from the analyzed cores were tested for depth of carbonation with no core having a depth of carbonation greater than 2 mm below the road surface. Barium chloride/potassium permanganate stain was used to identify sulfate minerals. Examples of the stained slabs are presented in figures 3-8 through 3-11.



(a) Stained slab

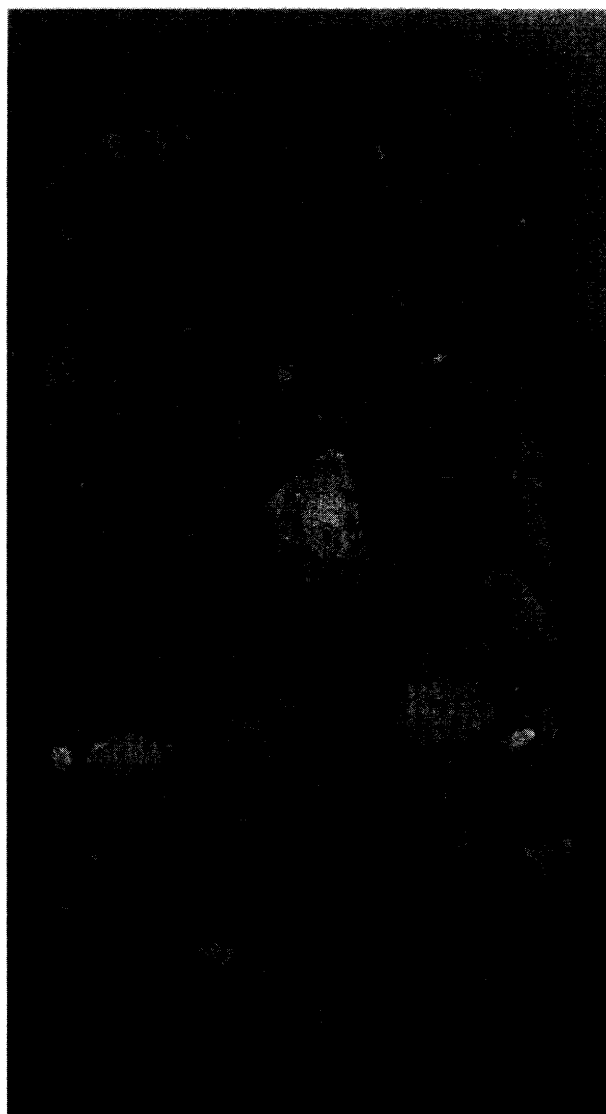


(b) Stereo optical micrograph of reactive porous siltstone particle



(c) Stereo optical micrograph of reactive volcanic particle

Figure 3-8. Slab 1B stained with sodium cobaltinitrite/rhodamine B from SD-090-019-001.



(a) Stained slab



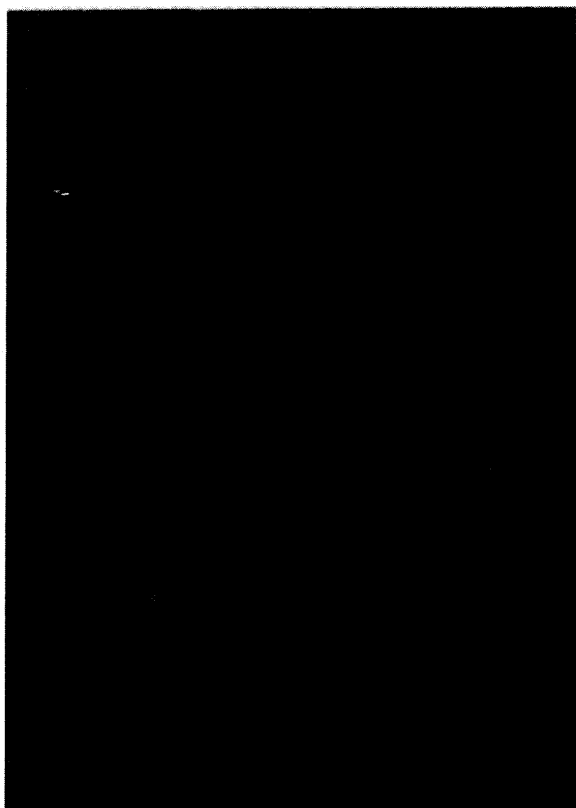
(b) Stereo optical micrograph of reactive rhyolite particle

Litho Type	* Volume (ml)	Volume %
limestone	530	35.8
siltstone	185	12.5
dolomite	195	13.2
rhyolite/volcanics	204	13.8
chert	117	7.9
gneiss/schist/phyllite	100	6.8
sandstone	84	5.7
shale	8	0.5
granite/pegmatite	53	3.6
quartzite	3	0.2
total	1479	100

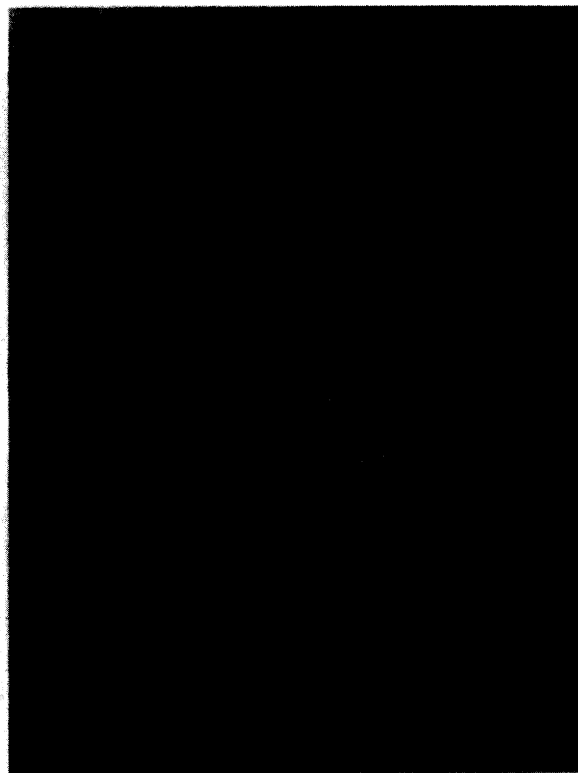
* Determined by H2O displacement from sample gathered at nearby river.

(c)

Figure 3-9. Slab 1B stained with sodium cobaltinitrite/rhodamine B from SD-090-019-001.



(a) Stained slab



(b) Reactive aggregate particle



(c) ASR gel filled void



(d) Reactive aggregate particle

Figure 3-10. Slab 2B stained with sodium cobaltinitrite/rhodamine B from SD-090-019-002.

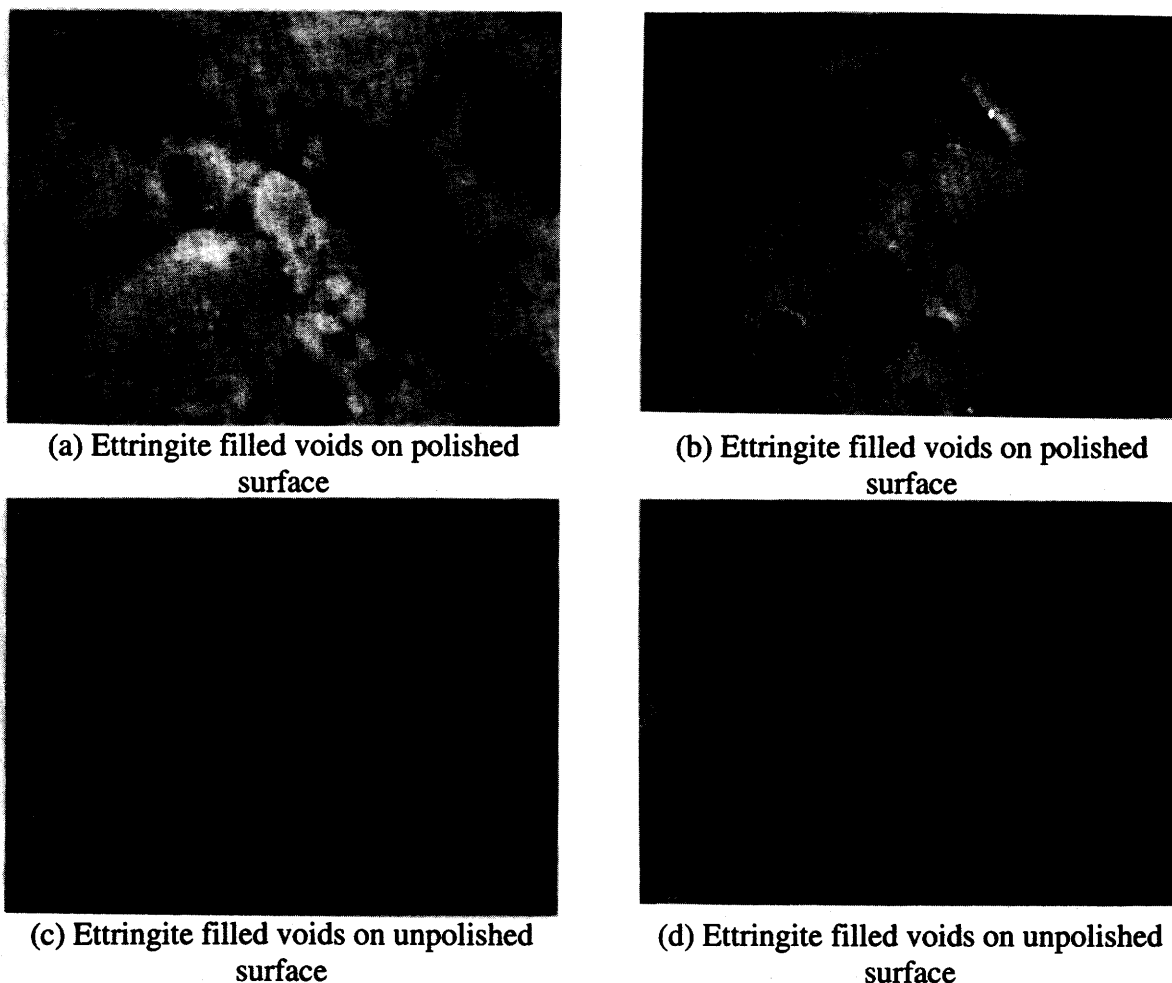


Figure 3-11. Stereo optical micrographs of air voids filled with sulfate minerals stained with potassium permanganate (note differences due to polishing).

Petrographic Optical Microscopy

Based upon stereo microscope observations and staining, thin sections were prepared from the selected cores. Surfaces were sectioned from the core adjacent to stained sections to avoid contamination from the stains. The reactive coarse aggregates were primarily the siltstones and rhyolites, although others were noted as reactive. The shale was commonly associated with ASR in fine aggregate. In addition to cracking associated with ASR, other cracking of non-reacted siltstone aggregates was noted. The siltstone aggregates had a very porous microstructure as seen in thin section. These aggregates may be susceptible to aggregate freeze-thaw deterioration, leading to some of the cracking seen in the concrete. In addition to possible ASR and aggregate freeze-thaw deterioration, evidence of alkali-carbonate reactivity (ACR) was noted where densified paste regions or "halos" with a large amount of calcite were seen surrounding dolomite coarse aggregates (Spry et al. 1996). Secondary deposits within cracks and voids were identified. In addition to specific phases identified (e.g., ASR gel, calcite), ettringite was common as a secondary deposit. In addition to these diagnostic features, hydrocalumite (Friedel's salt) secondary deposits were found. Given the high chloride concentration needed to precipitate hydrocalumite, this is taken as a diagnostic feature of deicer attack. Petrographic micrographs are presented in figures 3-12 and 3-13.

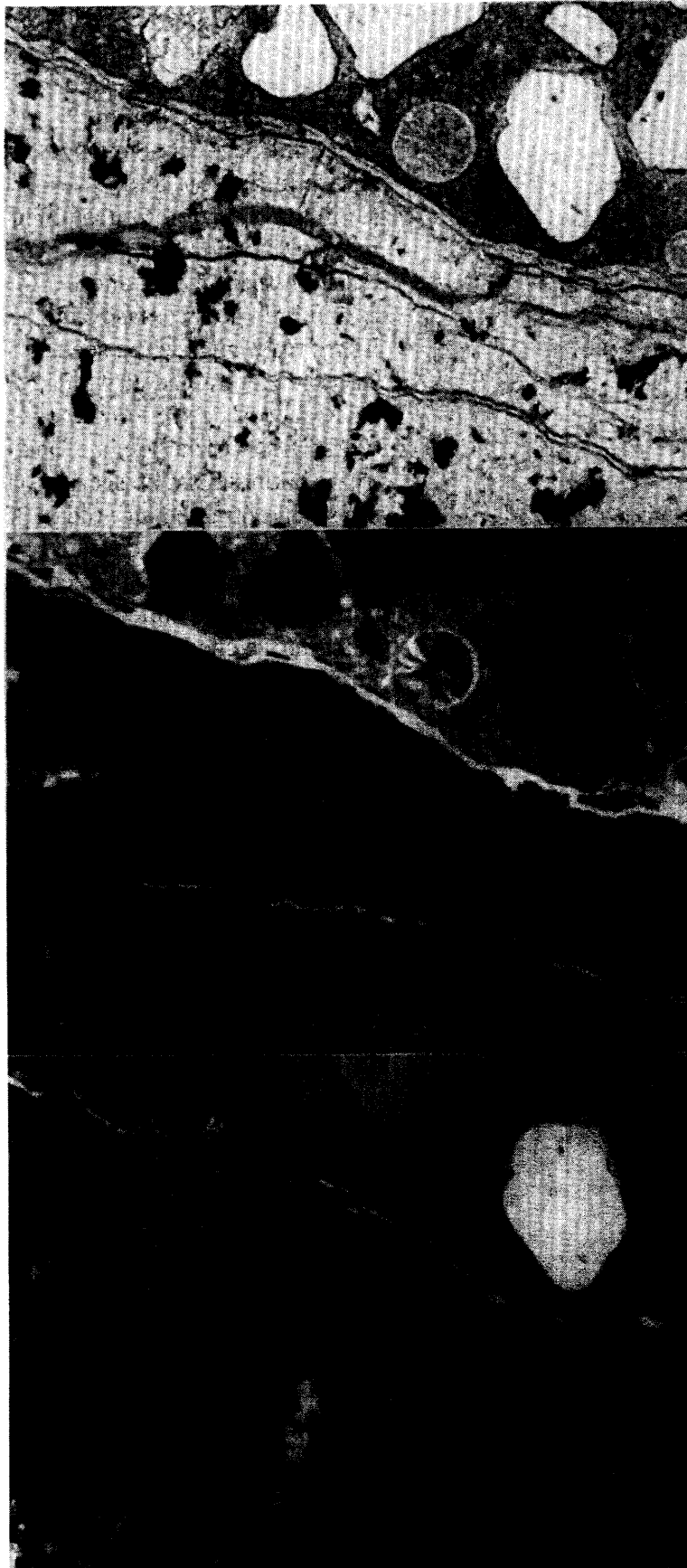


Figure 3-12. Core SD-090-019-001B, thin-section micrographs of same rhyolite aggregate that was stained with sodium cobaltinitrite ASR stain as shown in figure 3-9 (b). From top to bottom: transmitted plane polarized light, epifluorescent mode, and transmitted cross polarized light. Ettringite can be seen filling the entrained air void, ASR gel can be seen in the crack within the aggregate, and hydrocalumite can be seen in the crack along the contact between the aggregate and the cement paste. This same area was analyzed with the SEM to collect quantitative chemical information about the gel, ettringite, and hydrocalumite.

90x magnification

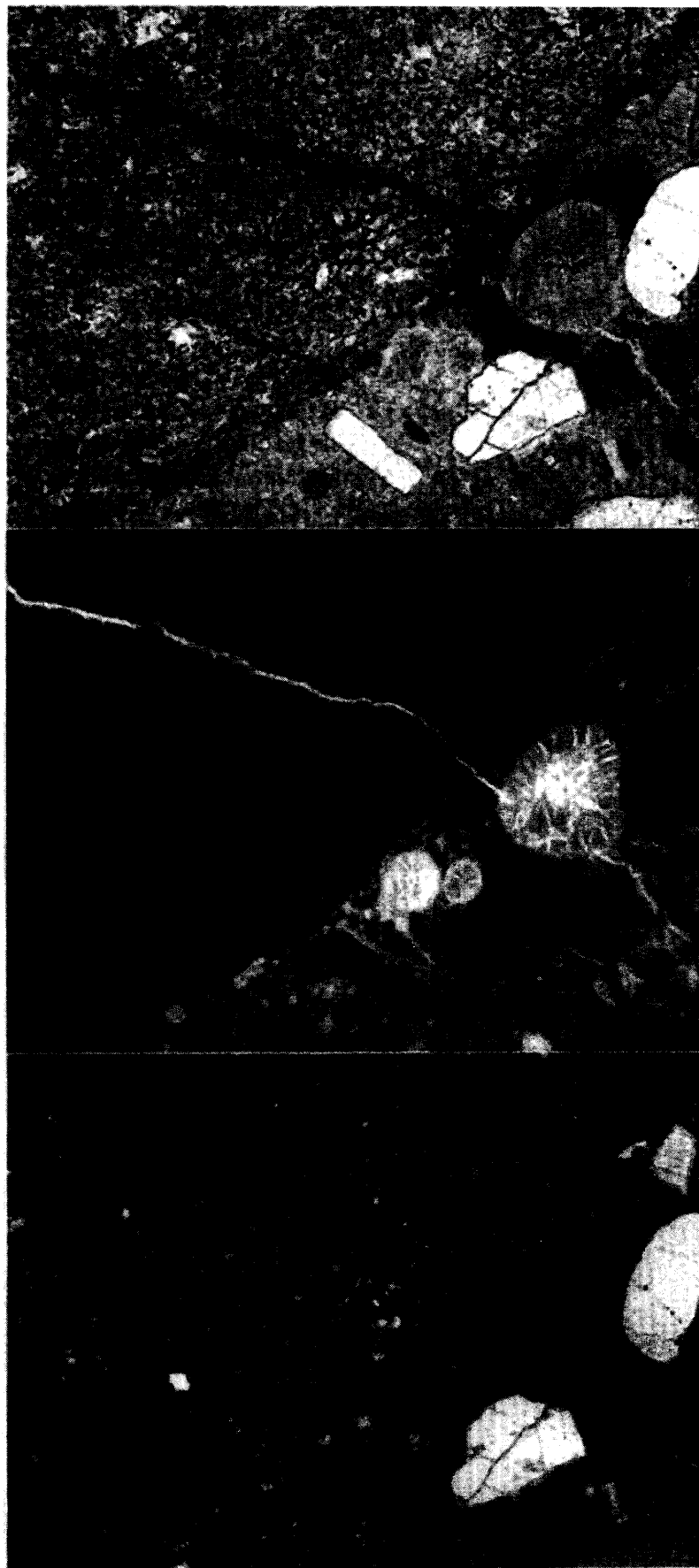


Figure 3-13. Core SD-090-019-001B, thin-section micrographs of same volcanic aggregate that was stained with sodium cobaltinitrite ASR stain as shown in figure 3-8 (c).

From top to bottom: transmitted plane polarized light, epifluorescent mode, and transmitted cross polarized light. Ettringite can be seen filling the entrained air void, ASR gel can be seen in the crack within the aggregate, and hydrocalumite can be seen in the small entrained air void in the lower right hand corner. This same area was analyzed with the SEM to collect quantitative chemical information about the gel, ettringite, and hydrocalumite.

90x magnification

Scanning Electron Microscopy (SEM)

A conventional SEM was used to identify secondary deposits seen in the petrographic microscope examination to confirm those observations. Figure 3-14 contains a backscattered electron image showing an ettringite filled void, a crack filled with hydrocalumite, and characteristic x-ray spectra from each phase illustrating their compositions. The SEM analysis confirmed the petrographic analysis with regards to the composition of the secondary deposits. The phase identified as hydrocalumite was confirmed, as were the presence of ettringite and the composition of various ASR reaction products. The results of x-ray microanalyses of the ettringite and the hydrocalumite phases are presented in tables 3-7 and 3-8, respectively. Figure 3-15 presents the ternary diagram showing the probable range of composition for the hydrocalumite deposits.

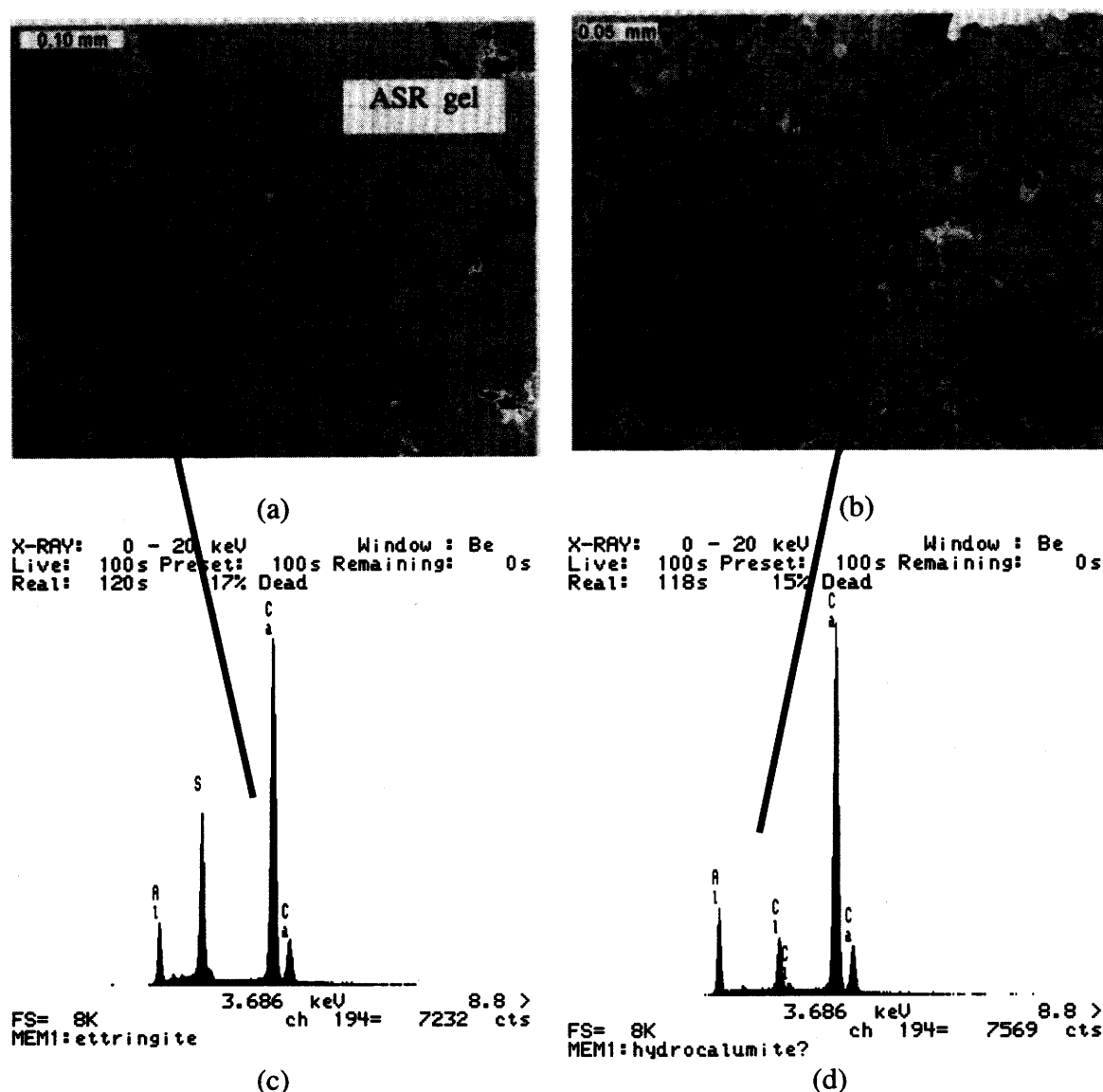


Figure 3-14. Ettringite (a) and hydrocalumite (b) infilling in void and crack, respectively. Example spectra from each phase are shown in (c) and (d), respectively.

Table 3-7. Summary of 10 analyses from ettringite deposits, compared to a calculated composition for dehydrated ettringite.

Element	Average Wt. %	Standard Deviation	Dehydrated Ettringite
Na	0.2	0.2	0.0
Mg	0.0	0.0	0.0
Al	7.9	0.3	6.9
Si	0.3	0.1	0.0
S	11.6	0.5	12.2
Cl	0.2	0.1	0.0
K	0.0	0.0	0.0
Ca	31.2	0.6	30.6
Ti	0.0	0.0	0.0
Mn	0.0	0.1	0.0
Fe	0.0	0.1	0.0
O	-	-	48.8
H	-	-	1.5
sum	51.3		100.0

Table 3-8. Summary of 13 analyses from hydrocalumite deposits, compared to calculated compositions for the 3 dehydrated end members of the hydrocalumite solid solution series.

Element	Average Wt. %	Standard Deviation	Dehydrated Cl-hydrocalumite	Dehydrated OH-hydrocalumite	Dehydrated CO ₃ ⁻² hydrocalumite
Na	0.0	0.1	0.0	0.0	0.0
Mg	0.0	0.1	0.0	0.0	0.0
Al	12.5	0.4	11.0	12.9	12.5
Si	0.4	0.4	0.0	0.0	0.0
S	0.0	0.0	0.0	0.0	0.0
Cl	5.0	0.2	14.5	0.0	0.0
K	0.0	0.1	0.0	0.0	0.0
Ca	36.0	0.8	32.8	38.3	37.3
Ti	0.0	0.0	0.0	0.0	0.0
Mn	0.0	0.1	0.0	0.0	0.0
Fe	0.3	0.2	0.0	0.0	0.0
C	-	-	0.0	0.0	2.8
O	-	-	39.2	45.9	44.6
H	-	-	2.5	2.9	2.8
sum	54.2		100.0	100.0	100.0

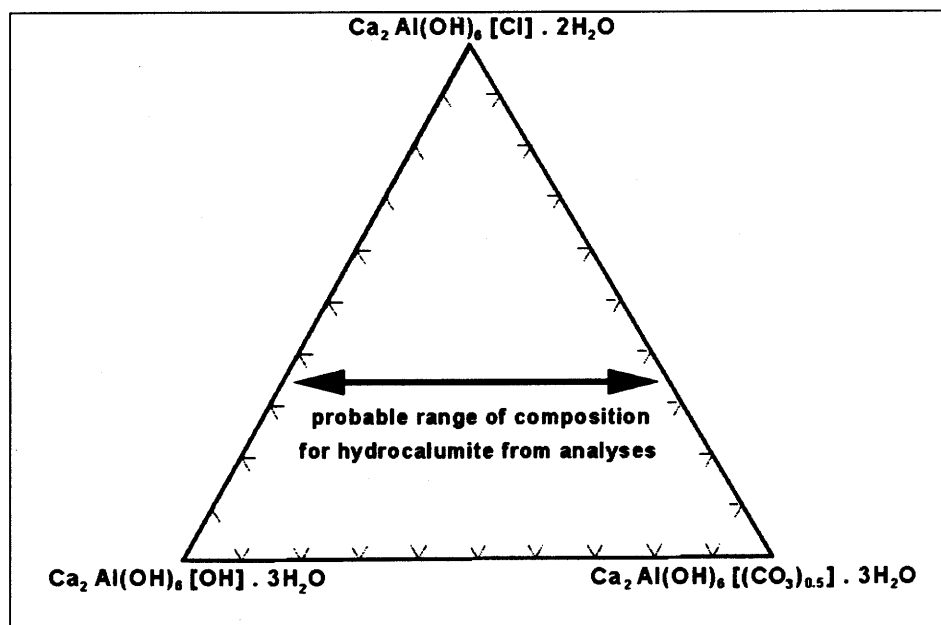


Figure 3-15. Ternary diagram showing the probable range of composition for the hydrocalumite deposits analyzed from SD-090-019.

Chemical Laboratory Tests

Ion chromatography was used to analyze the sulfate content of soil samples taken from the grade below the individual core holes. The complete analysis is presented in the final report. To summarize, the soil base below the test sites would be classified as a negligible sulfate exposure using the criteria set forth in ACI 201.2R-92 *Guides to Durable Concrete*.

Interpretation and Diagnosis

Having performed the described laboratory analyses and applied the diagnostic flowcharts as shown in figures 3-16 through 3-20, several possible MRDs were identified in SD-090-019-001, including ASR, ACR, aggregate freeze-thaw, and deicer attack. This is consistent with the visual observations of the distress reported from the field where mixtures of diagnostic features were apparent. To finalize the diagnosis, the diagnostic tables were consulted. The diagnostic features identified in the analysis processes are listed below in table 3-9 along with their associated MRD type and significance as related to this pavement. A brief discussion follows of each possible MRD identified in the laboratory analysis:

ASR - This MRD seems to be the most dominant given its extent in the sections sampled. From the standpoint of the guidelines, all diagnostic features of ASR were present with the exception of known poor performance for the aggregate used.

ACR - This MRD was identified as a possible but in the final analysis is not listed as probable as a major contributor. Although there was strong evidence of the reactivity of some dolomite aggregates, the extent and magnitude of this reaction was not great.

Aggregate Freeze-Thaw - Like ASR, this appeared to be a dominant distress in terms of extent. The likelihood or certainty of diagnosis is also very high given that, with the exception of known

poor performance for the aggregate used, 75 percent of all diagnostic features for aggregate freeze-thaw were present.

Deicer Attack - This MRD is probably the most difficult to diagnose as it can often be present and hidden by other MRDs. The key diagnostic feature that makes deicer attack probable is the occurrence of hydrocalumite as an infilling material in cracks and voids.

As stated previously, it is not rare to find a pavement with diagnostic features representative of more than one distress mechanism present. In most of these cases, as with this one, the failure of the concrete cannot be attributed to one particular cause. However, in this case some general observations can be made. First, the ASR, aggregate freeze-thaw, and potential ACR distresses may not have occurred if a higher quality aggregate source was used. As is most often the case, contractors use the best possible aggregate source economically feasible but in some locations, such as central South Dakota, the possibilities are limited. The other distress mechanism identified, deicer attack, is more problematic as deicers are clearly required on this portion of the interstate system. A lower water-to-cement ratio (w/c) would likely reduce the concrete permeability and thus reduce the likelihood of a recurrence of this distress.

Recommended Treatment/Rehabilitation Alternatives

Using the procedures presented in Guideline III in *Volume 2: Guidelines Description and Uses*, feasible treatment and rehabilitation alternatives were selected. The two most significant MRD mechanisms found were aggregate freeze-thaw deterioration and ASR. Because the two mechanisms are acting in concert, it is difficult to rate the severity of each independently, but the level of spalling and patching at the transverse joints indicates that the severity level is likely a medium severity in Section 001 and medium to high in Section 002. The extent was at both joints and cracks and at corners. As a result, feasible treatment/rehabilitation alternatives include:

- Sealing less deteriorated joints and cracks.
- Partial- and full-depth repairs.
- The application of a high molecular weight methacrylate (HMWM).
- Overlay.

The use of patching is still feasible even though ASR was observed since most deterioration is isolated in the vicinity of joints and cracks. Further, lithium compounds are not suggested since they are ineffective in delaying aggregate freeze-thaw damage.

Ultimately, as the pavement continues to deteriorate, a reconstruction/recycling option becomes more viable. If recycling is considered, precautions must be taken to avoid aggregate freeze-thaw deterioration and/or ASR in the newly constructed pavement.

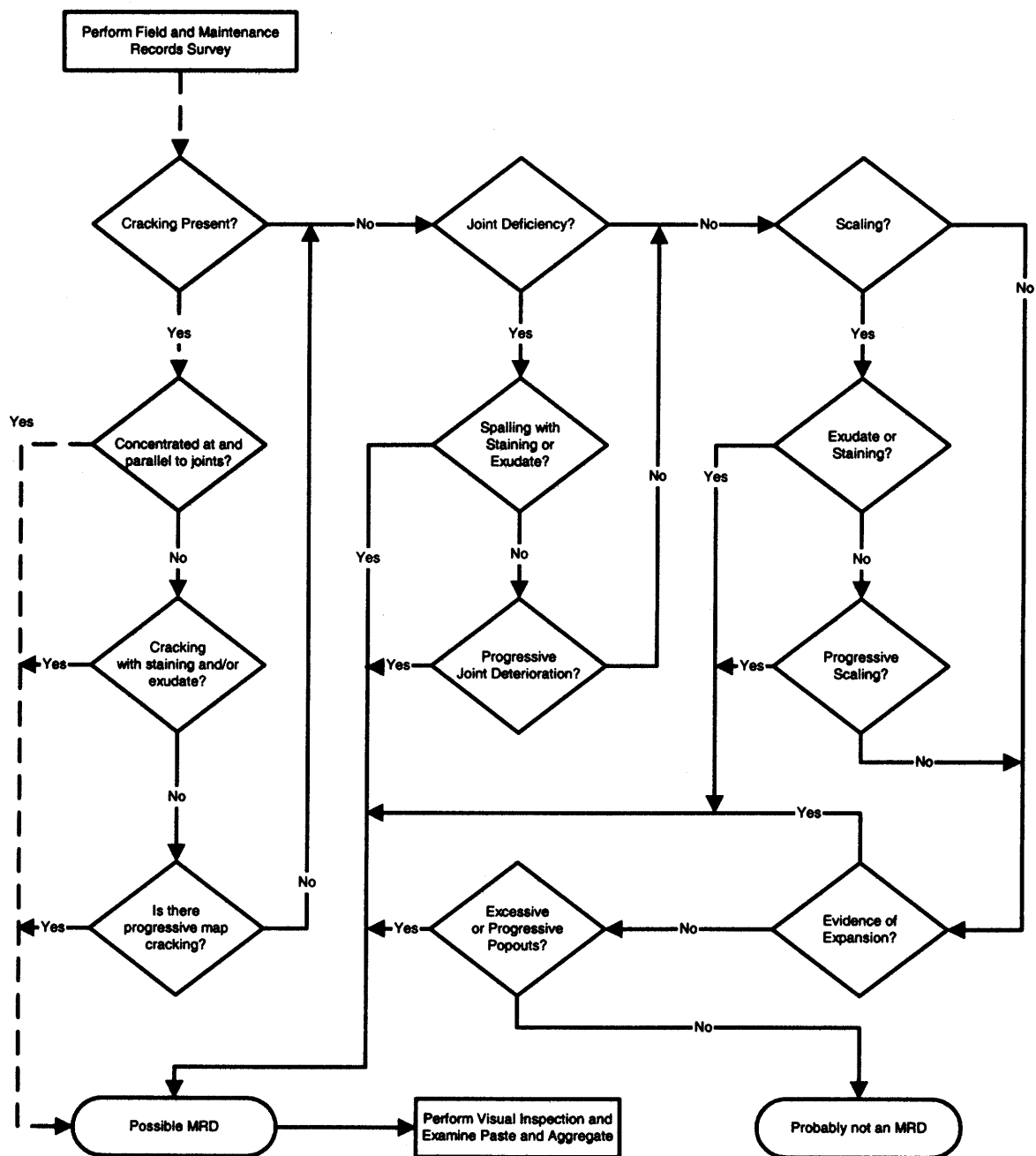


Figure 3-16. Flowchart for assessing the likelihood of MRD causing the observed distress in the pavement as applied to the Spearfish, South Dakota site.

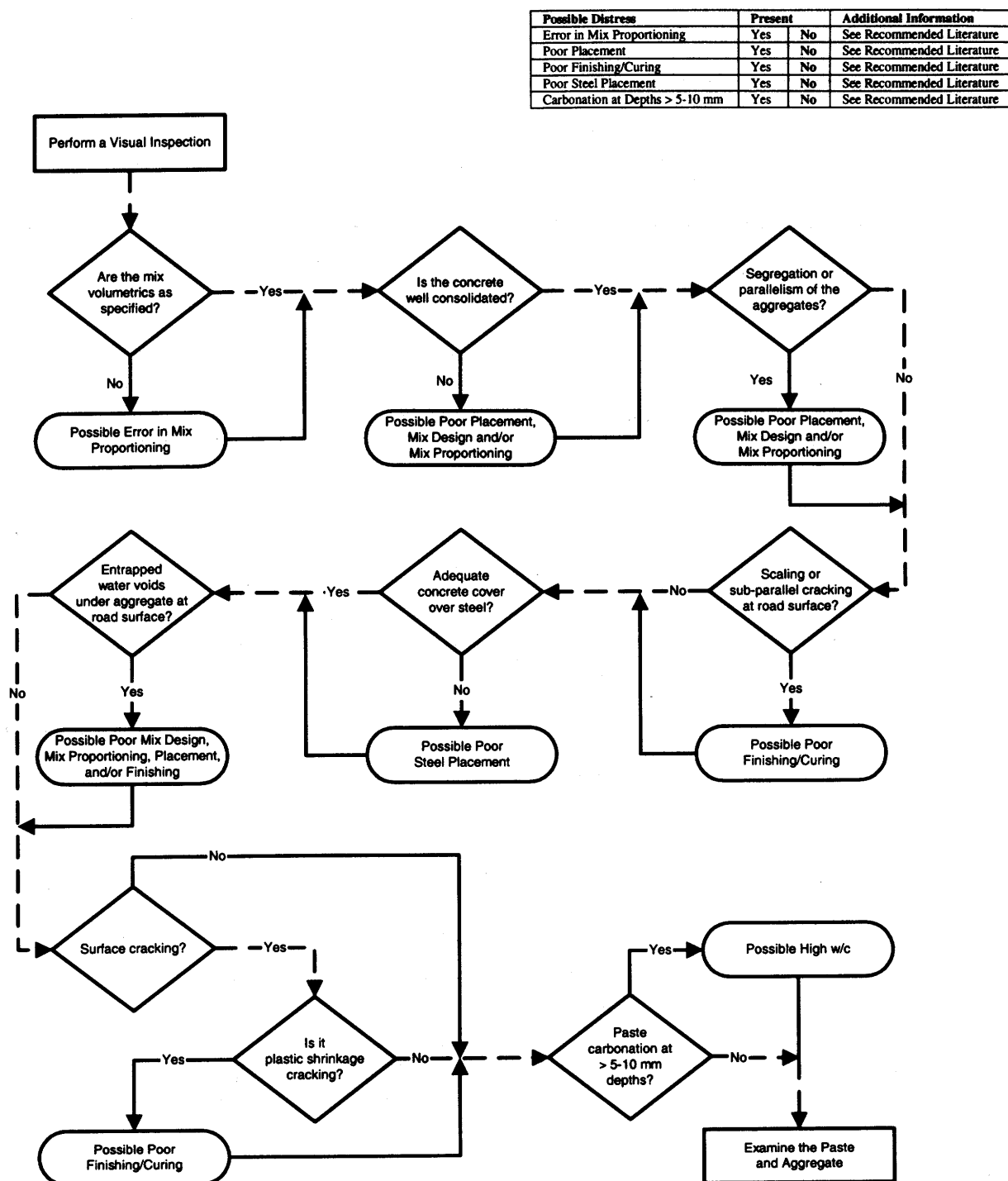


Figure 3-17. Flowchart for assessing general concrete properties based on visual examination as applied to the Spearfish, South Dakota site.

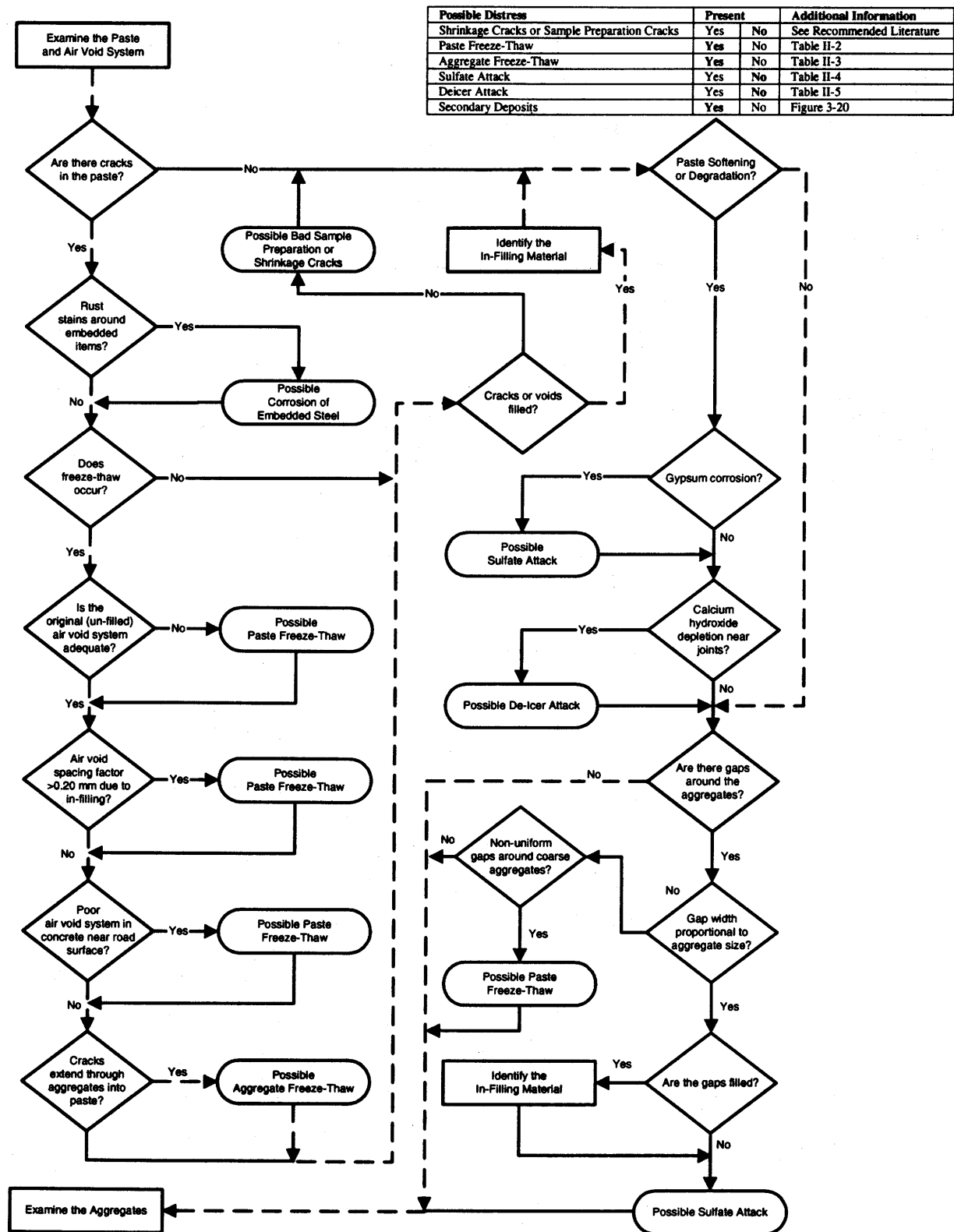


Figure 3-18. Flowchart for assessing the condition of the concrete paste as applied to the Spearfish, South Dakota site.

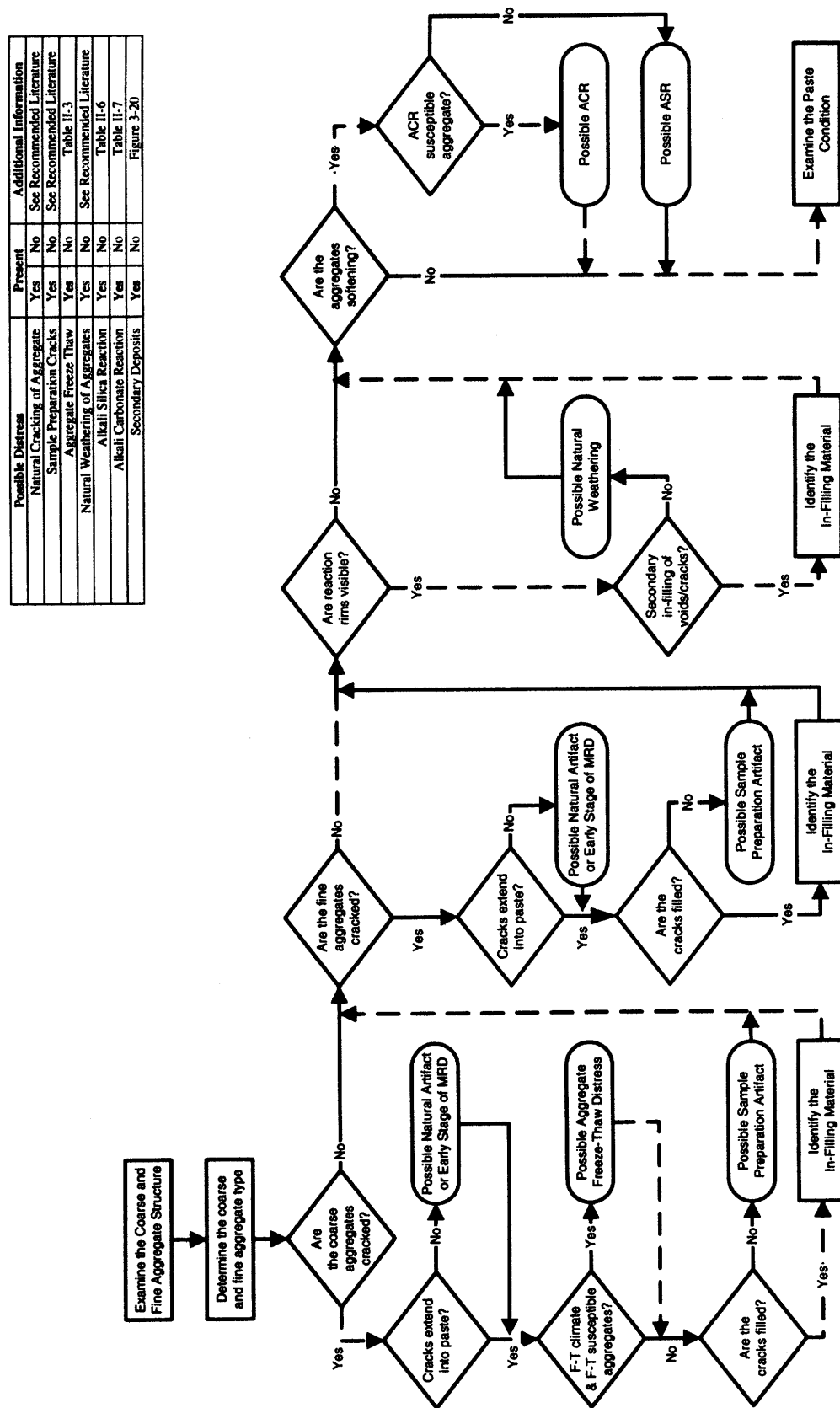


Figure 3-19. Flowchart for assessing the condition of the concrete aggregates as applied to the Spearfish, South Dakota site.

Possible Distress	Present	Additional Information
Sulfate Attack	Yes	Table II-4
De-icer Attack	Yes	Table II-5
Alkali Silica Reaction	Yes	Table II-6
Alkali Carbonate Reaction	Yes	Table II-7
Corrosion of Embedded Steel	Yes	Table II-1

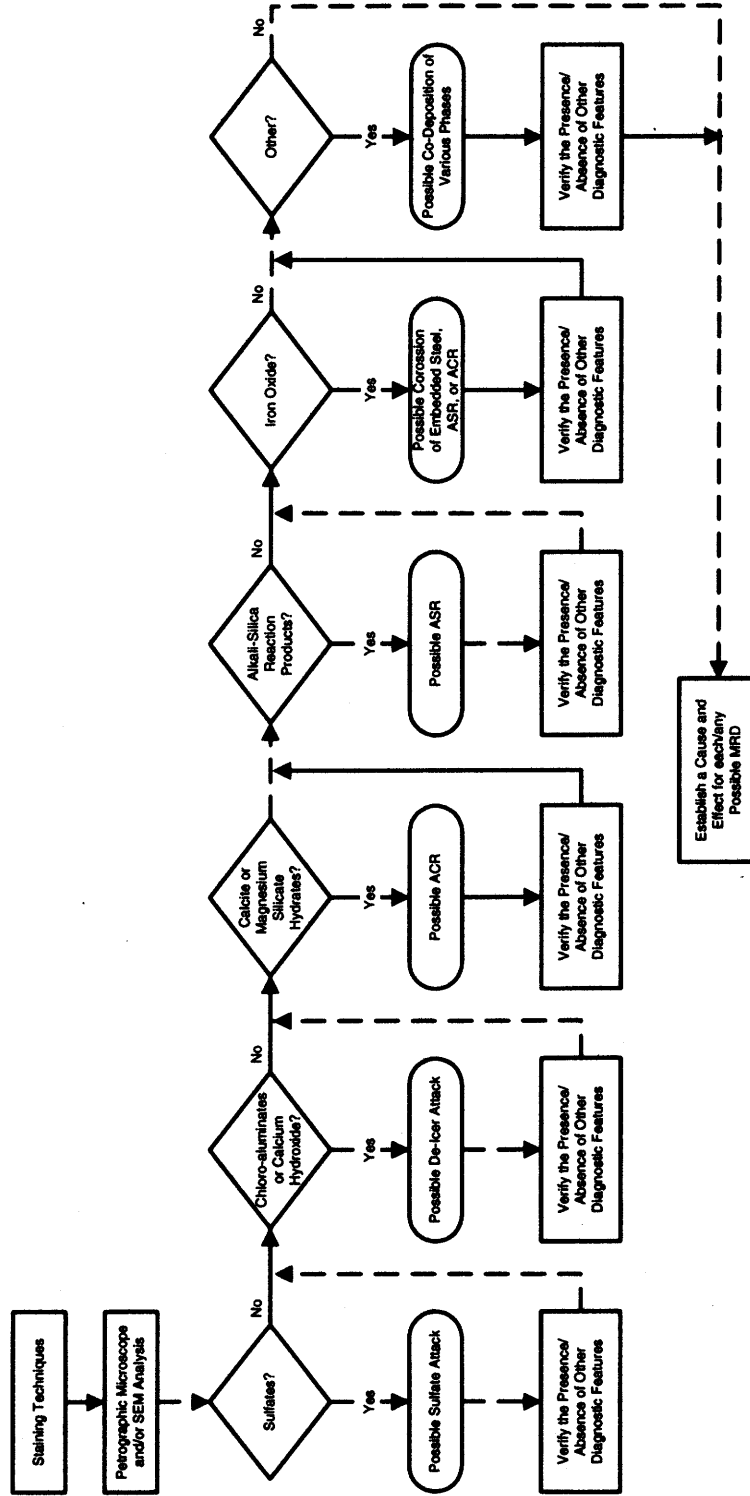


Figure 3-20. Flowchart for identifying infilling materials in cracks and voids as applied to the Spearfish, South Dakota site.

Table 3-9. Identified diagnostic features along with their associated MRD type and significance as related to SD-090-019.

Diagnostic Feature	Method of Characterization	Associated with MRD Type	Significance
Secondary deposits filling air voids	Staining Stereo OM Petrographic OM SEM	Paste freeze-thaw, deicer attack, ASR, ACR, Sulfate attack (both internal and external)	Low
Staining at joints or cracks	Field evaluation	Deicer attack	Moderate
Secondary deposits of chloroaluminates	Petrographic OM SEM		High
Cracking near joints/cracks	Field evaluation	Aggregate freeze-thaw	Moderate
Staining/Spalling	Field evaluation		Moderate
Cracks through non-reactive coarse aggregates	Visual inspection Stereo OM Petrographic OM SEM		High
Poor void structure in the aggregate	Petrographic OM CSEM LVSEM		High
Map Cracking with exudate	Visual inspection	ASR	High
ASR reaction product in cracks and voids	Stereo OM Petrographic OM		High
Reaction rims on aggregates	Visual inspection Stereo OM Petrographic OM SEM		Moderate
Microcracking radiating from reacted cracked aggregate	Stereo OM Petrographic OM SEM		High
Map Cracking	Field evaluation	Sulfate attack	Moderate
Significant sulfate deposits in cracks and voids	Staining Stereo OM Petrographic OM SEM		Low

Recommended Prevention Strategies

- For the distresses noted, the best preventative strategy is to use a different source of aggregate. Testing in accordance with the guidelines should show that the current source would be unacceptable without mitigation. Mitigation strategies for aggregate freeze-thaw deterioration that could be used if current aggregate source is all that is available include:

- Heavy media separation.
- Blending with non-susceptible aggregates.
- Crushing to a non-susceptible size (potentially blending with larger non-susceptible aggregates).

To address the potential for ASR, the following strategies can be employed to reduce the reactivity of the aggregate:

- Heavy media separation.
- Blending with non-susceptible aggregates.
- Washing.

If aggregate benefaction is not feasible or cost effective, other strategies can also be employed including:

- Reducing the total mixture alkalinity to less than 3 kg/m³.
- Using a blended cement containing a pozzolan or ground slag.
- Through supplementation or addition, use pozzolans or ground slag in the mixture.
- Add lithium nitrate.

Regardless of the approach, the design PCC mixture must be tested to ensure that the aggregate freeze-thaw deterioration and ASR have been mitigated.

2.2 TH 65 IN MORA, MINNESOTA (MN-065-064)

Project Description

The Minnesota DOT provided several candidate projects with durability problems. One of the projects—located on TH 65 in downtown Mora—was experiencing severe durability problems concentrated at the transverse joints. This project was selected as the primary case study site for the wet-freeze climatic region. This area receives approximately 660 mm of annual precipitation and has a freezing index of 1030 °C-days.

Table 3-10 presents a summary of the design information for this project. This project extends from milepost 64.2 to 65.0 and is located in both the northbound and southbound lanes. It is a four-lane divided roadway separated by a concrete median; some sections also include an additional lane for left-turn traffic. The pavement, which was constructed in 1989, consists of a 200-mm jointed plain concrete pavement (JPCP) with a 75-mm granular base and a 305-mm granular subbase. The transverse joints are skewed and have a variable joint spacing pattern of 4.0-4.6-5.2-4.6 m. Load transfer is provided by aggregate interlock only; no additional load transfer devices have been employed. The only variation in the two sections is the transverse joint sealant—Section 001 uses silicone sealant and Section 002 uses hot-pour sealant. The longitudinal joints are not sealed. A 2.4-m-wide AC shoulder is placed at the outer edge; there is no inside shoulder due to the concrete median.

Table 3-10. Summary of design features for MN-065-064.

Category	Design Feature	Description
General Information	Project limits	MP 64.2 – 65.0
	Highway type	Divided
	Number of lanes	4
	Direction	Northbound/southbound
	Construction date	1989
	Cumulative ESALs	~300,000
Pavement Cross Section	Pavement type	JPCP
	PCC slab thickness	200 mm
	Base	75-mm granular
	Subbase	305-mm granular
	Subgrade type	Unknown
Transverse Joint	Joint spacing	4.0-4.6-5.2-4.6 m
	Joint skew	1:12
	Load transfer	Aggregate interlock
	Sealant type	Silicone (001); hot-pour (002)
Longitudinal Joint	Load transfer	
	Sealant type	None
Outer Shoulder	Surface type	AC
	Width	2.4 m
Inner Shoulder	Surface type	n/a
	Width	n/a
Climatic Conditions	Region	Dry-freeze
	Annual precipitation ¹	660 mm
	Freezing index ¹	1030 °C-days

¹ Climatic data are for Minneapolis, Minnesota.

Distress Survey Results

Although the design and construction details are the same, the initial investigation revealed that the southbound lanes were in better condition than the northbound lanes. Thus, two sections were selected for survey, one in each direction. Section 001 is located in the northbound outer lane beginning at milepost 64.6, and Section 002 is located in the southbound outer lane beginning at milepost 64.4. Both sections are constructed at grade. Tables 3-11 and 3-12 provide a summary of the distress survey results for Sections 001 and 002, respectively.

As previously mentioned, Section 001 is exhibiting the worst performance, with most of the deterioration limited to the transverse joints. Joint spalling and bituminous patching are predominant along the transverse joints. The spalling appears to be materials-related and progressed to medium severity in most cases. In some cases, the surface has scaled off and aggregate particles have been exposed. Every transverse joint has been patched over a portion of its length to help address the spalling problem. In fact, the transverse joints were so deteriorated that faulting could not be measured. In addition, maintenance forces on hand during the surveys indicated that removal of the material during the patching operation often extended through the entire depth of the slab. The only other distress noted was a longitudinal crack that extended the length of one slab.

Table 3-11. Summary of pavement condition surveys for MN-065-064-001.

	Distress Type	Distress Measure	Severity Level			Comments
			Low	Moderate	High	
Cracking	Corner Breaks	number	0	0	0	
	Longitudinal Cracking	linear meters	3.5	0.0	0.0	
	Transverse Cracking	number of cracks	0	0	0	
		linear meters	0.0	0.0	0.0	
Transverse Joints		percent of slabs	0			
	Sealant		fair to good condition			silicone sealant
	Spalling	number	1	7	0	
		linear meters	0.4	2.7	0	
	Faulting	millimeters	n/a			
		millimeters	n/a ¹			
Long. Joints	Width	millimeters	9.4			
	Sealant		n/a			not sealed
	Spalling	linear meters	0.0	0.0	0.0	
	Shoulder Dropoff	millimeters	0.0			
Surface Conditions	Map Cracking	number of slabs	0			
		square meters	0.0			
	Scaling	number of slabs	0			
		square meters	0.0			
	Polished Aggregate	square meters	0.0			
	Popouts	number/sq. meter	0.0			
Other	Blowups	number	0			
	Flexible Patches	number	0	33	0	
		square meters	0.0	28.3	0.0	
	Rigid Patches	number	0	0	0	
		square meters	0.0	0.0	0.0	
	Pumping/Bleeding	number	0			
		linear meters	0.0			

¹ Faulting could not be measured due to deterioration at transverse joints.

Section 002 is in better overall condition but still exhibits some deterioration at the transverse joints. Medium-severity spalling is observed at 6 of the 33 joints (18 percent) and bituminous patches are observed at 12 of the 33 joints (36 percent). However, the deterioration at the affected joints is less severe than that observed on Section 001. Faulting could be measured on this section and averaged 2.0 and 1.7 mm at 0.30 and 0.75 m from the outer slab edge. The only other distresses include a single transverse crack and a single longitudinal crack.

MRD Field Characterization

A more detailed evaluation of the attributes of the MRDs was also conducted in the field. Table 3-13 provides the results of this characterization. Figure 3-21 shows some typical distress manifestations. Although a definitive diagnosis should not be drawn from this evaluation, it does provide information that can help diagnose the distress in conjunction with the laboratory results.

Table 3-12. Summary of pavement condition surveys for MN-065-064-002.

Distress Type		Distress Measure	Severity Level			Comments
			Low	Moderate	High	
Cracking	Corner Breaks	number	0	0	0	
	Longitudinal Cracking	linear meters	0.0	2.7	0.0	
	Transverse Cracking	number of cracks	1	0	0	
		linear meters	4.3	0.0	0.0	
		percent of slabs	3			
Transverse Joints	Sealant		fair condition			hot-pour sealant
	Spalling	number	0	6	0	
		linear meters	0.0	3.3	0.0	
	Faulting	millimeters	2.0			measured at 0.30 m
		millimeters	1.7			measured at 0.75 m
	Width	millimeters	15.7			
Long Joints	Sealant		n/a			not sealed
	Spalling	linear meters	0.0	0.0	0.0	
	Shoulder Dropoff	millimeters	0.0			
Surface Conditions	Map Cracking	number of slabs	0			all slabs affected
		square meters	0.0			entire area
	Scaling	number of slabs	0			
		square meters	0.0			
	Polished Aggregate	square meters	0.0			
	Popouts	number/sq. meter	0.0			
Other	Blowups	number	0			
	Flexible Patches	number	0	12	0	
		square meters	0.0	7.0	0.0	
	Rigid Patches	number	0	0	0	
		square meters	0.0	0.0	0.0	
	Pumping/Bleeding	number	0			
		linear meters	0.0			

On both pavement sections, the MRD is confined to the transverse joints; it is not exhibited over the entire slab. The distress is exhibited as hairline cracks that typically run parallel to the transverse joint. The cracking appears to initiate at the transverse joint and progresses outward. As the deterioration progresses, scaling occurs at the surface and exposes the aggregate particles. For the most part, the cracking and deterioration is confined to 150 mm on either side of the joint. The cracks do not have any staining or exudate in or around the cracks.

Interestingly, adjacent to Section 001 was a left-turn lane that was part of the original road constructed in the 1950's. This turn-lane appeared to be in excellent condition and it was decided that the turn-lane should also be sampled, thereby providing an insight into a concrete pavement from the same environment, made from similar materials that performed well.

Table 3-13. Summary of MRD characterization for MN-065-064.

Description		Section 001	Section 002	Comments
Cracking	Location	Joints	Joints	Assumed on spalled joints
	Orientation/shape	Parallel to transverse joints	Parallel to transverse joints	Assumed on spalled joints
	Extent	Within 150 mm of joint	Within 150 mm of joint	
	Crack size	Hairline	Hairline	
Staining	Location	None	None	
	Color	n/a	n/a	
Exudate	Present	None	None	
	Color	n/a	n/a	
	Extent	n/a	n/a	
Scaling	Location	None	None	
	Area of surface	n/a	n/a	
	Depth	n/a	n/a	
Vibrator Trails	Visible	None	None	
	Discolored	n/a	n/a	
	Distressed	n/a	n/a	
	Change in texture	n/a	n/a	

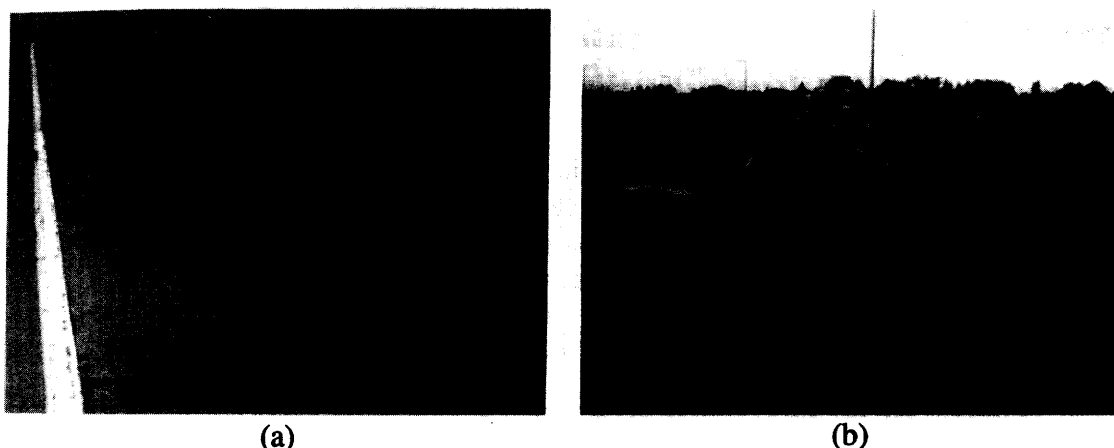


Figure 3-21. Typical distress manifestations observed at MN-065-064.

Laboratory Analysis

Core Selection/Visual Inspection

Based on the field survey and site inspection by researchers, the distress was determined to be concentrated at the transverse joints. In addition, the northbound turning lane was recognized as being in good condition even though it was approximately 40 years older than the badly distressed northbound Section 001. The guidelines for sampling were applied and four cores were retrieved from each section. Also, one mid-panel core (core D in standard pattern) was retrieved from the northbound (Section 001) left-turn lane. The cores selected for laboratory analysis were A from Section 002, cores B and D from Section 001, and core D from the left-turn lane. Pictures of these cores are shown in figure 3-22.

Inspecting the cores visually before and after slicing, mix proportions were only noted. If required to understand the distress, an estimate of the relative phase abundance is obtained simultaneously with determination of the hardened air content. The concrete was well consolidated with no apparent segregation or parallelism of the aggregates. Scaling was present in the deteriorated areas but not on the cores examined. Also, no evidence of sub-parallel cracking was apparent on these cores, no entrapped water voids were seen under aggregates, and no surface cracking was seen in the cores. In the mid-panel core D from Section 001, abundant infilling of the entrained air voids was seen and the paste appeared "soft." The mid-panel core from the left-turn lane also had abundant air void infilling but had a much harder paste. Also, the turn-lane concrete had a coarse aggregate that was not crushed and had a larger (25.4 mm) top size. This is in contrast to the concrete in Section 001, which used a crushed aggregate with a 19-mm top size. The concrete at the joint and in contact with the subbase had a depth of carbonation of 5-10 mm. This indicates some deterioration of the paste at those locations.

Stereo Optical Microscopy/Staining Tests

The rock type for the coarse aggregate was characterized as varying, but was dominantly mafic rock types typical of the Superior Lobe. The fine aggregate was the same, but with more quartz. No unusual alteration of the aggregate was observed. For this study, the most useful role for the stereo microscope was for observing stained specimens and determination of the hardened air content. The barium chloride/potassium permanganate stain described in Guideline II colors sulfate minerals a brilliant pink to purple hue as shown in figure 3-23.

Hardened Air-Void Analysis According to ASTM C 457

The hardened air-void content was determined in accordance with ASTM C 457. For the work performed in this study, the modified point count method was used for analysis and the required software was written in house using the free image analysis program from NIST Image 1.62. The results of the analysis are presented in table 3-14.

Table 3-14. Results of ASTM C 457 on concrete from MN-065-064-001.

Core	Original		Existing		Volume Percent		
	Air Content (vol. %)	Spacing Factor (mm)	Air Content (vol. %)	Spacing Factor (mm)	Paste (vol. %)	Coarse Aggregate (vol. %)	Fine Aggregate (vol. %)
Site 1 Core C	5.9	0.227	5.9	.270	26.4	39.2	28.5
Site 1 Core B	3.6	.271	3.5	.302	32.4	36.4	27.5
Site 1 Core D	6.3	.302	6.2	.303	30.3	42.8	20.6
Left Turn Ln.	4.5	.191	4.4	.220	21.9	53.9	19.7

As can be seen, the original air-void system and the existing air-void system (after infilling) are both inadequate in terms of the Power's spacing factor for each. This indicates a cement paste that is not adequately protected from the cyclic stresses of freezing and thawing. This usually results in cracking of the paste that is then susceptible to ingress of water and deicers.

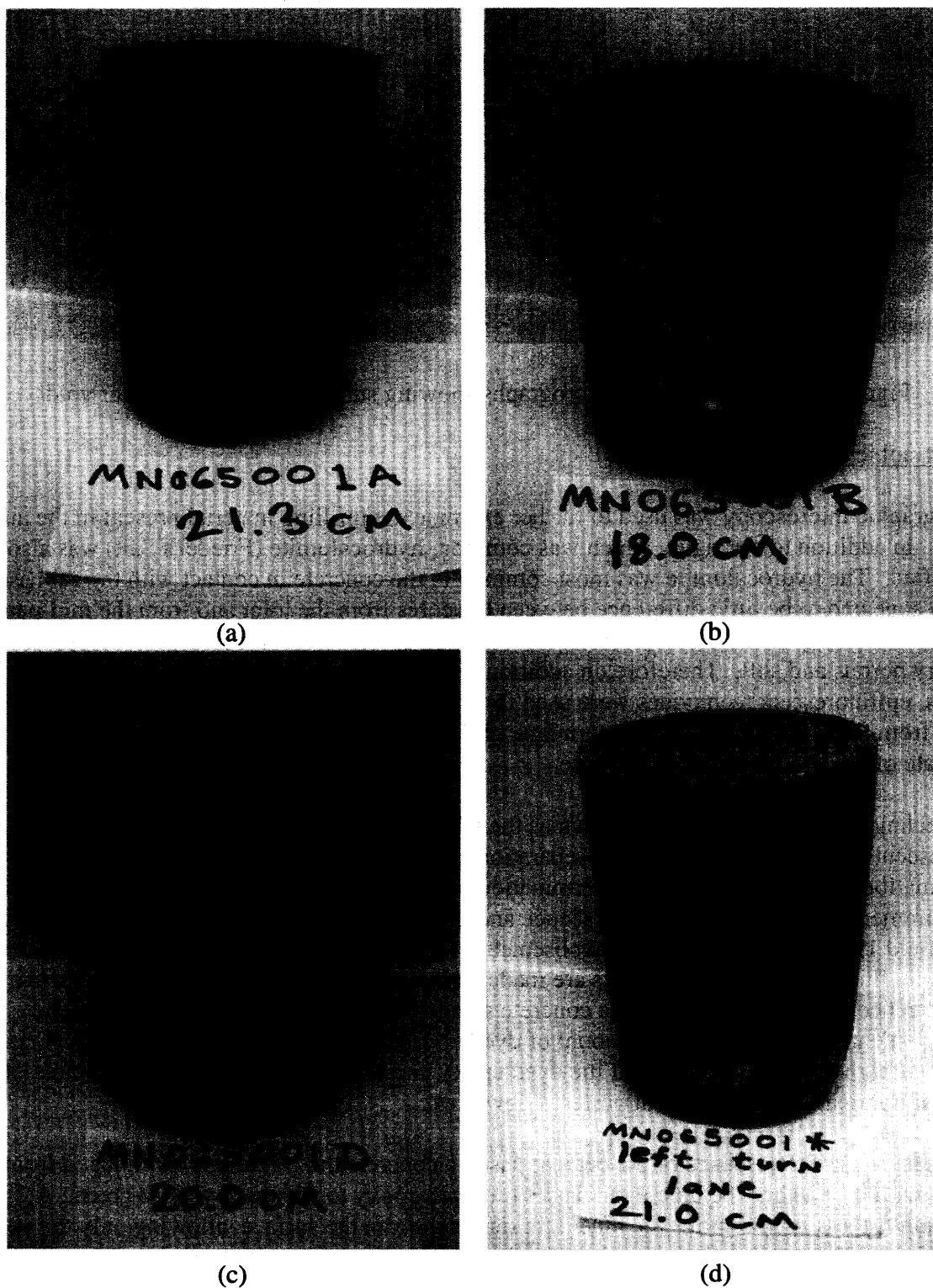


Figure 3-22. Cores evaluated for MN-065-064.

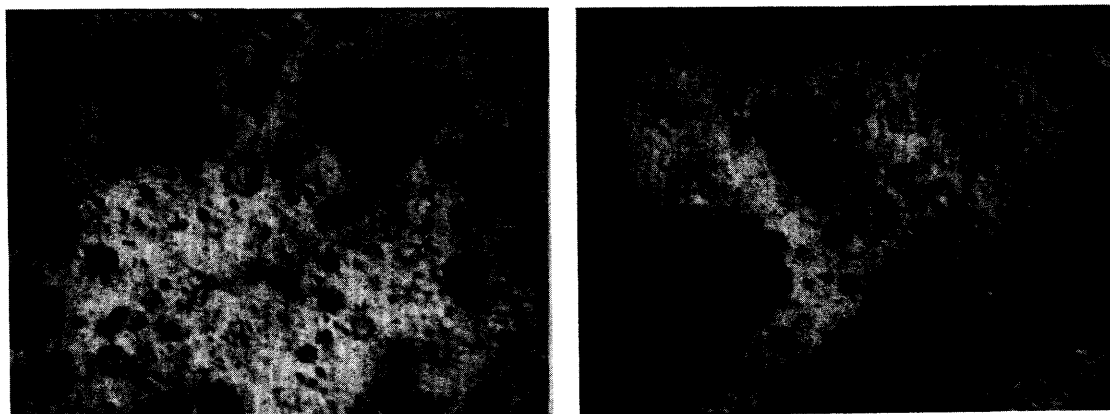


Figure 3-23. Stereo optical micrographs showing sulfate minerals filling air voids.

Petrographic Optical Microscopy

Petrographic microscopy was used to further examine the infilling material present in the air voids. In addition to ettringite, which was common, hydrocalumite (Friedel's Salt) was also identified. The hydrocalumite was most common in the concrete in contact with the subbase. There appeared to be little difference between the cores from the joint and from the mid-panel of Section 001. In general, there was extensive infilling of voids and the cement paste appeared to be very porous and soft. Therefore, in addition to identifying infilling material within voids and cracks, epifluorescent techniques were used for examining the cement paste in the mid-panel cores from Section 001 and the left-turn lane of the northbound section. This analysis leads to an estimate of the w/c ratio for the concrete.

The technique used is commonly known as the UV dye method for determining w/c and uses a fluorescent dye epoxy impregnation preparation and microscopic observation using UV illumination. This method of w/c determination relies upon the relationship between measurements of cement paste fluorescence and the w/c values of known concrete standards (Mayfield 1990; Elsen et al. 1995; Jakobsen et al. 1997). To determine the w/c of a sample of concrete, fluorescence measurements are made from the cement paste, and related back to fluorescence measurements from the concrete standards. The intensity of the fluorescence measurements depends upon the amount of dyed epoxy absorbed by the cement paste. Cement pastes of higher w/c absorb more of the dyed epoxy because they possess a larger volume of capillary porosity than do cement pastes of lower w/c .

To measure the fluorescence of the cement paste, a concrete thin section is illuminated from above with blue light. The blue light causes the dyed epoxy to fluoresce yellow-green. A blocking filter is used to remove the blue light reflected from the surface, allowing only the yellow-green fluorescence to reach the camera (Walker 1992). The camera generates a video signal, which is converted to an RGB digital image on a computer monitor. In the image, each pixel is assigned a 0-255 intensity, where 0 represents pure white (high intensity) and 255 represents pure black (low intensity). The G band of the image contains the most information about the fluorescence, and is used to make the cement paste fluorescence measurement.

To ensure that the illumination of the blue light and the performance of the camera are constant, a method of calibration is needed. Prior to collecting any measurements, a thin section composed of quartz sand in a matrix of dyed epoxy is used to calibrate the system. A digital image of the calibration slide is collected. In the image, the quartz sand appears dark, and the dyed epoxy matrix appears bright. If a histogram is plotted of the image, two distinct peaks are present, one for the quartz sand, and the other for the dyed epoxy matrix. It is important that the positions of the peaks on the x-axis do not shift in order to ensure consistent measurements. Figure 3-24 shows a summary of histograms collected from our calibration thin section. If the peak positions are out of alignment, then adjustments need to be made, either in the illumination, shutter speed of the camera, or gain and offset of the digital capture card. It has been reported that the fluorescence of the dyed epoxy decreases under constant illumination, but recovers to its initial fluorescence if allowed to sit in darkness for a period of 2 hours (Jakobsen et al. 1995). Furthermore, the drop-off in fluorescence is most dramatic within the first 2 minutes, so it is important not to pause too long over any given area before collecting a fluorescence measurement.

Another set of parameters that can affect the fluorescence measurements is consistency in thickness of the thin sections, uniformity of impregnation by the dyed epoxy, and the consistency in dosage of dye. It is imperative that the thin sections used are of high quality (Elsen et al. 1995; Jakobsen et al. 1997).

Since concrete is a combination of cement paste, aggregate, and air bubbles, it is necessary to distinguish between the cement paste fluorescence and the fluorescence from aggregates and air bubbles. Generally, the aggregates are less porous than the cement paste, and therefore fluoresce at lower intensity levels, although this may not always be the case, especially when porous aggregates are used. At the other extreme, total porosity, the air bubbles fluoresce at a higher intensity level than the cement paste. At intermediate intensity values, most of the fluorescence can be attributed to the cement paste. Although this is a good approximation, intensity level alone is not enough to determine whether any given pixel represents cement paste, aggregate, or air bubble. Rigorous schemes have been proposed to ensure that the pixels used to make the cement paste fluorescence measurements do not include air bubbles or aggregate, but they were not employed here (Elsen et al. 1995; Gerold 2000). Instead, the distinction between cement paste, aggregate, or air bubble was based solely on fluorescence intensity.

Figures 3-25 through 3-31 summarize the fluorescence measurements from the different standards. Three thin sections were prepared from each w/c standard, and 10 fluorescence measurements were made from different locations on each thin section for a total of 30 measurements per w/c standard. Each fluorescence measurement represents a 2.493-mm x 1.870-mm region on the thin section; therefore, a total area of about 140 mm² was measured per w/c standard. Each measurement consists of a 640 x 480 pixel image, so a total of 9.216 million pixels were collected per w/c standard. Regions containing coarse aggregates were avoided during the sampling. The regions sampled were chosen by the operator, which may introduce bias.

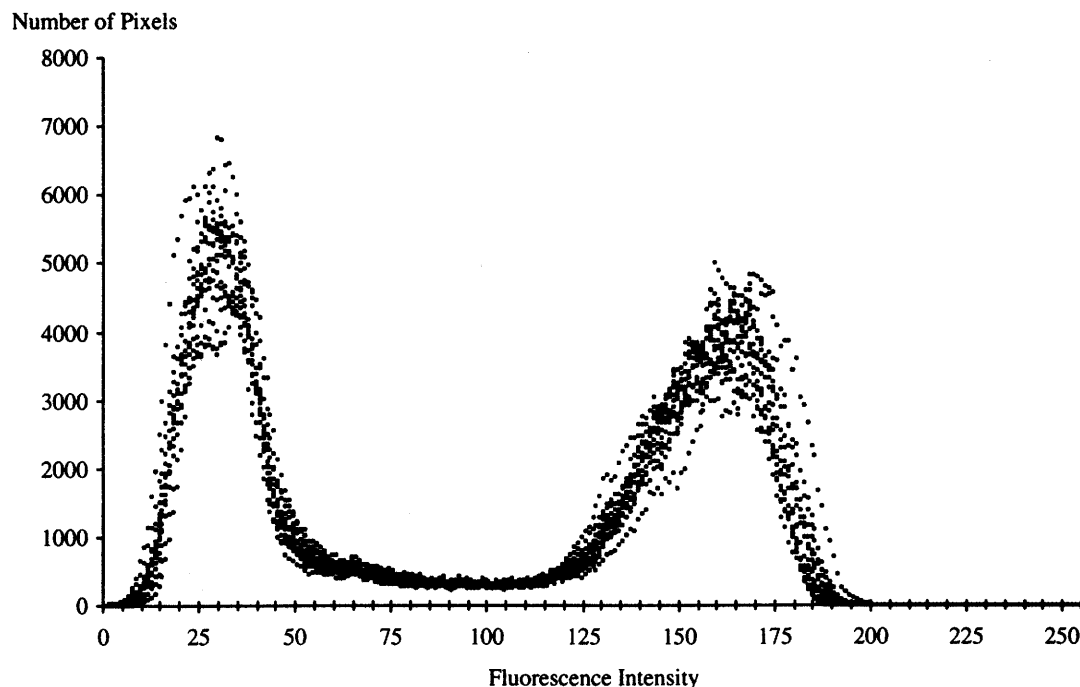


Figure 3-24. Histogram of 16 fluorescence measurements from calibration thin section composed of quartz sand in a dyed epoxy matrix. The peak on the left represents the dyed epoxy matrix, and the peak on the right represents the quartz sand.

It is clear from figures 3-25 through 3-31 that there is considerable variability within the individual standards, although the three distinct fluorescence levels attributed to air bubbles, cement paste, and aggregate can be distinguished in each of the standards. Assuming that the intermediate intensity levels represent the cement paste, channels 75 through 175 were used to quantify the cement paste fluorescence of the standards. The choice of channels 75 through 175, however, does not ensure that the pixels included in the measurement exclusively represent cement paste, nor does it ensure that some pixels that represent cement paste are not omitted. One concern is that the choice of channels 75 to 175 may exclude unhydrated cement grains, which appear as dark specks against the background of cement hydration products and capillary porosity. The overall fluorescence of the cement paste is related to both the capillary porosity as well as the quantity of unhydrated cement grains. In these measurements, variations in capillary porosity alone seem sufficient to distinguish variations in w/c (see figure 3-32). However, with the inclusion of unhydrated cement grains, the variation in intensity versus w/c would perhaps be more pronounced.

There is no doubt that it would be advantageous to employ a more rigorous method to ensure that only those pixels that represent cement paste are used in the measurements, but the simple method employed here performed adequately. The major weakness in the strict use of channels 75 to 175 is that the fluorescence of the cement paste and aggregates are both influenced to some degree by the fluorescence of the surrounding phases. For instance, the cement paste surrounding air bubbles often appears brighter than the rest of the cement paste due to the

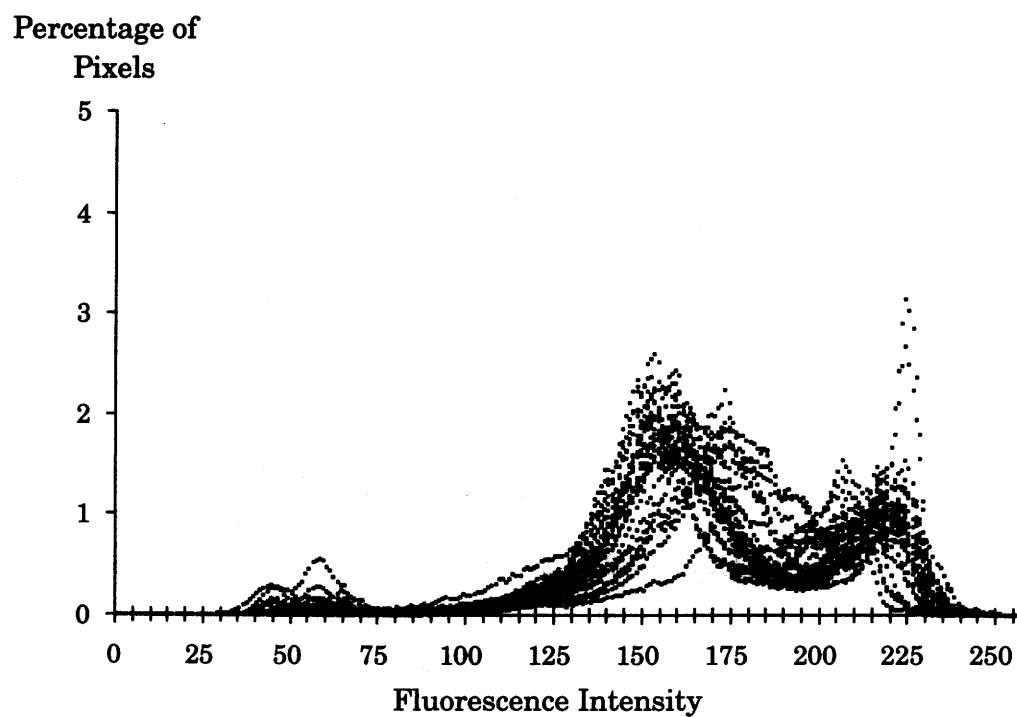


Figure 3-25. Histogram of 30 fluorescence measurements from 0.38 w/c standard.

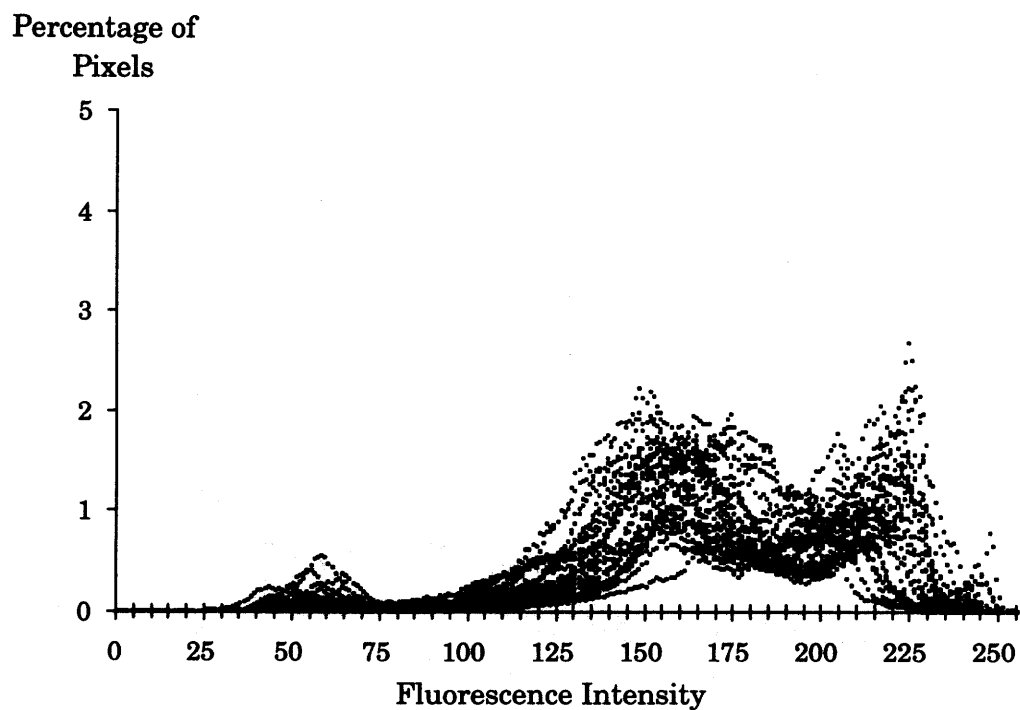


Figure 3-26. Histogram of 30 fluorescence measurements from 0.41 w/c standard.

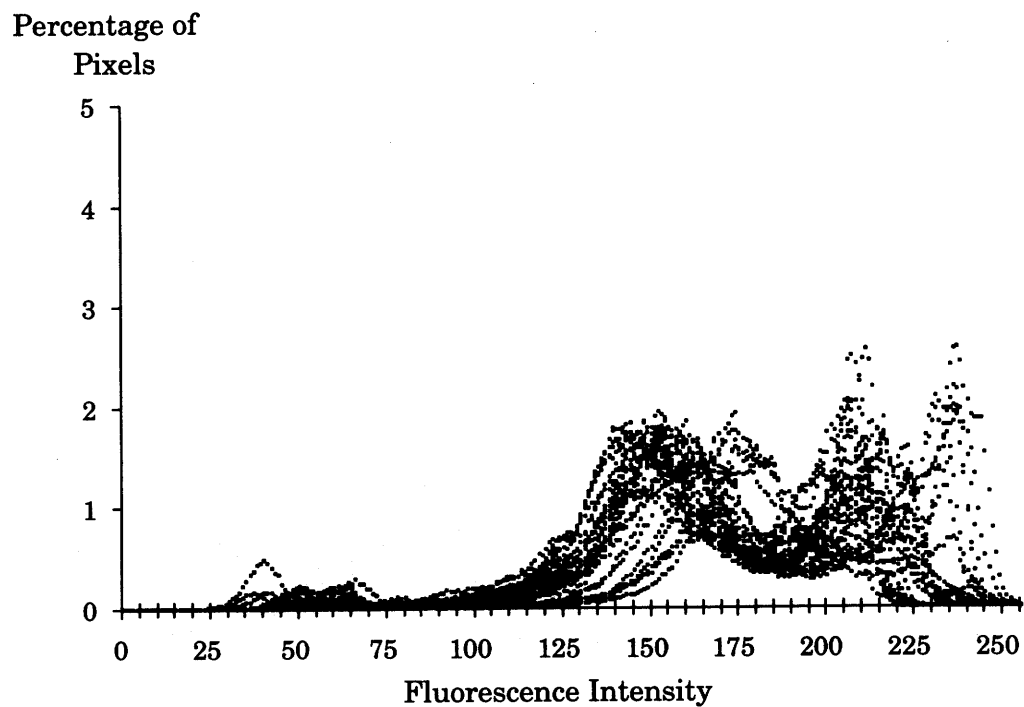


Figure 3-27. Histogram of 30 fluorescence measurements from 0.42 w/c standard.

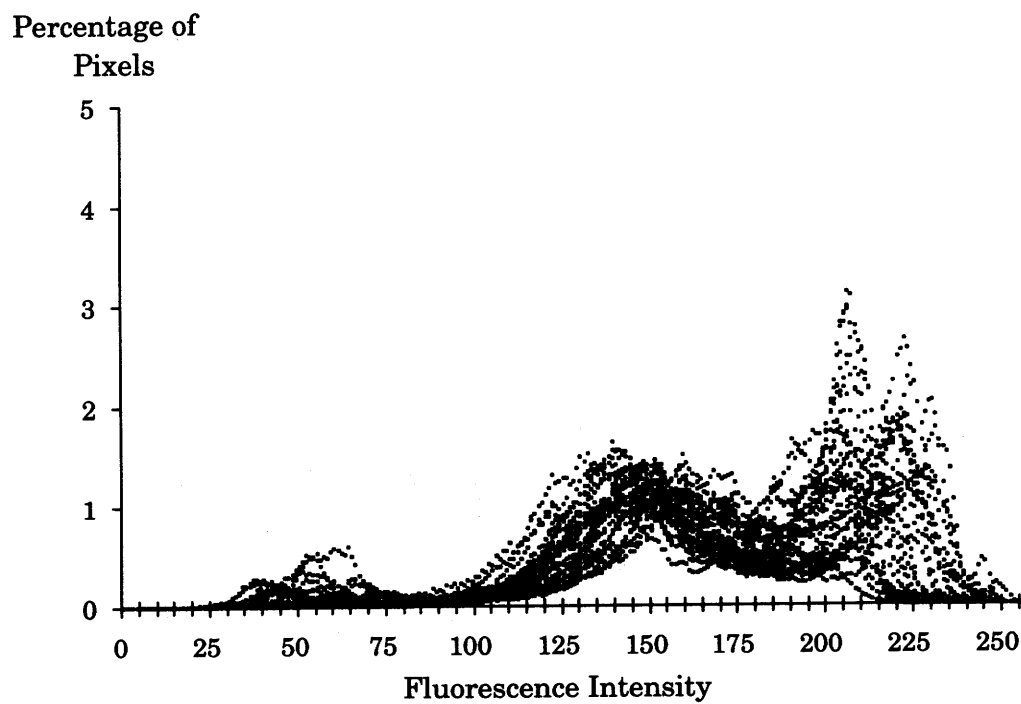


Figure 3-28. Histogram of 30 fluorescence measurements from 0.52 w/c standard.

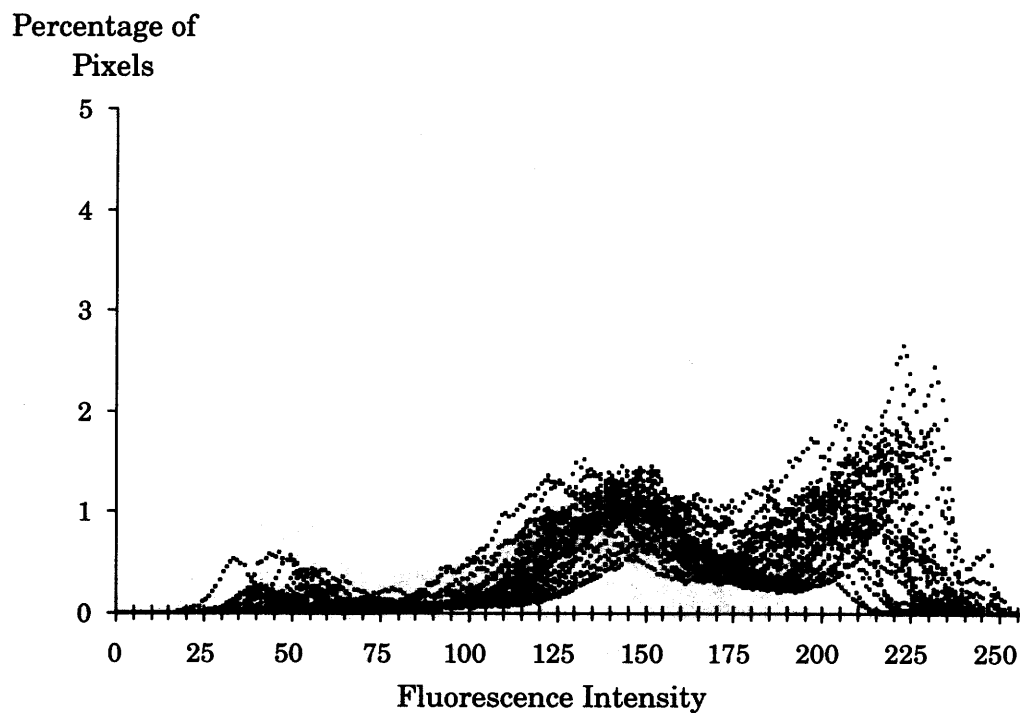


Figure 3-29. Histogram of 30 fluorescence measurements from 0.56 w/c standard.

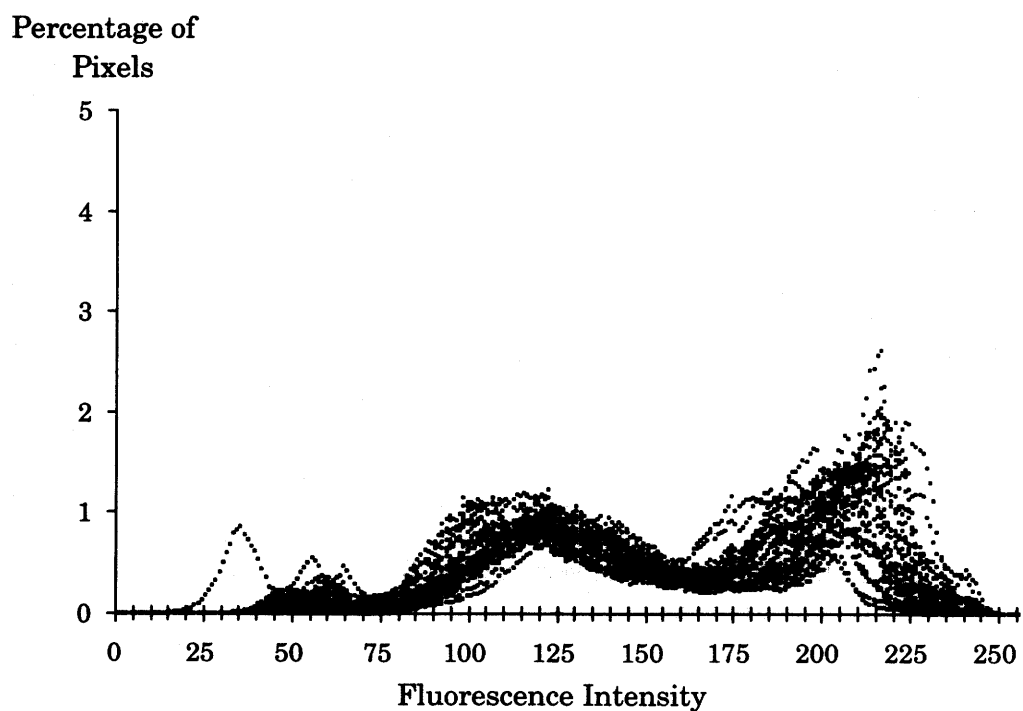


Figure 3-30. Histogram of 30 fluorescence measurements from 0.74 w/c standard.

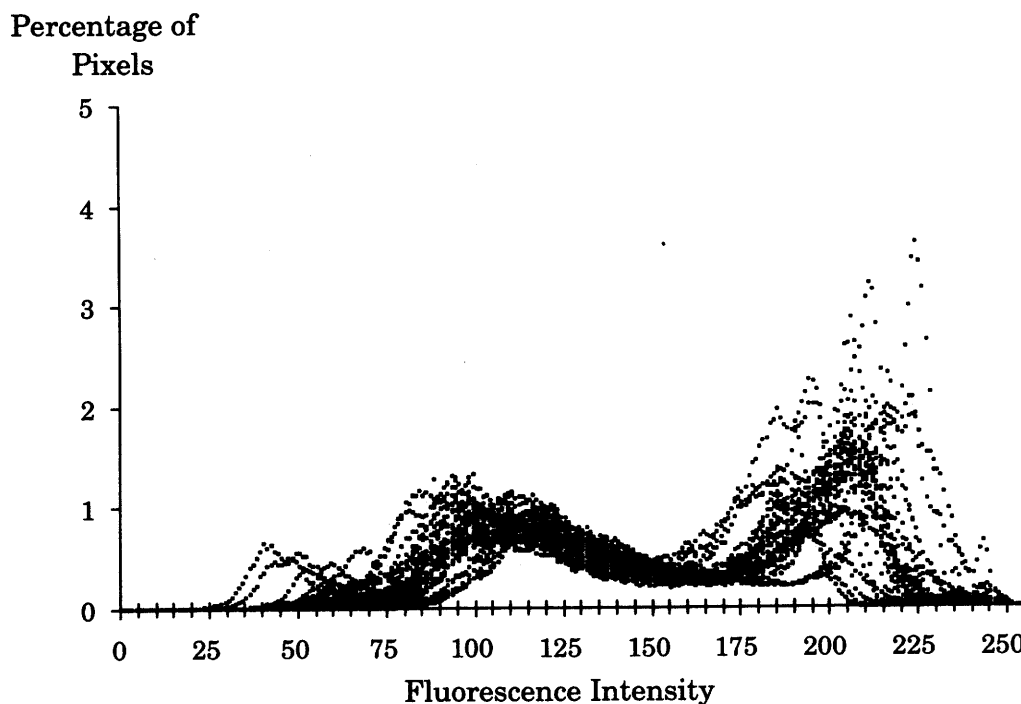


Figure 3-31. Histogram of 30 fluorescence measurements from 0.80 w/c standard.

proximity to the air bubbles. For this reason, some researchers exclude cement paste that neighbors air bubbles from recorded fluorescence measurements (Elsen et al. 1995). Similarly, translucent aggregates, such as quartz, may appear brighter if surrounded by brightly fluorescing cement paste. Depending on the appearance of a series of images, it may be necessary to interactively change the interval of channels that is used to represent the fluorescence of the cement paste. However, this would require the operator to repeatedly make decisions that could introduce bias to the measurements, hence the rigid choice of channels 75 to 175 used here.

The first step in quantifying the fluorescence for each individual measurement was to normalize the number of pixels contained in channels 75 through 175 to 100. This step is necessary to account for differences in the volumes of cement paste between standards. For instance, the low w/c standards contained a higher volume of cement paste in order to maintain the workability of the plastic concrete. Next, an average intensity value was determined from the normalized number of pixels in channels 75 through 175. The average intensity value was used as a measurement of cement paste fluorescence. Figure 3-32 plots the average fluorescence intensity values versus the w/c of the standards, along with a best-fit line. The equation for the best-fit line from figure 3-32 can then be used to convert average fluorescence intensity measurements from unknown concrete samples to values for w/c.

The concrete samples analyzed here are from mid-panel of the traffic lane and from mid-panel of a left-turn lane. Thin sections were prepared from the cores at different depths to make cement paste fluorescence measurements. Figures 3-33 through 3-38 summarize the measurements from the old concrete and the new concrete.

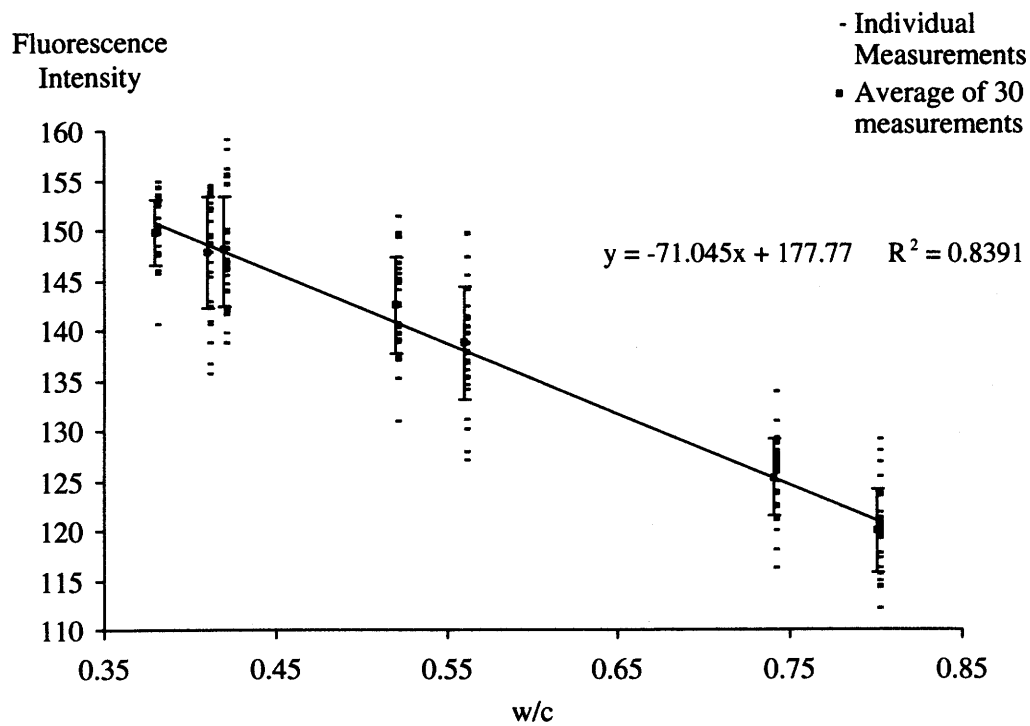


Figure 3-32. Average cement paste fluorescence measurements versus w/c. Error bars represent one standard deviation.

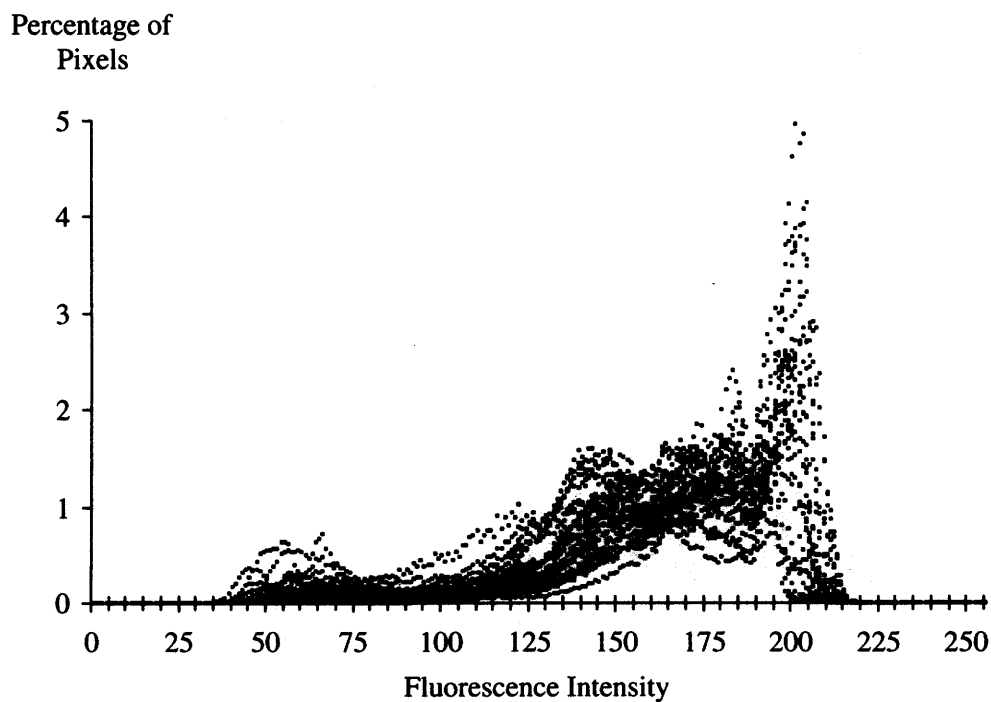


Figure 3-33. Histogram of fluorescence measurements from 1950 concrete from mid-panel of the left-turn lane of site MN-065-064-001.

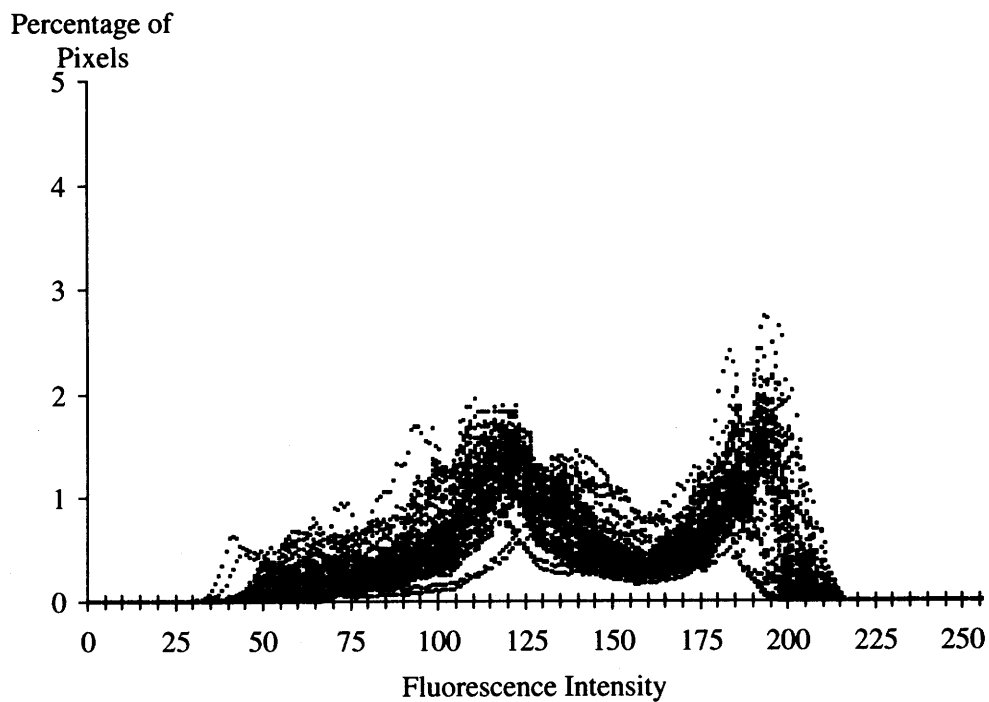


Figure 3-34. Histogram of fluorescence measurements from 1990 concrete from mid-panel of the traffic lane of site MN-065-064-001.

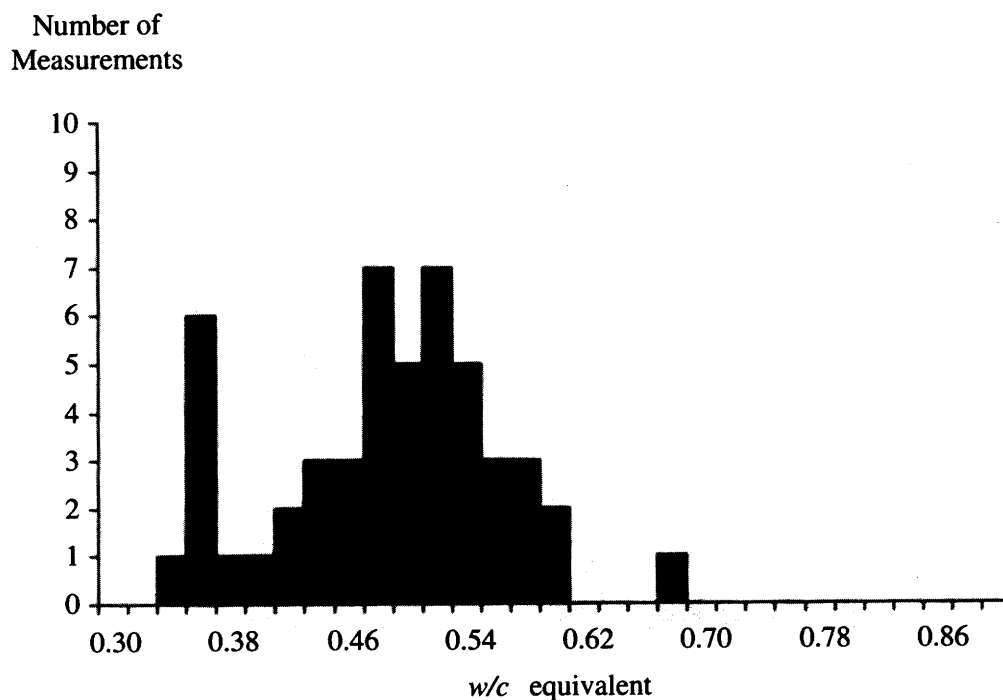


Figure 3-35. Distribution of the w/c values from the 1950 concrete from mid-panel of the left-turn lane of site MN-065-064-001.

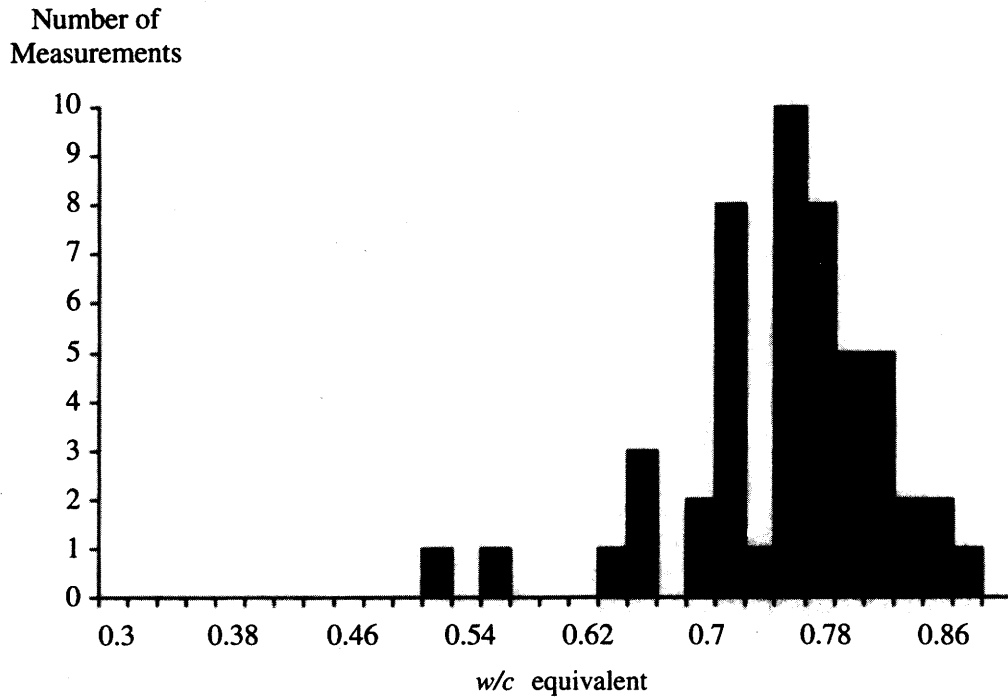


Figure 3-36. Distribution of the w/c values from the 1990 concrete from mid-panel of the traffic lane of site MN-065-064-001.

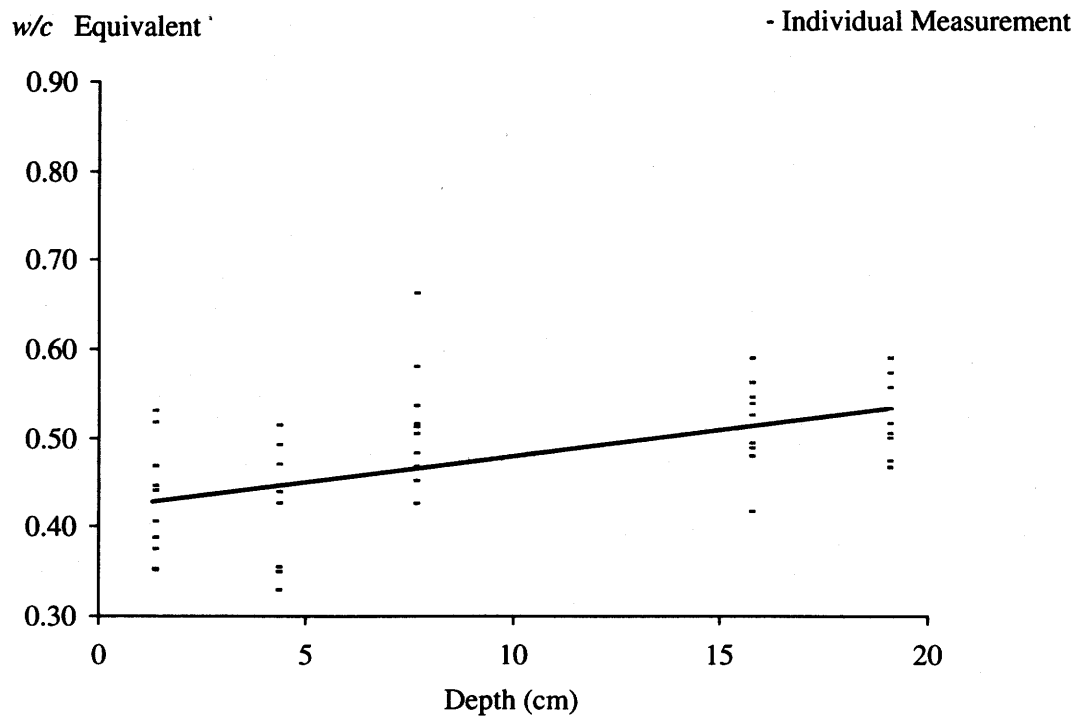


Figure 3-37. The w/c values versus depth from the 1950 concrete from mid-panel of the left-turn lane of site MN-065-064-001.

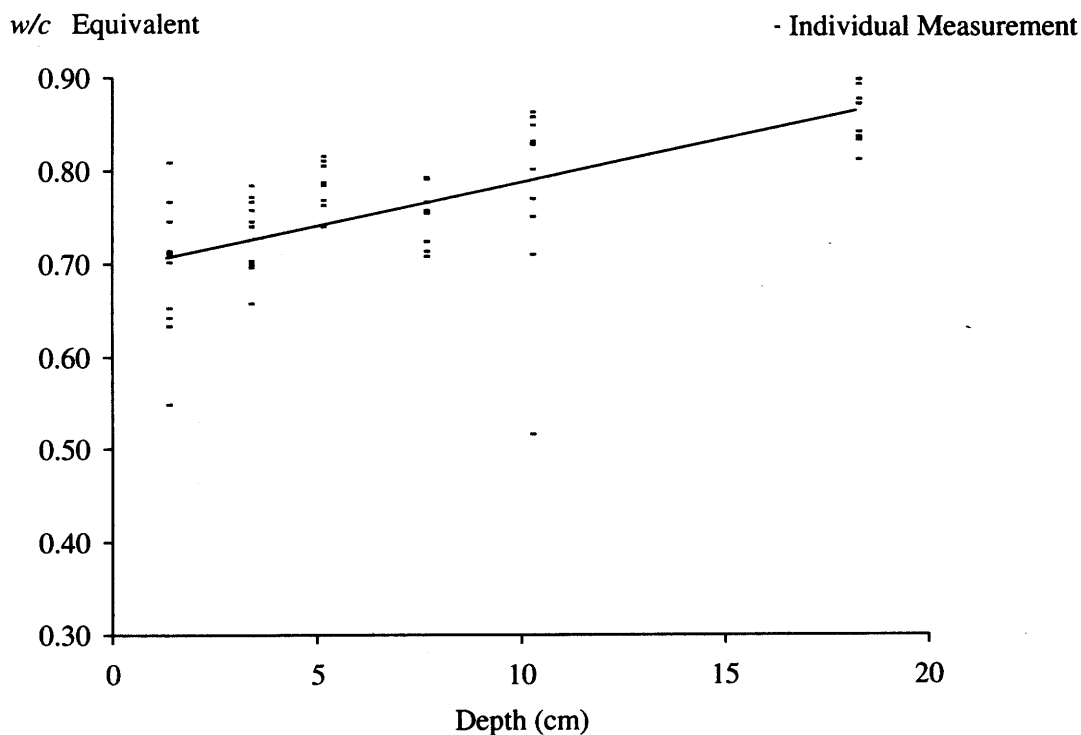


Figure 3-38. The w/c values versus depth from the 1990 concrete from mid-panel of the traffic lane of site MN-065-064-001.

When using the fluorescent method of w/c determination, it is important to realize that the capillary porosity is not solely a function of the w/c . As both proponents and critics of the technique are quick to point out, the capillary porosity is influenced by a number of different parameters. For example, the degree of hydration, the use of cementitious additives such as fly ash, and the amount of weathering or leaching of the cement paste all influence the capillary porosity, just to name a few (Jakobsen et al. 1997; Neville 1999). Certainly, to make an accurate estimation of w/c , appropriate standards of similar hydration and composition should be used. Since it would be difficult to produce suitable standards for every situation, another approach would be to refer to the fluorescence measurement of w/c as an "equivalent w/c ". This makes it clear that the w/c value determined for a sample of concrete is expressed in terms of an *equivalent w/c* as compared to the standards. In the case of site MN-065-064-001, the w/c standards came from concrete that had cured for 65 days. The concrete from the 1950's has had a long time to hydrate, and it might not be appropriate to directly compare it to the 65-day cure standards. The concrete from 1990 may have undergone some leaching and weathering, so again, it might not be appropriate to directly compare it to the standards as a measure of constructed w/c . However, if it is understood that the w/c measurement is an equivalent to the 65-day cured laboratory standards, then the results are not as misleading.

Scanning Electron Microscopy (SEM)

SEM was used to identify infilling material in voids and cracks. As indicated earlier, the principal materials identified were ettringite and hydrocalumite as shown in the typical SEM micrographs and x-ray analyses presented in figures 3-39 and 3-40.

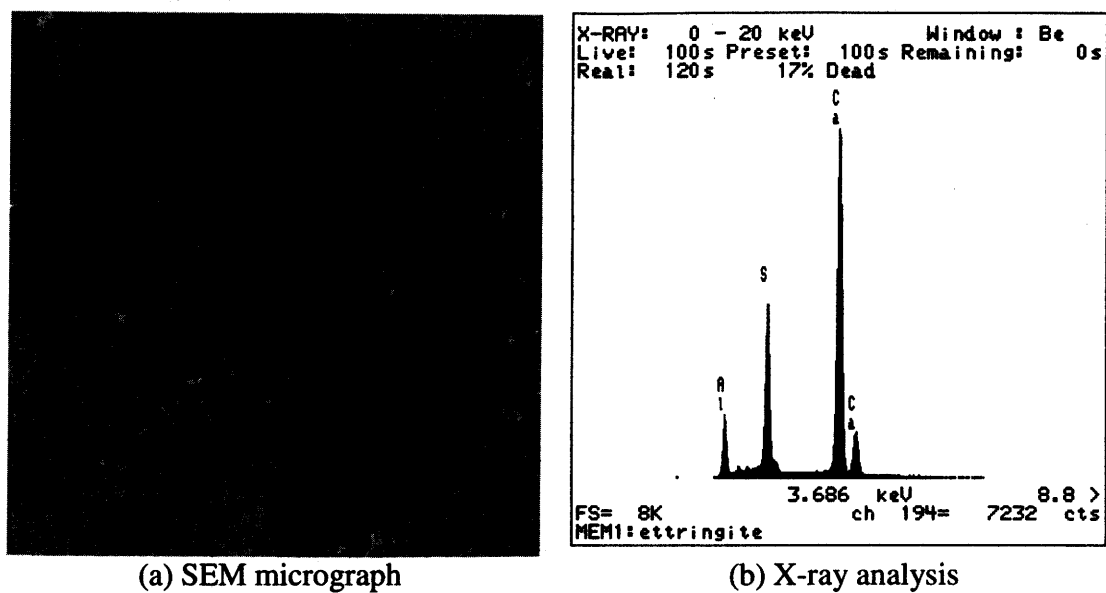


Figure 3-39. Typical SEM micrograph and x-ray analysis for ettringite infilling air void.

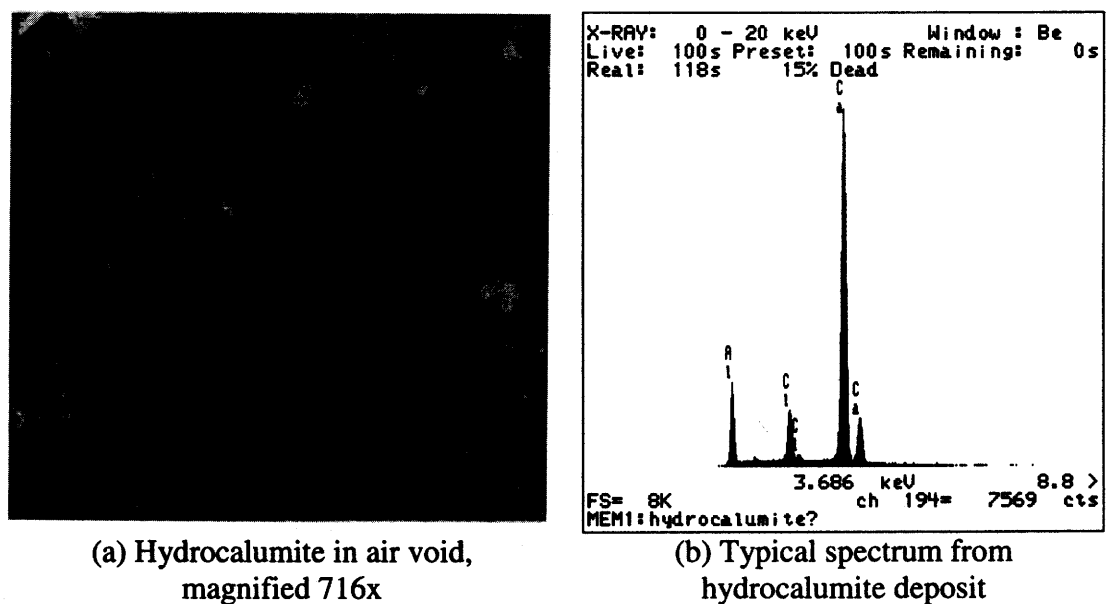


Figure 3-40. Typical SEM micrograph and x-ray analysis for hydrocalumite infilling air void.

Table 3-15 presents the quantitative results from a single spectrum collected from an ettringite deposit, compared to a calculated composition for dehydrated ettringite. Table 3-16 is a summary of 10 analyses of hydrocalumite deposits, compared to calculated compositions for the 3 dehydrated end members of the hydrocalumite solid solution series. The ternary diagram presented previously in figure 3-15 shows the probable range of composition for the hydrocalumite deposits analyzed from the pavement. Hydrocalumite describes a solid solution series with 3 end-member compositions and a range in substitutions between Cl^- , OH^- , and CO_3^{2-} . The hydrocalumite analyses were low in chlorine as compared to the pure Cl^- hydrocalumite end member shown above. Oxygen and carbon were not analyzed so the true composition of the hydrocalumite cannot be determined.

Table 3-15. Quantitative results from single spectrum collected from ettringite deposit, compared to a calculated composition for dehydrated ettringite.

Element	Analysis Results (wt%)	Dehydrated Ettringite (theoretical)
Na	0.0	0.0
Mg	0.0	0.0
Al	7.5	6.9
Si	0.2	0.0
S	13.0	12.2
Cl	0.0	0.0
K	0.0	0.0
Ca	31.9	30.6
Ti	0.0	0.0
Mn	0.0	0.0
Fe	0.0	0.0
O	Not Measured	48.8
H	Not Measured	1.5
sum	52.8	100.0

Interpretation and Diagnosis

This test site illustrates a key point with the laboratory analysis of MRD. Namely, standard procedures will provide adequate data for diagnosing the majority of MRD cases. But in some cases, a more in-depth or “unique” analysis must be conducted to fully understand the MRD mechanisms identified. In this case, a more in-depth investigation of the effective w/c led to a better insight into why the distresses observed were occurring.

In the context of a guideline, it is impossible to design an analytical approach that will identify all possible types of MRD in every situation. For more difficult or complex cases of MRD, a State highway agency (SHA) may have to contract with outside labs for petrographic services if such services are not available within the organization. Even if an outside contract is required, the guidelines still assist the analyst or engineer in refining the questions that you want the external petrographer to answer.

Table 3-16. Summary of 10 analyses and theoretical composition of hydrocalumite deposits.

Element	Measured		Theoretical		
	Average Wt%	Standard Deviation	Dehydrated Cl ⁻ hydrocalumite	Dehydrated OH ⁻ hydrocalumite	Dehydrated CO ₃ ⁻² hydrocalumite
Na	0.0	0.0	0.0	0.0	0.0
Mg	0.0	0.0	0.0	0.0	0.0
Al	13.2	0.3	11.0	12.9	12.5
Si	0.0	0.0	0.0	0.0	0.0
S	0.0	0.0	0.0	0.0	0.0
Cl	6.6	0.4	14.5	0.0	0.0
K	0.0	0.0	0.0	0.0	0.0
Ca	37.2	0.5	32.8	38.3	37.3
Ti	0.0	0.0	0.0	0.0	0.0
Mn	0.0	0.0	0.0	0.0	0.0
Fe	0.5	0.1	0.0	0.0	0.0
C	Not Measured		0.0	0.0	2.8
O	Not Measured		39.2	45.9	44.6
H	Not Measured		2.5	2.9	2.8
sum	57.4		100.0	100.0	100.0

Having performed the described laboratory analyses and applied the diagnostic flowcharts reproduced in figures 3-41 to 3-45, two possible MRDs were identified in MN-065-064-001, including paste freeze-thaw and deicer attack. To finalize the diagnosis, the diagnostic tables were consulted. The diagnostic features identified in the analysis processes are listed below in table 3-17 along with their associated MRD type and significance as related to this pavement. A brief discussion follows of each possible MRD identified in the laboratory analysis:

Paste Freeze-Thaw – Clearly, there were two distinguishing features of this distressed concrete. The first was the softness and high effective *w/c* for this concrete. The porous paste was evident even in the mid panel when compared to the passing lane constructed with similar aggregates but approximately 40 years before the failed concrete. Of course, changes in cement characteristics and other factors may be contributors to the observed paste characteristics. However, it is unlikely that these factors would result in a difference of the magnitude seen in these pavement sections. It is most probable that a high *w/c* contributed to the observed distress. In addition, the original air system was marginal and once infilling occurred; the hardened air system became inadequate to protect the weakened paste.

Deicer Attack – This MRD may be opportunistic or it may be a contributor. Given the degree of distress seen near the joint, it is reasonable to infer that deicer attack was a factor. Also, the presence of hydrocalumite is an indicator that this concrete was exposed to a high chloride environment, given the necessary high chloride concentration required for this phase to precipitate.

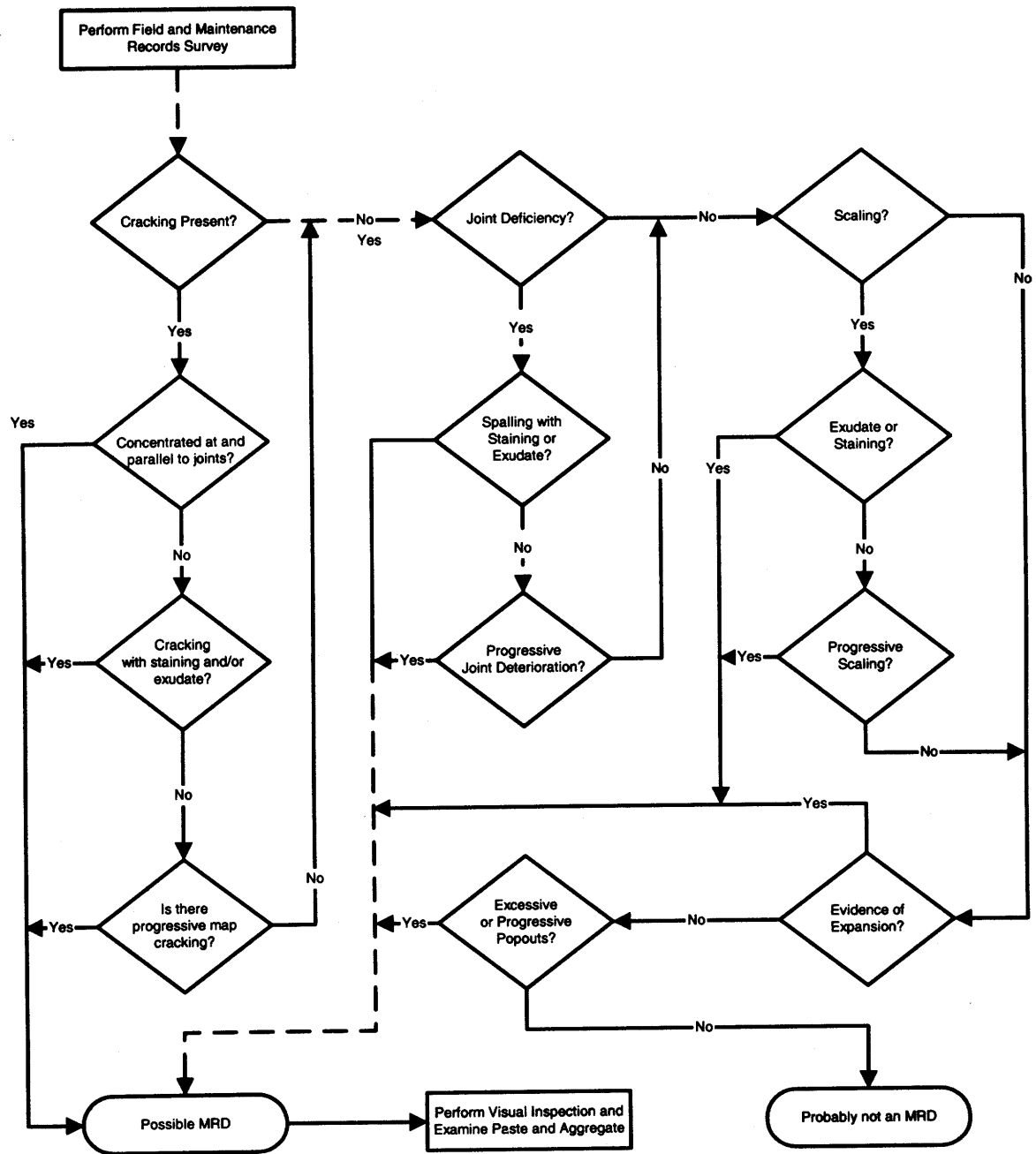


Figure 3-41. Flowchart for assessing the likelihood of MRD causing the observed distress in the pavement as applied to MN-065-064.

Possible Distress	Present		Additional Information
Error in Mix Proportioning	Yes	No	See Recommended Literature
Poor Placement	Yes	No	See Recommended Literature
Poor Finishing/Curing	Yes	No	See Recommended Literature
Poor Steel Placement	Yes	No	See Recommended Literature
Carbonation at Depths > 5-10 mm	Yes	No	See Recommended Literature

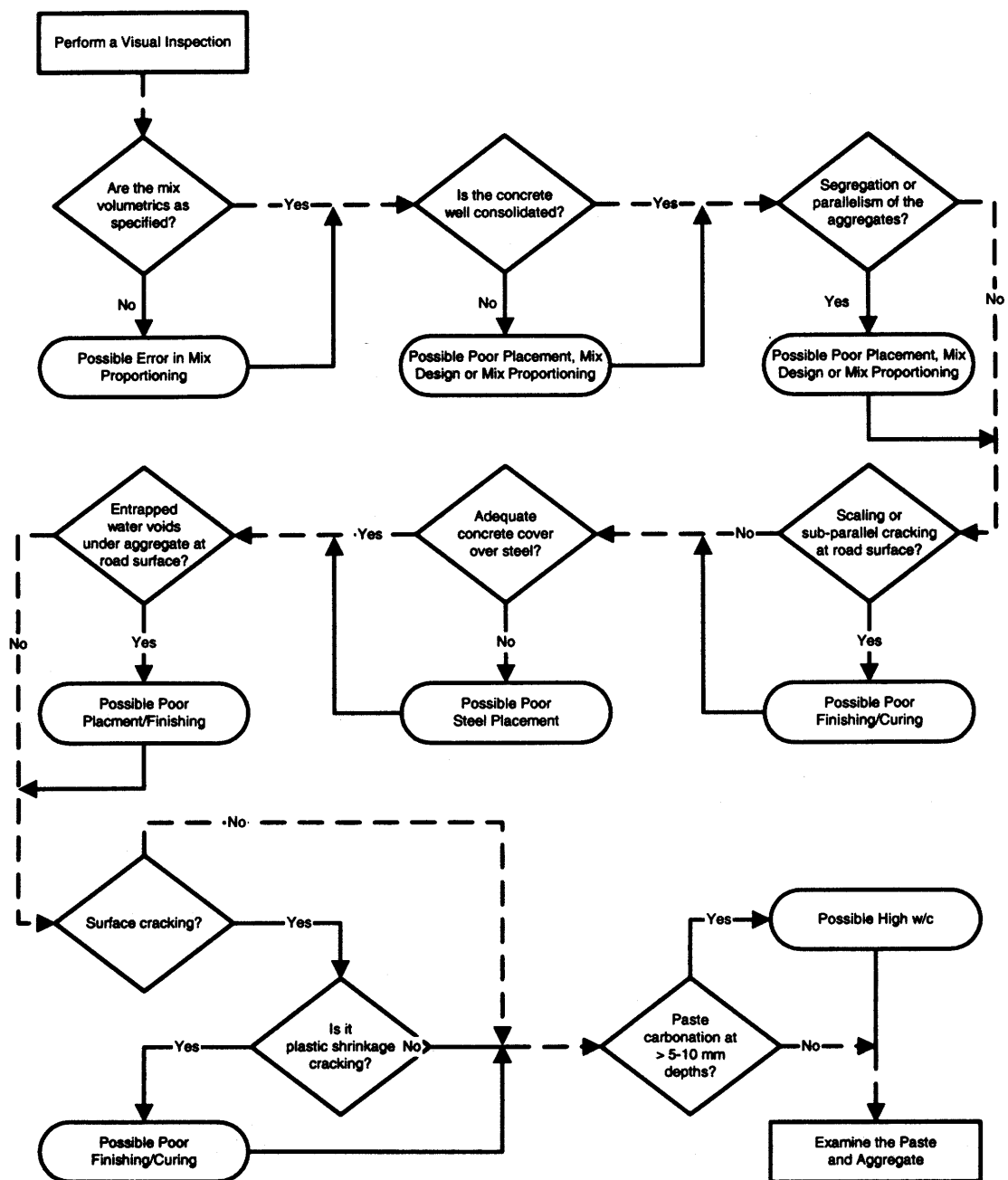
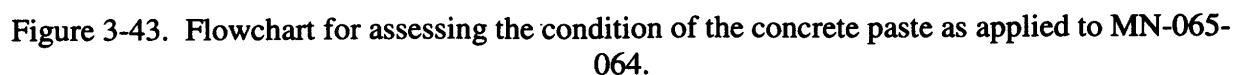


Figure 3-42. Flowchart for assessing general concrete properties based on visual examination as applied to MN-065-064.

52

Possible Distress	Present	Additional Information
Natural Cracking of Aggregate	Yes	See Recommended Literature
Sample Preparation Cracks	Yes	See Recommended Literature
Aggregate Freeze-Thaw	Yes	Table II-3
Natural Weathering of Aggregates	Yes	See Recommended Literature
Alkali Silica Reaction	Yes	Table II-6
Alkali Carbonate Reaction	Yes	Table II-7
Secondary Deposits	Yes	Figure 3-45

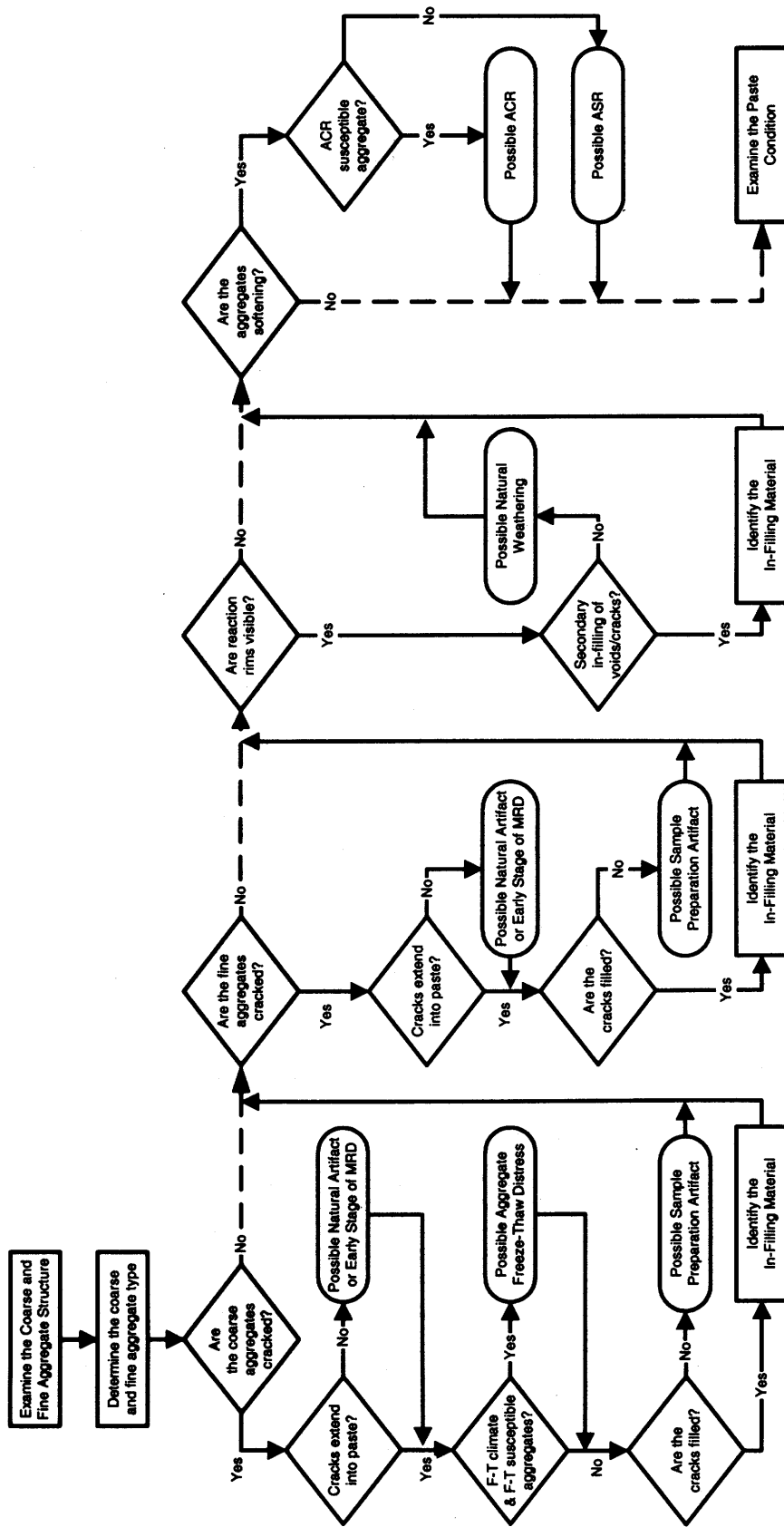


Figure 3-44. Flowchart for assessing the condition of the concrete aggregates as applied to MN-065-064.

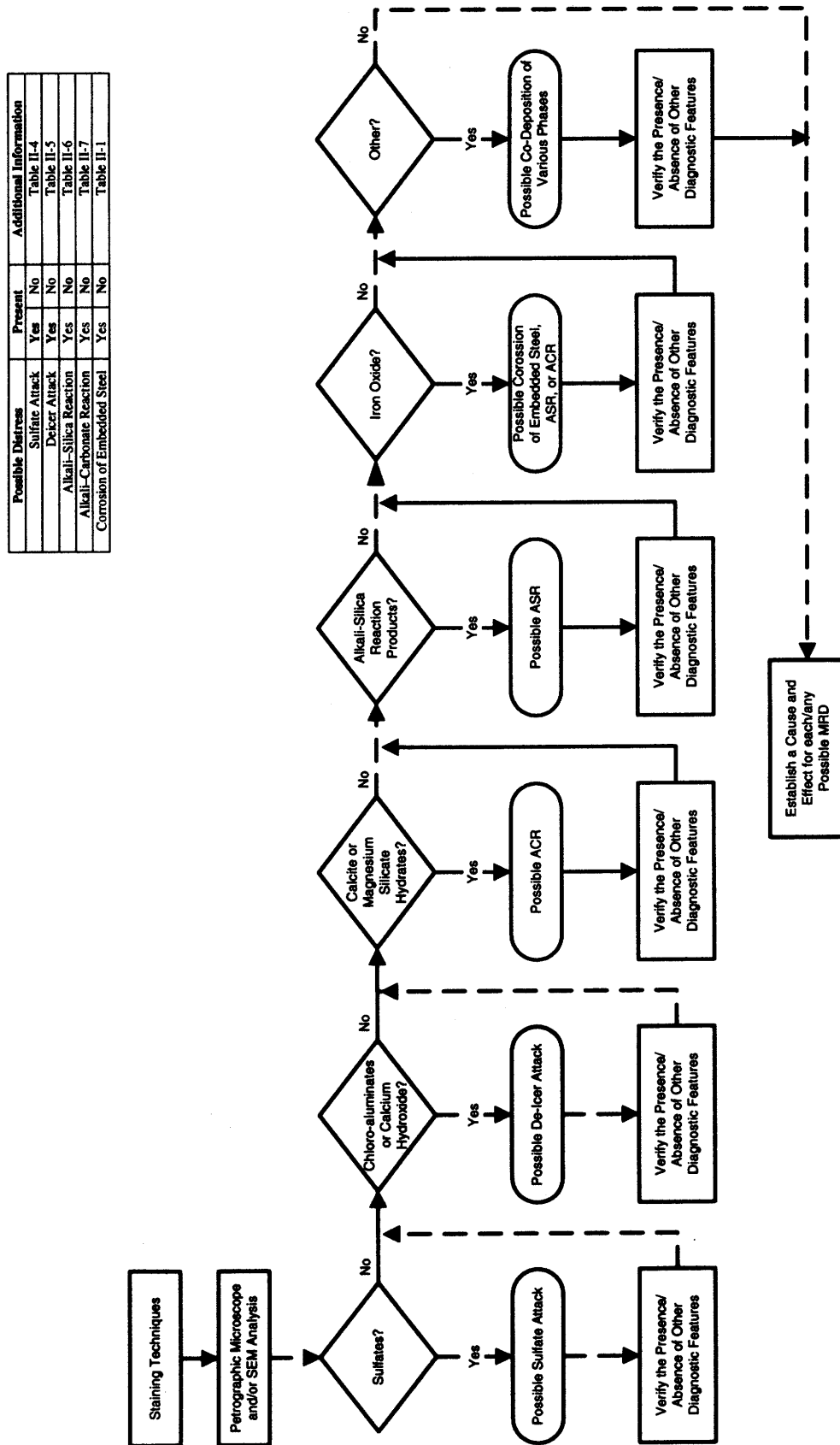


Figure 3-45. Flowchart for identifying infilling materials in cracks and voids as applied to MN-065-064.

Table 3-17. Diagnostic features identified along with their associated MRD type and significance as related to MN-065-064.

Diagnostic Feature	Method of Characterization	Associated with MRD Type	Significance
Secondary deposits filling air voids and cracks	Visual Stereo OM Petrographic OM SEM	Paste freeze-thaw, deicer attack, sulfate attack (both internal and external)	Low
Surface scaling or Sub-parallel cracking	Field evaluation Visual	Paste freeze-thaw	Medium-Low
Inadequate air-void system	Visual Stereo OM		High
Scaling of slab surface	Field evaluation Visual Stereo OM	Deicer attack	Medium
Secondary deposits of chloroaluminates	Petrographic OM SEM		High
Secondary deposits of ettringite in air voids and cracks	Petrographic OM SEM	Sulfate attack (both internal and external)	Low

In summary, a combination of heavy deicer use, an inadequate air-void system, and a weak paste resulting from a high w/c all combined to cause the distress in this pavement. With care in batching future concrete mixes and possibly alternative deicers, this type of distress may be minimized in future construction.

Recommended Treatment/Rehabilitation Alternatives

The application of the procedures presented in Guideline III in *Volume 2: Guidelines Description and Uses* is not straightforward in this case since the high w/c is a major factor in the observed failure, yet it is not considered a common MRD. Even so, the guideline can be used to select feasible treatment and rehabilitation alternatives for paste freeze-thaw deterioration and deicer attack. Based on the visual assessment, Section 001 is clearly suffering high-severity distress in the vicinity of joints, with patching observed at every joint. Section 002 is in slightly better condition, but still would be considered high severity based on the depth of spalling and the number of patches observed. It was also noted by maintenance crews that the deterioration extended through the full depth of the slab. Based on this assessment, the following treatment/rehabilitation options are available:

- Full-depth repairs
- Reconstruction/recycling

The use of full-depth patching is still feasible, although it should only be used as a stop-gap measure with the full realization that deterioration will likely continue at the patch boundary. Ultimately, as the pavement continues to deteriorate, a reconstruction/recycling option becomes more viable.

Recommended Prevention Strategies

For the distresses noted, the best preventative strategy is to ensure that the concrete specified is constructed. It seems evident that the w/c as constructed was well in excess of that specified and that the as-constructed air-void system was inadequate to protect against paste freeze-thaw damage. Further, the deicer attack was also a result of these two factors. If this concrete was constructed as specified, it is unlikely that deterioration would have occurred. Thus, the use of a w/c equal to or less than 0.45 and the addition of an effective air entraining admixture at a dosage sufficient to create an adequate air-void system would be all that was needed to address the observed MRD.

2.3 NEAR RALEIGH, NORTH CAROLINA (NC-440-015)

Project Description

Pavements with durability problems in the wet-nonfreeze climatic region were not as easy to locate. However, the North Carolina DOT did provide a viable section that was selected as the primary site for the wet-nonfreeze region (this area receives approximately 1070 mm of annual precipitation and has a freezing index of 58°C-days). The section is located on I-440 near Raleigh and exhibits surface cracking over the entire slab area. The project extends approximately 3 km from Pool Road to Raleigh Boulevard in both directions. The highway is a divided roadway with a minimum of three and in some cases up to five lanes in each direction.

The project was constructed in 1982 and consists of a 250-mm JPCP and a 100-mm cement-treated base. A 25-mm AC separator layer is located between the PCC slab and the base course. The transverse joints are doweled, sealed with silicone, and employ a variable joint spacing pattern of 7.6-7.0-5.8-5.5 m. The longitudinal joints were formed using a plastic joint insert and have not been sealed. AC shoulders are located along the inside and outside edge and are 1.8 and 3.0 m wide, respectively. The design information is summarized in table 3-18.

Distress Survey Results

An initial windshield survey was conducted over the entire project. Following this cursory survey, two sections—one in each direction—were selected for more detailed surveys. Both sections are located in the outer traffic lane. Table 3-19 presents a summary of the distress survey results for Section 001; the results for Section 002 are summarized in table 3-20.

Both sections are in similar condition. The predominant distress is map cracking over the entire pavement surface. Several flexible patches (low to medium severity) have also been placed on each section. Faulting is not to the extent where it is creating any reduction in ride quality. The only observed difference is the presence of two transverse cracks on Section 002. Due to the surface cracking, these cracks have begun to deteriorate and have been patched with AC. The transverse joints, which have been sealed with a silicone sealant, are in fair condition. However, it appears that as this MRD continues to progress, it could result in problems in the future.

Table 3-18. Summary of design features for NC-440-015.

Category	Design Feature	Description
General Information	Project limits	Pool Road to Raleigh Blvd.
	Highway type	Divided
	Number of lanes	6
	Direction	Eastbound/westbound
	Construction date	1982
	Cumulative ESALs	
Pavement Cross Section	Pavement type	JPCP
	PCC slab thickness	250 mm
	Base	100-mm cement-treated base (CTB) ¹
	Subbase	
	Subgrade type	
Transverse Joint	Joint spacing	7.6-7.0-5.8-5.5 m
	Joint skew	None
	Load transfer	Dowels
	Sealant type	Silicone
Longitudinal Joint	Load transfer	
	Sealant type	None
Outer Shoulder	Surface type	AC
	Width	3.0 m
Inner Shoulder	Surface type	AC
	Width	1.8 m
Climatic Conditions	Region	Wet-nonfreeze
	Annual precipitation	1070 mm
	Freezing index	58 °C-days

¹ Also includes 25-mm AC separator layer between the CTB and PCC slab.

Table 3-19. Summary of pavement condition surveys for NC-440-015-001.

	Distress Type	Distress Measure	Severity Level			Comments
			Low	Moderate	High	
Cracking	Corner Breaks	number	0	0	0	
	Longitudinal Cracking	linear meters	0.0	0.0	0.0	
	Transverse Cracking	number of cracks	0	0	0	
		linear meters	0.0	0.0	0.0	
		percent of slabs	0			
Transverse Joints	Sealant		fair condition			silicone sealant
	Spalling	number	2	0	0	
		linear meters	0.5	0.0	0	
	Faulting	millimeters	n/a ¹			
		millimeters	1.2			
	Width	millimeters	8.1			
Long Joints	Sealant		n/a			not sealed
	Spalling	linear meters	0.0	0.0	0.0	
	Shoulder Dropoff	millimeters	n/a			not measured
Surface Conditions	Map Cracking	number of slabs	24			all slabs affected
		square meters	578.0			entire area
	Scaling	number of slabs	0			
		square meters	0.0			
	Polished Aggregate	square meters	0.0			
	Popouts	number/sq. meter	0.0			
Other	Blowups	number	0			
	Flexible Patches	number	5	0	0	
		square meters	0.8	0.0	0.0	
	Rigid Patches	number	0	0	0	
		square meters	0.0	0.0	0.0	
	Pumping/Bleeding	number	0			
		linear meters	0.0			

¹ Faulting could not be measured due to high traffic volumes.

Table 3-20. Summary of pavement condition surveys for NC-440-015-002.

Distress Type		Distress Measure	Severity Level			Comments
			Low	Moderate	High	
Cracking	Corner Breaks	number	0	0	0	
	Longitudinal Cracking	linear meters	0.0	0.0	0.0	
	Transverse Cracking	number of cracks	2	0	0	
		linear meters	7.4	0.0	0.0	
		percent of slabs	8			
Transverse Joints	Sealant		fair condition			silicone sealant
	Spalling	number	0	0	0	
		linear meters	0.0	0.0	0.0	
	Faulting	millimeters	0.6			measured at 0.30 m
		millimeters	0.7			measured at 0.75 m
Long. Joints	Width	millimeters	7.6			
	Sealant		n/a			not sealed
	Spalling	linear meters	0.0	0.0	0.0	
	Shoulder Dropoff	millimeters	3.0			
Surface Conditions	Map Cracking	number of slabs	24			all slabs affected
		square meters	576.0			entire area
	Scaling	number of slabs	0			
		square meters	0.0			
	Polished Aggregate	square meters	0.0			
	Popouts	number/sq. meter	0.0			
Other	Blowups	number	0			
	Flexible Patches	number	0	2	0	
		square meters	0.0	0.4	0.0	
	Rigid Patches	number	0	0	0	
		square meters	0.0	0.0	0.0	
	Pumping/Bleeding	number	0			
		linear meters	0.0			

MRD Field Characterization

An evaluation of the MRDs is a key component of this project, so they are thus examined closely in the field. This detailed investigation, along with the comprehensive laboratory investigation, will help diagnose the type and cause of the distresses. The findings from this evaluation are summarized in table 3-21 and typical photos are shown in figure 3-46.

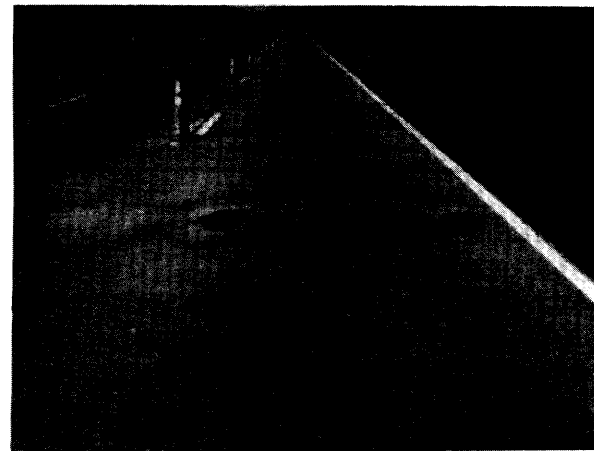
The primary distress, and the reason this section was selected as part of this project, is the extensive surface cracking exhibited over the entire pavement area. These hairline cracks run parallel to the longitudinal joints and are more prevalent near the outer edge of the slab (i.e., near the longitudinal joints). Some cracks are stained immediately around the cracks, which further highlights the presence of the cracks. The staining is typically dark gray areas around the crack; no exudate appears to be present in the cracks.

Table 3-21. Summary of MRD characterization for NC-440-015.

Description		Section 001	Section 002	Comments
Cracking	Location	Entire slab	Entire slab	
	Orientation/shape	Parallel to longitudinal joint	Parallel to longitudinal joints	
	Extent	Entire slab	Entire slab	
	Crack size	Hairline	Hairline	
Staining	Location	Around cracks	Around cracks	Not all cracks have staining
	Color	Dark gray	Dark gray	
Exudate	Present	None	None	
	Color	n/a	n/a	
	Extent	n/a	n/a	
Scaling	Location	None	None	
	Area of surface	n/a	n/a	
	Depth	n/a	n/a	
Vibrator Trails	Visible	None	None	
	Discolored	n/a	n/a	
	Distressed	n/a	n/a	
	Change in texture	n/a	n/a	



(a)



(b)

Figure 3-46. Typical cracking pattern at NC-444-015. Note distress over entire slab length with spalling occurring at joints.

For the most part, these surface cracks are not causing any immediate concerns or problems. At a few joints and at the two transverse cracks, the surface cracks have begun to deteriorate and create loose pieces and some large spalls were seen on the side of the road. These areas have been patched with AC. Otherwise, the cracks are not adversely affecting the ride quality.

Laboratory Analysis

Core Selection/Visual Inspection

Based on the field survey and site inspection by researchers, the distress was determined to be widespread and uniform. Therefore it wasn't necessary to emphasize the joints as compared to the mid-panel concrete in selecting cores to analyze. As a result only two cores were examined, cores A and E. In addition, a large spall found by the side of Site 1 was selected for examination. Pictures of the cores and spall are shown in figure 3-47.

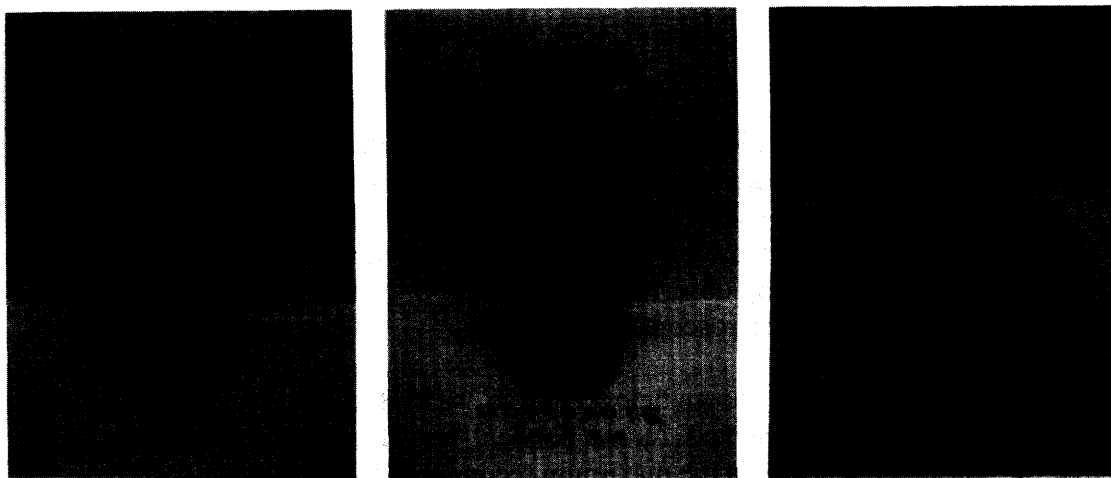
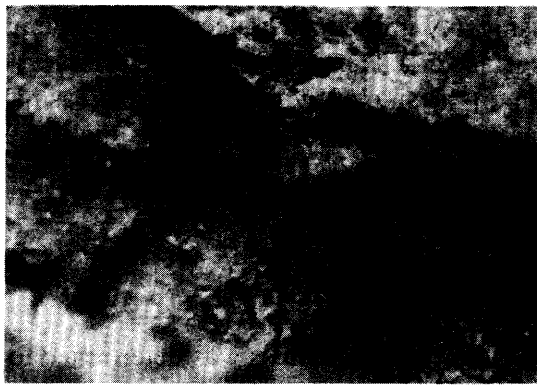


Figure 3-47. Cores and specimens evaluated from NC-440-015.

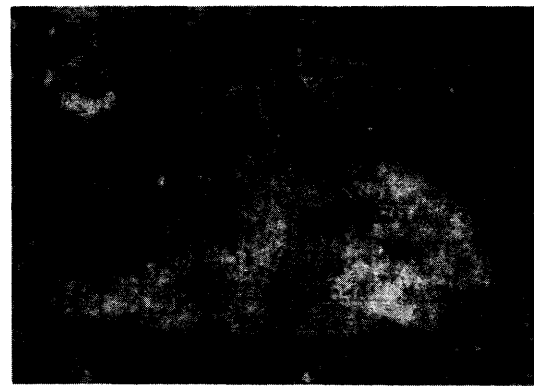
As with the other sites, mix proportions were not documented in the construction records and were only noted in the visual inspection as being normal. The concrete cores were 265 mm in depth, considerably greater than the design thickness of 250 mm. The concrete was well consolidated with no apparent segregation or parallelism of the aggregates. No scaling was present and there was no evidence of sub-parallel cracking or entrapped water voids under aggregates and surface cracking was seen in the cores that was thought not to be shrinkage cracks. Cracks extended from aggregates and through the paste. Secondary deposits were seen in some entrapped air voids and darkened rims were seen on coarse aggregate particles.

Stereo Optical Microscopy

As with the other sites, the stereo optical microscope was used to inspect the concrete in greater detail and perform the ASTM C 457 analysis. Infilling in cracks and voids was common with some entrapped air voids exhibiting large amounts of gel products. Figure 3-48 shows examples of infilling. The aggregate shown stained in figure 3-48 was prepared in thin section for additional study. Coarse aggregates in contact with the cement paste showed darkened rims.



(a) Desiccated ASR gel lining large entrapped air void.



(b) Granite coarse aggregate that picked up the stain, especially in cracks within the aggregate. Matching face from this aggregate prepared in thin section to examine material in cracks.

Figure 3-48. Stereo optical micrographs of ASR gel and reactive coarse aggregate from NC-440-015.

The coarse aggregate type was identified as granite and the fine aggregate appeared to be the same rock type. The fine aggregate was very angular, further indicating it may be a crushed version of the coarse aggregate used. The paste was hard and varied in color from yellow on one site to green on the other. This was attributed to different cement types being used in different sections, a fact later confirmed by observation of the unhydrated cement grains in the concrete using the petrographic optical microscope.

The results of ASTM C 457 are shown below in table 3-22. Both the air-void parameters and phase abundance results are presented. As can be seen, the value of Power's spacing factor measured for this concrete exceeds the maximum recommended to ensure freeze-thaw protection. In general this is not a concern for this pavement as the environment is considered a wet/no-freeze zone. However, the fact is that some freezing does occur and there may be some minor contribution of paste freeze-thaw damage to the overall observed distress.

Table 3-22. Results of ASTM C 457 on concrete from NC-440-015.

Core	Original		Existing		Volume Percent		
	Air Content (vol. %)	Spacing Factor (mm)	Air Content (vol. %)	Spacing Factor (mm)	Paste (vol. %)	Coarse Aggregate (vol. %)	Fine Aggregate (vol. %)
Site 1 Core A	6.6	.278	6.4	.320	29.6	41.7	22.2
Site 1 Core E	6.5	.252	6.5	.276	30.0	44.4	21.2

Staining Tests

The results of staining indicate that both sulfate minerals and ASR gel are present as infilling material in cracks and voids. Figure 3-49 below shows some typical results for these tests. The characteristic yellow of the sodium cobaltinitrite stain is seen on the left and the brilliant purple color associated with the barium chloride/potassium permanganate is seen on the right. The phenolphthalein stain indicated a depth of carbonation of approximately 5 mm at the road surface and at the bottom of the slab.

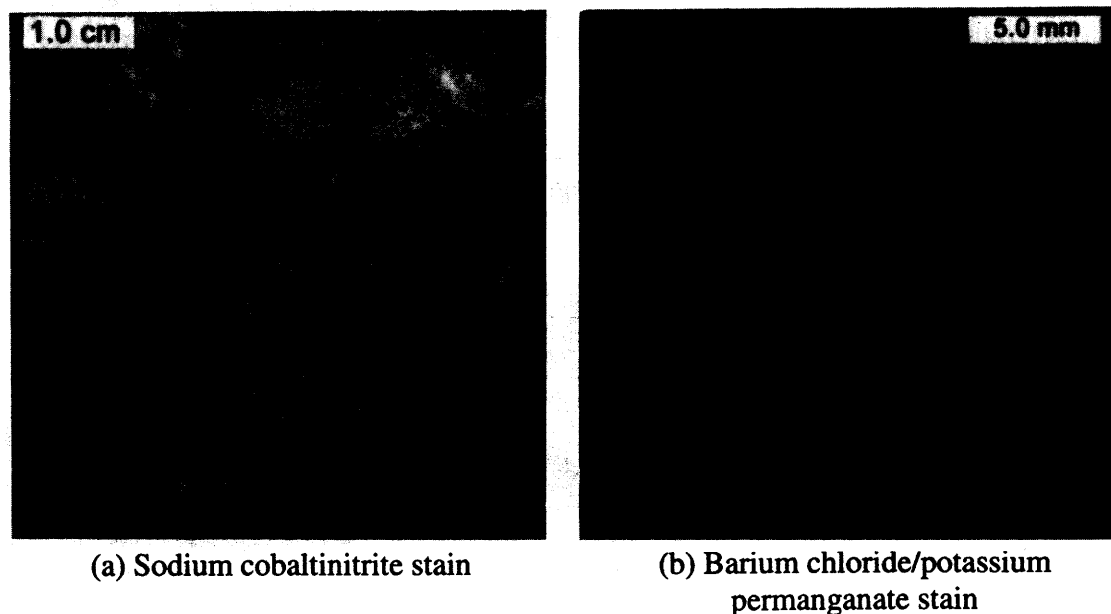


Figure 3-49. Typical stereo optical micrographs of stained concrete. Note that the broad banding occurs from the montage process to create a single image.

Petrographic Optical Microscopy

The petrographic microscope further confirmed dense reaction rims on coarse aggregates in contact with the cement paste. Cracks within the aggregate were filled with crystalline ASR product and ettringite. The ettringite was generally very dense and tightly packed. In addition to the granite aggregates reacting, some reactive chert was seen in the fine aggregate. Also, the fine aggregate contained some reactive particles that were a red to tan color and occurred as a “coating” on other particles. The reaction seems to convert the coating to a gel product, which appears desiccated in thin section. Apart from consuming the tan to red coating, the reaction appears to cause no damage to the surrounding concrete. Some typical petrographic optical micrographs of reacting aggregate and ASR gel “blobs” are shown in figures 3-50 through 3-54.

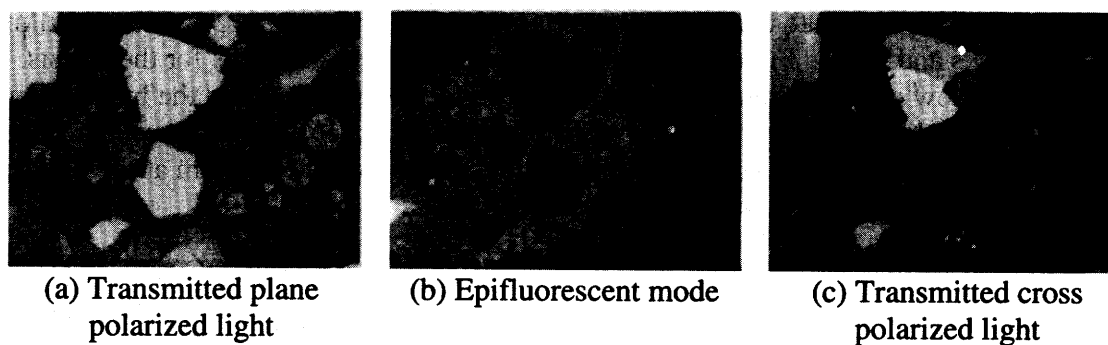


Figure 3-50. Petrographic micrographs from spall obtained from NC-440-015 showing ettringite filled entrained air voids. Ettringite growths are unusually dense.

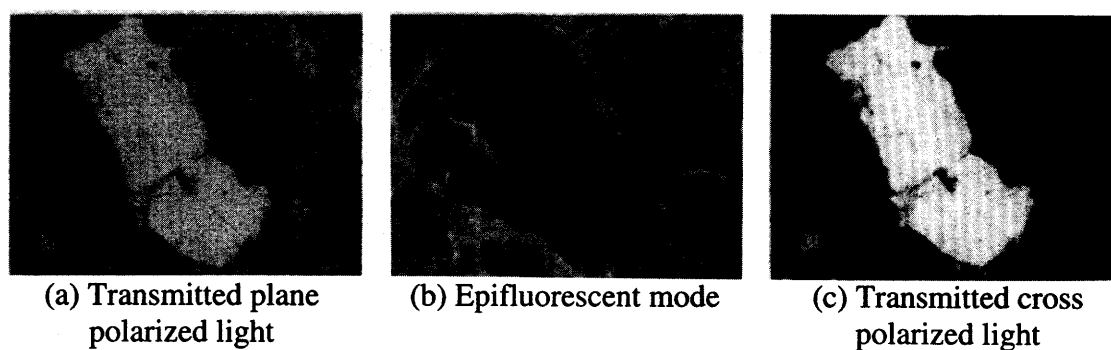


Figure 3-51. Petrographic micrograph of a tan to red coating observed on some of the fine aggregates that appears to undergo ASR from spall obtained from NC-440-015.

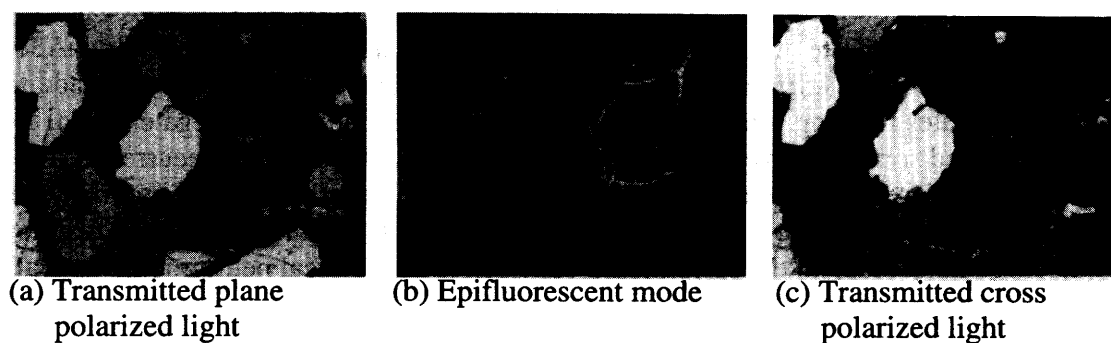


Figure 3-52. Petrographic micrograph of ettringite and “ASR gel blob” from spall obtained from NC-440-015. The term ASR gel is misleading in this example, since the reaction product is slightly birefringent and, therefore, crystalline.

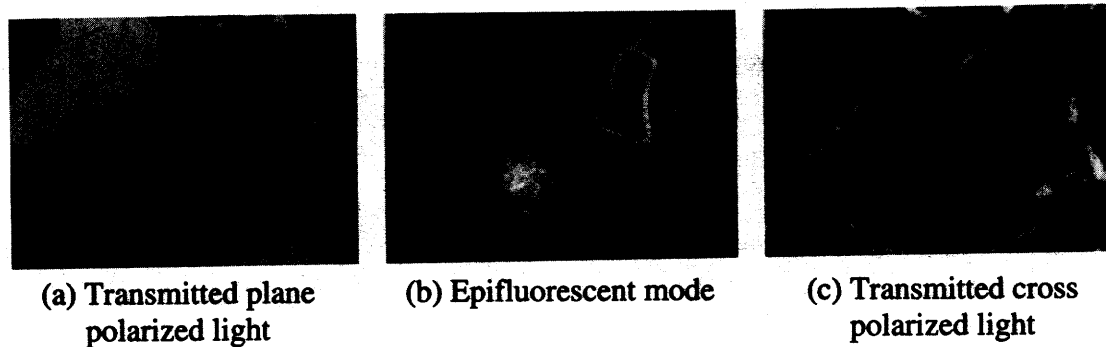


Figure 3-53. Petrographic micrograph of ettringite intermixed with ASR gel. As in figure 3-52, the ASR “gel” in this image is birefringent and crystalline.

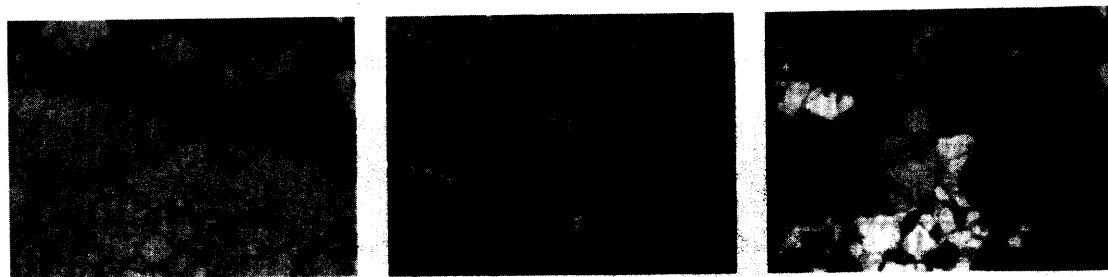
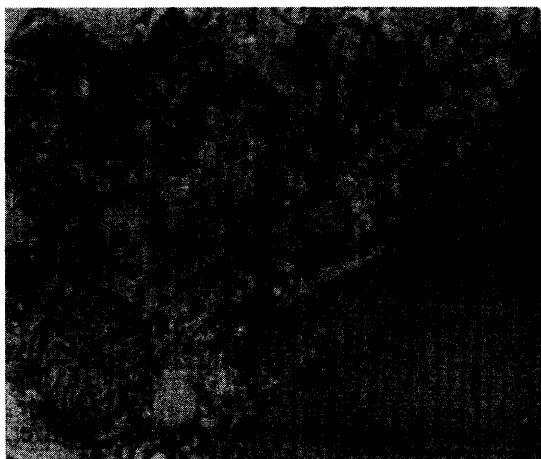


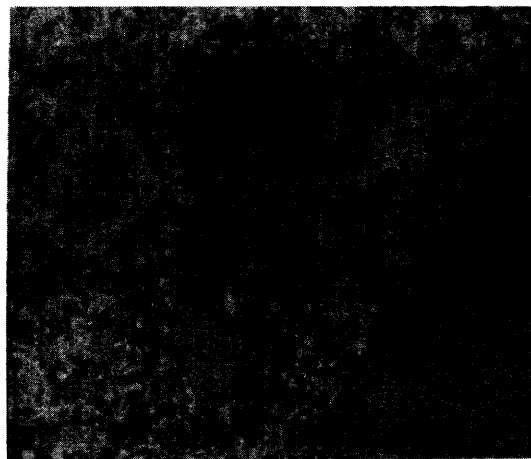
Figure 3-54. Petrographic micrograph of ASR gel in crack within coarse aggregate. The gel deposit in this image was analyzed with the SEM. Again, the ASR “gel” in this image is birefringent and crystalline.

Scanning Electron Microscopy

Using the SEM, quantitative measurements of ettringite and ASR “gel” compositions were made. Ettringite deposits were extensive and found both in entrained air voids and in cracks in the cement paste and in cracks along the contact with coarse aggregates. Measurements were made of the coarse aggregate ASR product pictured in figure 3-54, both within the crack in the coarse aggregate, and in the region where the crack comes into contact with the cement paste. Measurements were also made of the gel blobs associated with the fine aggregates. The presence of small amounts of iron in the ASR product is unusual. Figures 3-55 and 3-56 are SEM micrographs of ettringite and ASR reaction product. Figure 3-57 shows the typical spectra for ettringite and ASR reaction product.

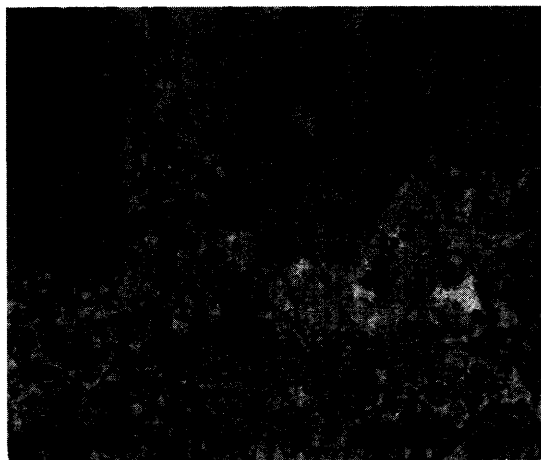


(a) Ettringite in entrained air void, and in crack along contact between cement paste and coarse aggregate.

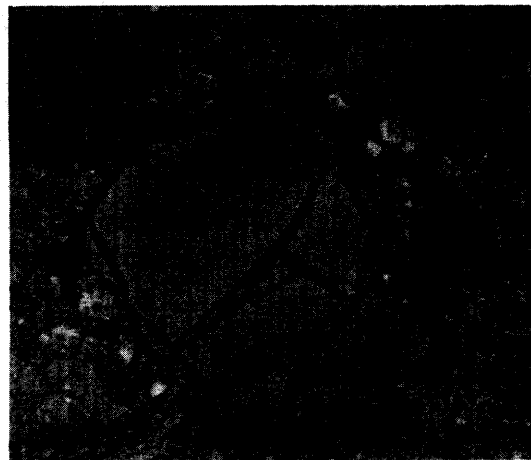


(b) Ettringite in entrained air void, and in crack along contact between cement paste and coarse aggregate. Large relict cement grain also visible.

Figure 3-55. SEM micrograph of ettringite filling air voids and crack.



(a) Two ettringite filled air voids connected by a crack, also filled with ettringite.



(b) ASR "gel blob" associated with fine aggregate. Spectrum shown in figure 3-57 contain data collected from this deposit.

Figure 3-56. SEM micrograph of ettringite and ASR reaction product.

Interpretation and Diagnosis

This test site was a good example of an "obvious" MRD, if there is such a thing. The visual inspection indicated a classic case of ASR distress. Further examination led to no other likely distress other than the potential of some paste freeze-thaw damage as a result of an inadequate air-void system. It should be pointed that with the visuals and stereo optical microscope inspection alone, a diagnosis of ASR is tempting. However, to be certain of your diagnosis, all other avenues must be explored. In this context the guidelines proved useful in keeping the analysis on track and not stopping at the first MRD identified.

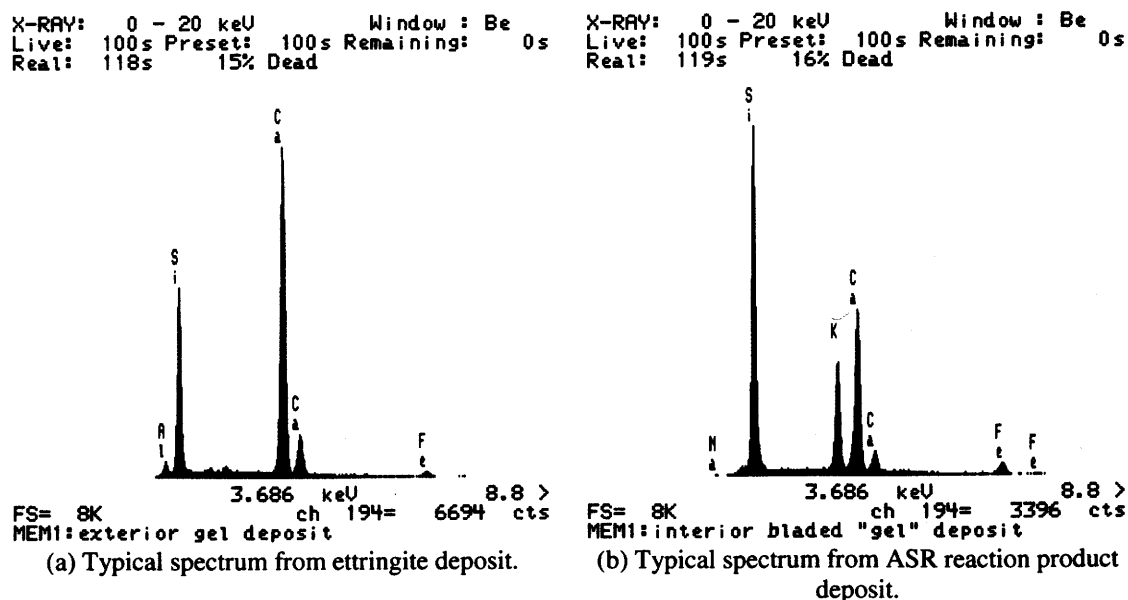


Figure 3-57. Typical spectra for ettringite and ASR reaction product.

Having performed the described laboratory analyses and applied the diagnostic flow charts as shown in figures 3-58 through 3-62, two possible MRDs were identified in NC-440-015, including paste freeze-thaw and ASR. To finalize the diagnosis, the diagnostic tables were consulted. The diagnostic features identified in the analysis processes are listed in table 3-23 along with their associated MRD type and significance as related to this pavement. A brief discussion of each possible MRD identified in the laboratory analysis:

Paste Freeze-Thaw – The probability of paste freeze-thaw damage is low. The fact that the air void system was inadequate and was further compromised by infilling should be noted. Microcracking resulting from paste freeze-thaw may have accelerated the ASR reaction by providing a path for water ingress into the concrete.

ASR – This MRD was clearly dominant in terms of extent. It is most likely that the major contributor to the overall observed distress is ASR.

In summary, ASR is the most likely cause of distress in this pavement. Any steps to remediate should focus on ASR mitigation. In future construction, more attention to the quality of the entrained air system may help improve performance.

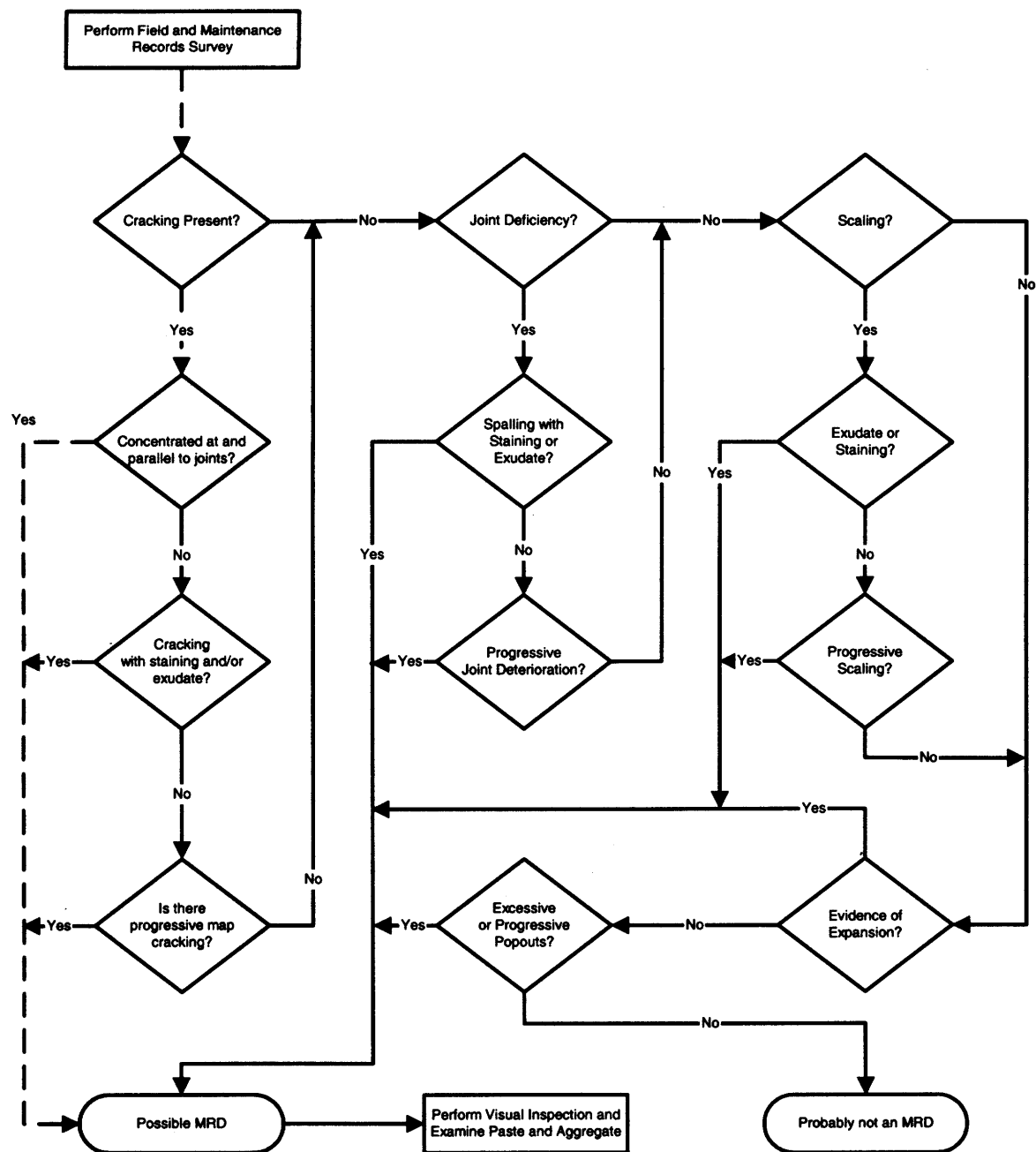


Figure 3-58. Flowchart for assessing the likelihood of MRD causing the observed distress in the pavement as applied to NC-440-015.

Possible Distress	Present		Additional Information
Error in Mix Proportioning	Yes	No	See Recommended Literature
Poor Placement	Yes	No	See Recommended Literature
Poor Finishing/Curing	Yes	No	See Recommended Literature
Poor Steel Placement	Yes	No	See Recommended Literature
Carbonation at Depths > 5-10 mm	Yes	No	See Recommended Literature

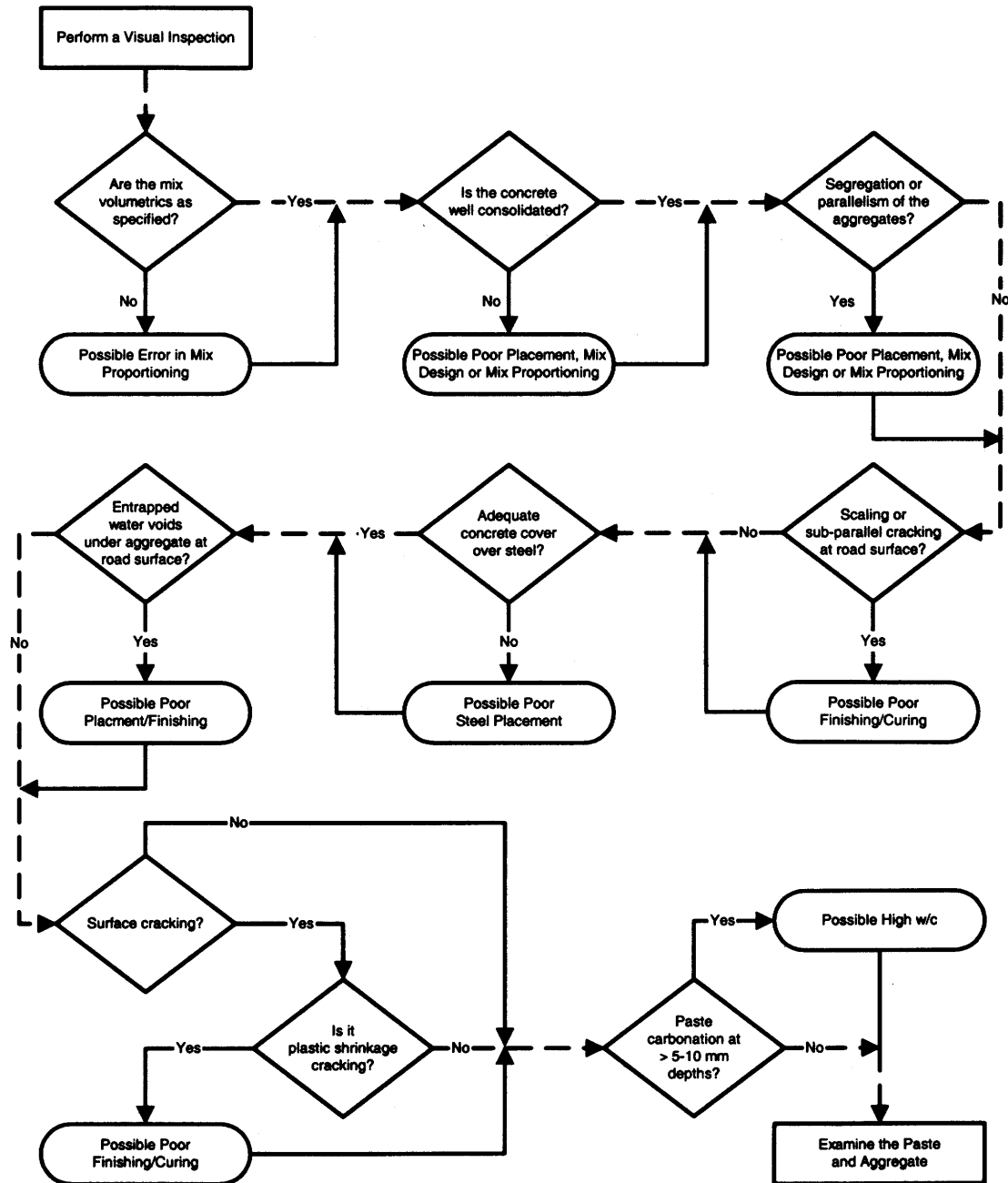


Figure 3-59. Flowchart for assessing general concrete properties based on visual examination as applied to NC-440-015.

Possible Distress	Present		Additional Information
Shrinkage Cracks or Sample Preparation Cracks	Yes	No	See Recommended Literature
Paste Freeze-Thaw	Yes	No	Table II-2
Aggregate Freeze-Thaw	Yes	No	Table II-3
Sulfate Attack	Yes	No	Table II-4
Deicer Attack	Yes	No	Table II-5
Secondary Deposits	Yes	No	Figure 3-62

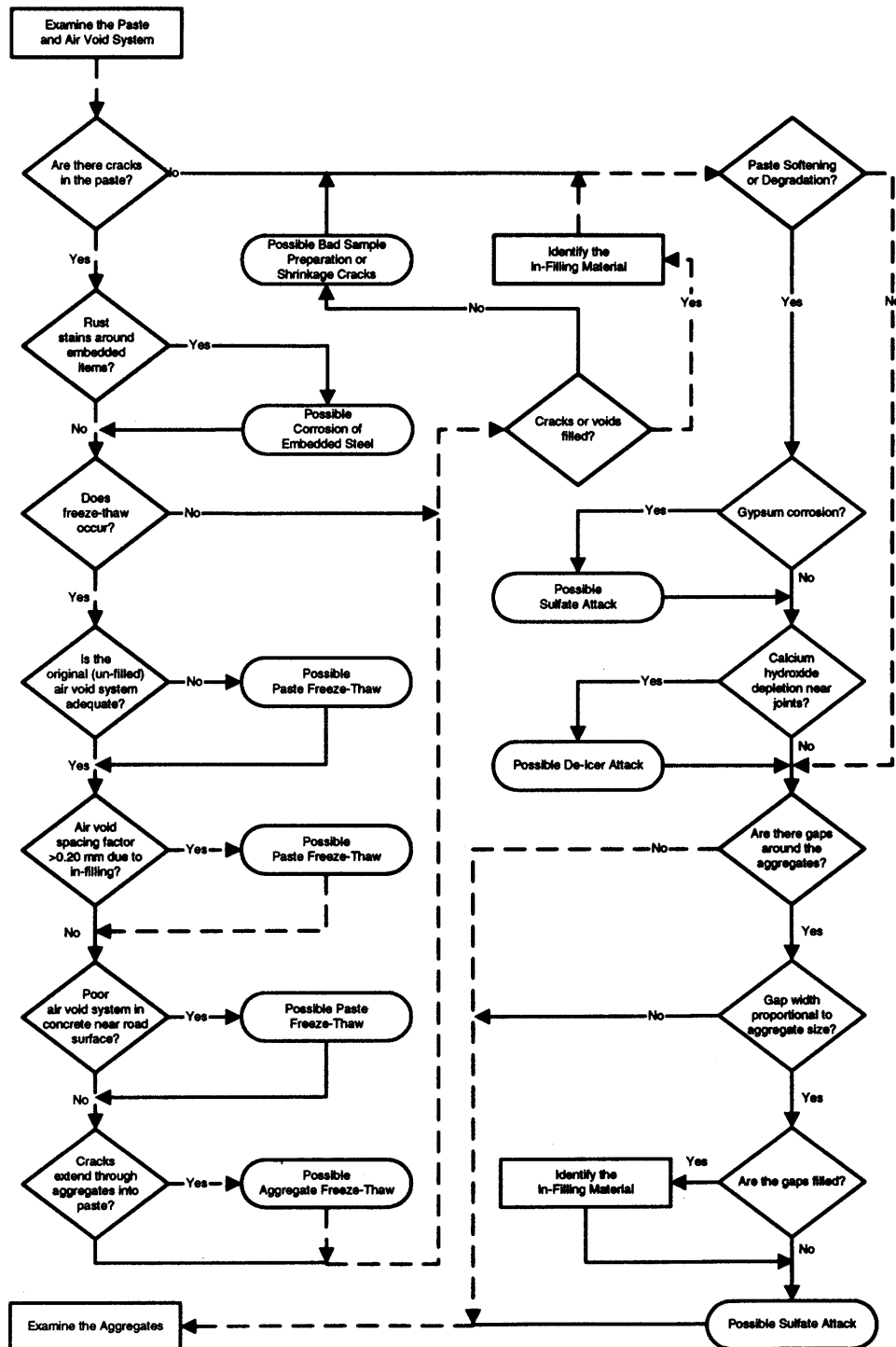


Figure 3-60. Flowchart for assessing the condition of the concrete paste as applied to NC-440-015.

Possible Distress	Present	Additional Information
Natural Cracking of Aggregate	Yes No	See Recommended Literature
Sample Preparation Cracks	Yes No	See Recommended Literature
Aggregate Freeze Thaw	Yes No	Table II-3
Natural Weathering of Aggregates	Yes No	See Recommended Literature
Alkali-Silica Reaction	Yes No	Table II-6
Alkali-Carbonate Reaction	Yes No	Table II-7
Secondary Deposits	Yes No	Figure 3-62

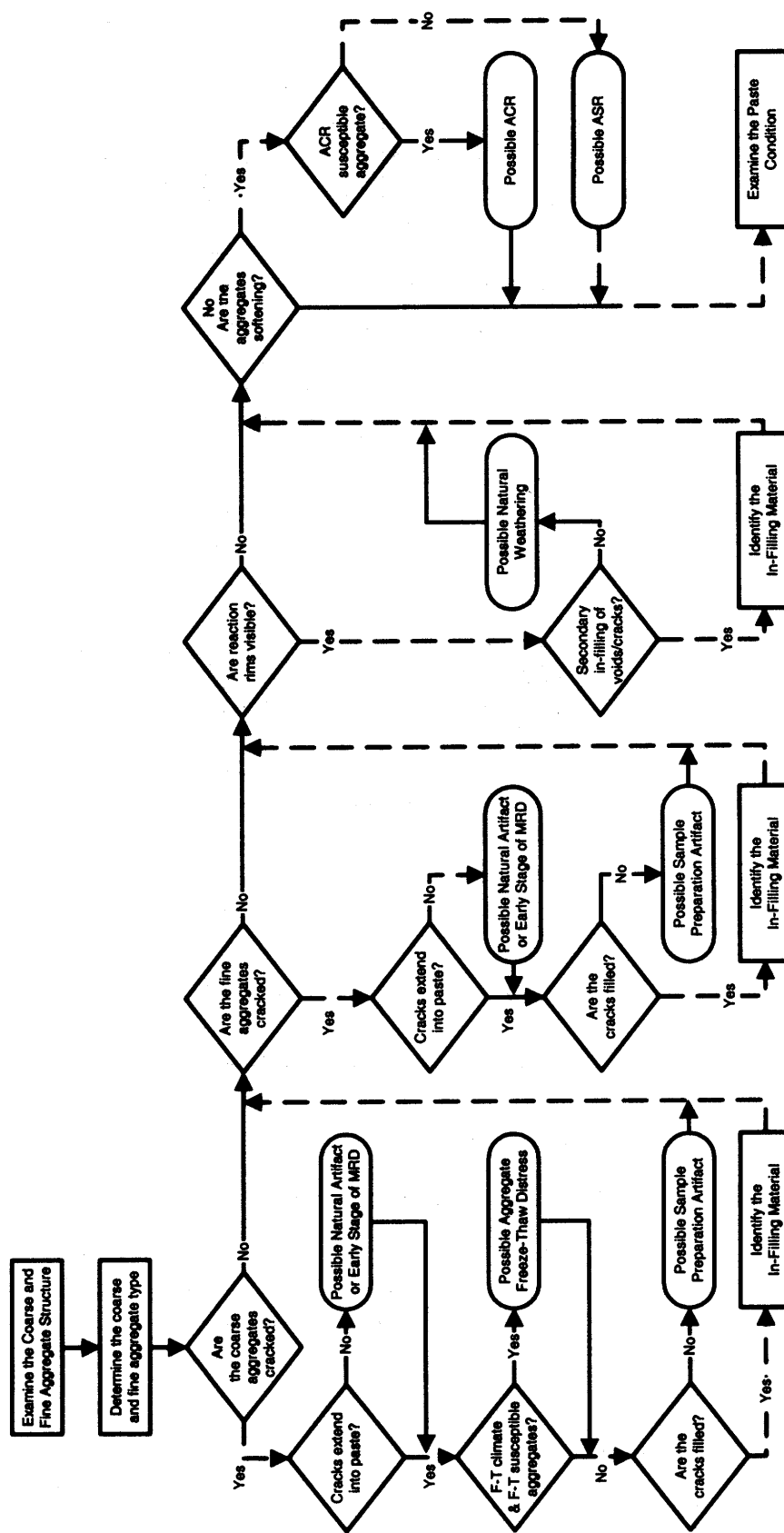


Figure 3-61. Flowchart for assessing the condition of the concrete aggregates as applied to NC-440-015.

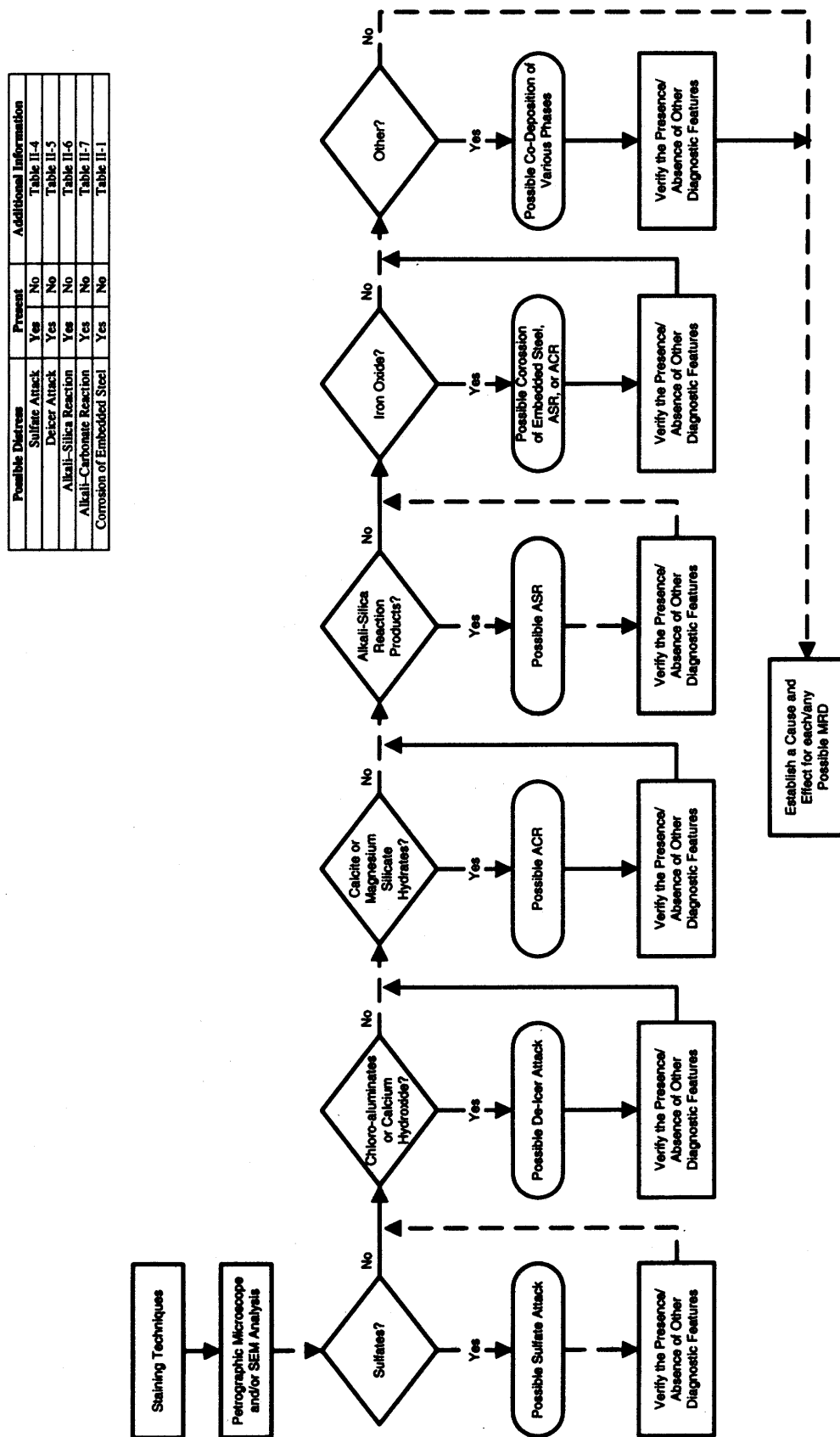


Figure 3-62. Flowchart for identifying infilling materials in cracks and voids as applied to NC-440-015.

Table 3-23. Diagnostic features identified along with their associated MRD type and significance as related to NC-440-015.

Diagnostic Feature	Method of Characterization	Associated with MRD Type	Significance
Secondary deposits filling air voids and cracks	Visual Stereo OM Petrographic OM SEM	Paste freeze-thaw, Deicer attack, Sulfate attack (both internal and external)	Low
Inadequate air-void system	Visual Stereo OM	Paste freeze-thaw	Low
Microcracking around aggregates	Stereo OM Petrographic OM		
Map cracking without exudate		ASR	Medium
ASR reaction products in cracks and voids	Petrographic OM SEM		High
Reaction rims on aggregates	Petrographic OM SEM		Low
Microcracking radiating from reacted aggregates	Stereo OM Petrographic OM		Medium
Significant sulfate deposits in cracks and voids	Staining Stereo OM Petrographic OM SEM	Sulfate attack (both internal and external)	Low

Recommended Treatment/Rehabilitation Alternatives

Using the procedures presented in Guideline III in *Volume 2: Guidelines Description and Uses*, feasible treatment and rehabilitation alternatives were selected. The most significant MRD mechanism found was ASR. The deterioration is characterized as map cracking (hairline) over the entire pavement surface, with some associated staining. Isolated areas of higher deterioration were noted, necessitating patching. The severity level would be classified as medium severity, with some isolated areas of high severity. As a result, feasible treatment/rehabilitation alternatives include:

- Application of a lithium compound.
- The application of a HMWM.
- Overlay.

Ultimately, as the pavement continues to deteriorate, a reconstruction/recycling option becomes more viable. If recycling is considered, precautions must be taken to avoid ASR in the newly constructed pavement.

Recommended Prevention Strategies

For the distresses noted, the best preventative strategy is to use a source of aggregate that is not ASR susceptible. Testing in accordance with the guidelines should show that the current source would be unacceptable without mitigation. Mitigation strategies for ASR that could be used if the current aggregate source is all that is available include:

- Heavy media separation
- Blending with non-susceptible aggregates
- Washing

If aggregate benefaction is not feasible or cost effective, other strategies can be employed including:

- Reducing the total mixture alkalinity to less than 3 kg/m³
- Using a blended cement containing a pozzolan or ground slag
- Through supplementation or addition, use pozzolans or ground slag in the mixture
- Add lithium nitrate

Regardless of the approach, the design PCC mixture must be tested to ensure that the ASR has been mitigated.

2.4 SR 58 NEAR BORON, CALIFORNIA (CA-058-141)

Project Description

This project is located on State Route 58 near Boron, California. This particular project has been documented in the literature as exhibiting cracking patterns typically associated with ASR (Stark et al. 1993). The project was constructed in 1970 and has exhibited MRD for many years. In 1988, the project was treated with HMWM. After an evaluation of several other possible projects located in California, this project was selected as the primary case study to represent the dry-nonfreeze climatic region. Los Angeles, which is the closest major metropolitan area, has an annual precipitation of about 300 mm and no degree-days below freezing.

State Route 58 is a four-lane divided highway running east and west. However, the test project is located in the eastbound lanes only, extending from milepost 141.8 to milepost 142.5. A summary of the design information for this project is presented in table 3-24. The pavement is a 230-mm JPCP with a variable (4.0-5.8-5.5-5.7 m) joint spacing. The transverse joints are skewed at a angle of 1-to-6 (longitudinal-to-transverse). No load transfer mechanisms are provided at the longitudinal or transverse joints. The inside and outside shoulders, both of which have an AC surface, are 1.2 and 3.0 m wide, respectively.

Chemistry lab data from the construction records indicated that the soil sulfate composition at this site was less than 200 ppm. As a result, this test site would be classified as a moderate sulfate exposure in accordance with ACI 201.2R-92.

Table 3-24. Summary of design features for CA-058-141.

Category	Design Feature	Description
General Information	Project limits	MP 141.8 – 142.5
	Highway type	Divided
	Number of lanes	4
	Direction	Eastbound
	Construction date	1970
	Cumulative ESALs	
Pavement Cross Section	Pavement type	JPCP
	PCC slab thickness	230 mm
	Base	
	Subbase	
	Subgrade type	Sand
Transverse Joint	Joint spacing	4.0-5.8-5.5-3.7 m
	Joint skew	1:6
	Load transfer	Aggregate interlock
	Sealant type	None
Longitudinal Joint	Load transfer	Aggregate interlock
	Sealant type	None
Outer Shoulder	Surface type	AC
	Width	3.0 m
Inner Shoulder	Surface type	AC
	Width	1.2 m
Climatic Conditions	Region	Dry-nonfreeze
	Annual precipitation	305 mm (in Los Angeles)
	Freezing index	0°C-days (in Los Angeles)

Distress Survey Results

This project is a relatively short project that exhibits significant MRD throughout its entire length. The section selected for detailed investigation under this study begins at milepost 141.8 and extends 150 m to the east. This section was constructed on approximately 2.5 m of fill material. Table 3-25 presents a summary of the distress survey results for Section 001.

Map cracking is located throughout the entire pavement area. The only other noteworthy distresses are spalling and patching, both of which are due to deterioration of the surface cracking. Five of the 33 transverse joints have joint spalling over a portion of its length (4 have progressed to medium severity). There are seven small AC patches, all of which are medium severity, that have been placed to address the spalling caused by surface cracking. Even though the joints do not contain any load transfer devices, faulting is not significant enough to affect ride quality.

Table 3-25. Summary of pavement condition surveys for CA-058-141-001.

Distress Type		Distress Measure	Severity Level			Comments
			Low	Moderate	High	
Cracking	Corner Breaks	number	0	0	0	
	Longitudinal Cracking	linear meters	0.0	0.0	0.0	
	Transverse Cracking	number of cracks	0	0	0	
		linear meters	0.0	0.0	0.0	
		percent of slabs	0			
Transverse Joints	Sealant		n/a			not sealed
	Spalling	number	1	4	0	
		linear meters	0.1	1.3	0.0	
	Faulting	millimeters	1.3			measured at 0.30 m
		millimeters	0.6			measured at 0.75 m
Long Joints	Width	millimeters	3.4			
	Sealant		n/a			not sealed
	Spalling	linear meters	0.0	0.0	0.0	
	Shoulder Dropoff	millimeters	3.4			
Surface Conditions	Map Cracking	number of slabs	32			all slabs affected
		square meters	561.0			entire area
	Scaling	number of slabs	0			
		square meters	0.0			
	Polished Aggregate	square meters	0.0			
	Popouts	number/sq. meter	0.0			
Other	Blowups	number	0			
	Flexible Patches	number	0	7	0	
		square meters	0.0	0.8	0.0	
	Rigid Patches	number	0	0	0	
		square meters	0.0	0.0	0.0	
	Pumping/Bleeding	number	0			
		linear meters	0.0			

MRD Field Characterization

During the distress surveys, detailed information was collected to characterize the MRD. This information is useful, in conjunction with a laboratory investigation, to help diagnose the type and cause of MRD. Table 3-26 summarizes the key attributes of the MRD.

Table 3-26. Summary of MRD characterization for CA-058-141.

Description		Section 001	Comments
Cracking	Location	Entire slab	
	Orientation/shape	Honeycomb	
	Extent	Entire slab	
	Crack size	Hairline/open	Longitudinal cracks are more open; spalling at interconnecting cracks
Staining	Location	Around cracks	
	Color	Dark gray	
Exudate	Present	Yes	Not observed at all cracks
	Color	White	
	Extent	Low	
Scaling	Location	None	
	Area of surface	n/a	
	Depth	n/a	
Vibrator Trails	Visible	None	
	Discolored	n/a	
	Distressed	n/a	
	Change in texture	n/a	

As described previously, the MRD on this project is characterized by map cracking over the entire pavement surface. The most predominant cracking at the surface runs parallel to the longitudinal joints. These cracks are more prevalent, wider, and more deteriorated than the cracks running in other directions. In more deteriorated areas, the transverse and diagonal surface cracks have interconnected, forming a criss-cross or honeycomb pattern. These interconnecting cracks have led to spalling and loose material on the pavement surface.

A dark gray staining has occurred in the area surrounding the cracks. However, due to the extensive cracking, the entire pavement surface has a darker appearance. The cracks were once sealed with an HMWM, but that material does not appear to be performing its intended function at this time. Although not widespread, exudate, typically white in color, is observed at a few cracks. Figure 3-63 shows typical distress patterns for this site.

Laboratory Analysis

Core Selection/Visual Inspection

Based upon the field survey, distress was widespread. The joints were badly deteriorated and coring at the transverse joint produced pieces rather than an intact core. Cores C, D, and E were relatively intact and were thus analyzed. Photos of these cores are shown in figure 3-64. All cores were cut to produce slabs for examination with stains.

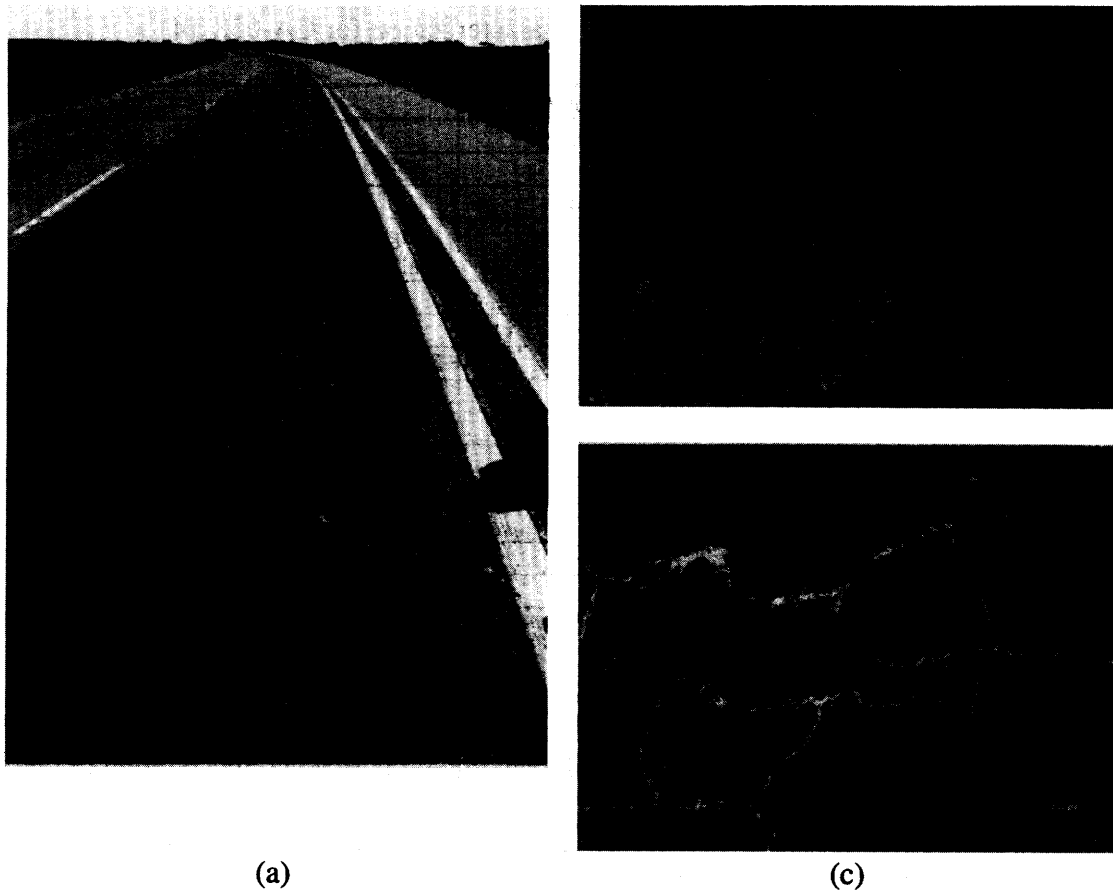


Figure 3-63. Typical conditions at CA-058-141.

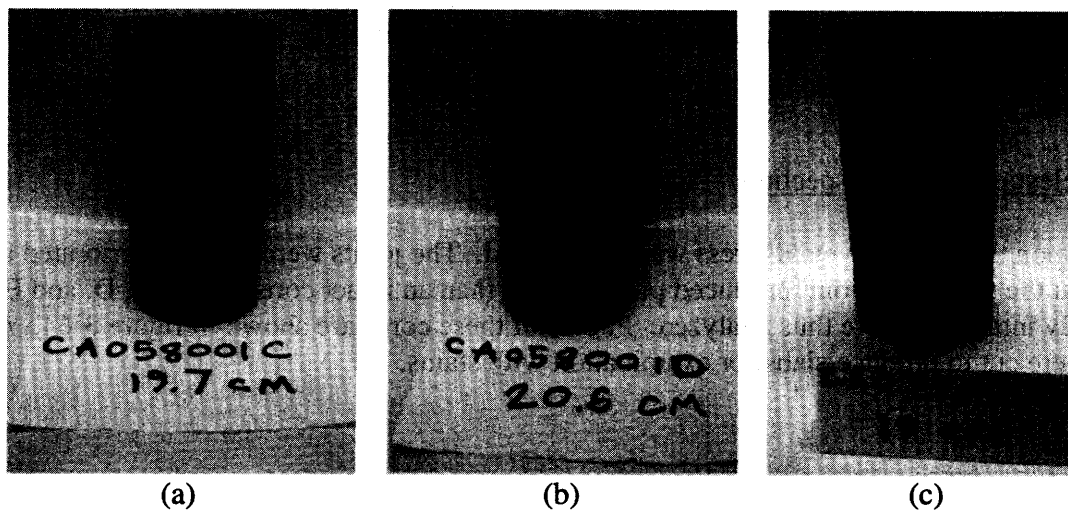


Figure 3-64. Photographs of core specimens analyzed from CA-058-141.

Mix proportions were estimated by inspecting the cores visually before and after slicing. In this case, construction records were unavailable to verify the mix design. The concrete was well consolidated with no apparent segregation or parallelism of the aggregates. No scaling or sub-parallel cracking was apparent on these sites. No entrapped water voids were seen under aggregates or embedded steel. Surface cracking was apparent that was not plastic shrinkage cracking. Darkened reaction rims were seen around some of the coarse aggregates. Abundant cracks filled with white deposits were visible with the unaided eye. The coarse aggregates used were a natural igneous (both intrusive and extrusive) and the natural fine aggregate used appear to be similar in lithology.

Stereo Optical Microscopy

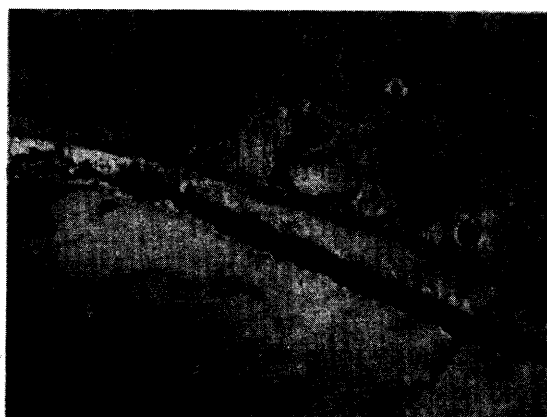
For this study, the stereo optical microscope was used primarily for observing stained specimens, selecting areas for preparing thin sections, and air void analysis. In this climate, air content is not an important factor in MRD unless it becomes excessive. Interestingly enough, according to the construction records obtained, this concrete was air entrained. As a result, only two cores were analyzed using ASTM C 457. A wide disparity in air content is noted but not considered abnormal considering the small sample size of only two cores. Also, a side benefit of performing the ASTM C 457 test is obtaining a measure of the relative phase abundance in the concrete. The results of the analysis are presented in table 3-27.

Table 3-27. Results of ASTM C 457 on concrete from CA-058-141.

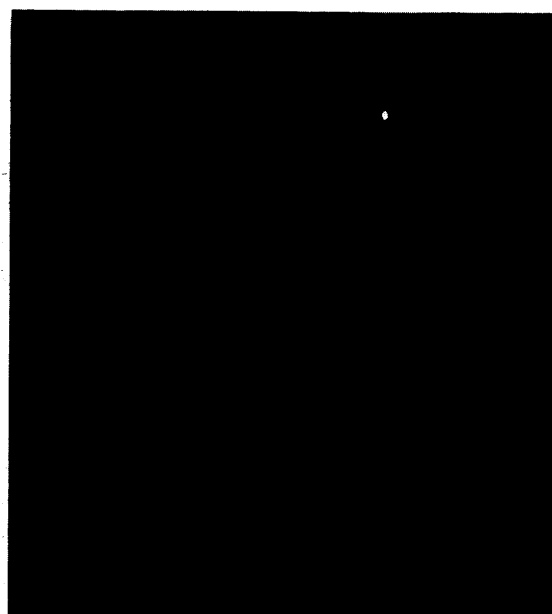
Core	Original		Existing		Volume Percent		
	Air Content (vol. %)	Spacing Factor (mm)	Air Content (vol. %)	Spacing Factor (mm)	Paste (vol. %)	Coarse Aggregate (vol. %)	Fine Aggregate (vol. %)
Site 1 Core C	1.9	0.230	1.1	0.430	23.0	54.3	20.9
Site 1 Core D	5.7	0.305	5.7	0.338	27.2	44.9	22.2

Staining Tests

Cores C and D were slabbed and stained using the sodium cobaltinitrite stain for identifying ASR reactive aggregates and reaction products. Also, slabs were stained with the potassium permanganate/barium chloride stain for identifying sulfate minerals. ASR reaction product was seen in cracks associated with the coarse aggregate. Ettringite was common in cracks and voids, and actually was more common than ASR reaction product. Examples of these stains as applied are shown in figure 3-65.



(a) Sodium cobaltinitrite yellow stain picked up in crack within felsic volcanic coarse aggregate



(b) An unpolished cut surface that has been stained to show ettringite filled cracks and voids

Figure 3-65. Stereo optical micrographs showing staining observed in core CA-058-141-001C.

Petrographic Optical Microscopy

Petrographic microscopy confirmed what was seen visually and by stereo optical microscopy. Alkali-silica gel was present in some cracks associated with some coarse aggregate, primarily felsic volcanics. Ettringite was common in cracks and air voids. This is seen in figures 3-66 and 3-67.

Scanning Electron Microscopy

In this case, the SEM was used simply as a means of confirming the results of the petrographic optical microscopy, stereo optical microscopy, and visual inspection. Using x-ray microanalysis, the ASR gel deposits shown in figure 3-68 were analyzed and these results are summarized in table 3-28. Many ettringite filled cracks were observed and an example is shown in the back-scattered electron (BSE) micrograph shown in figure 3-68.

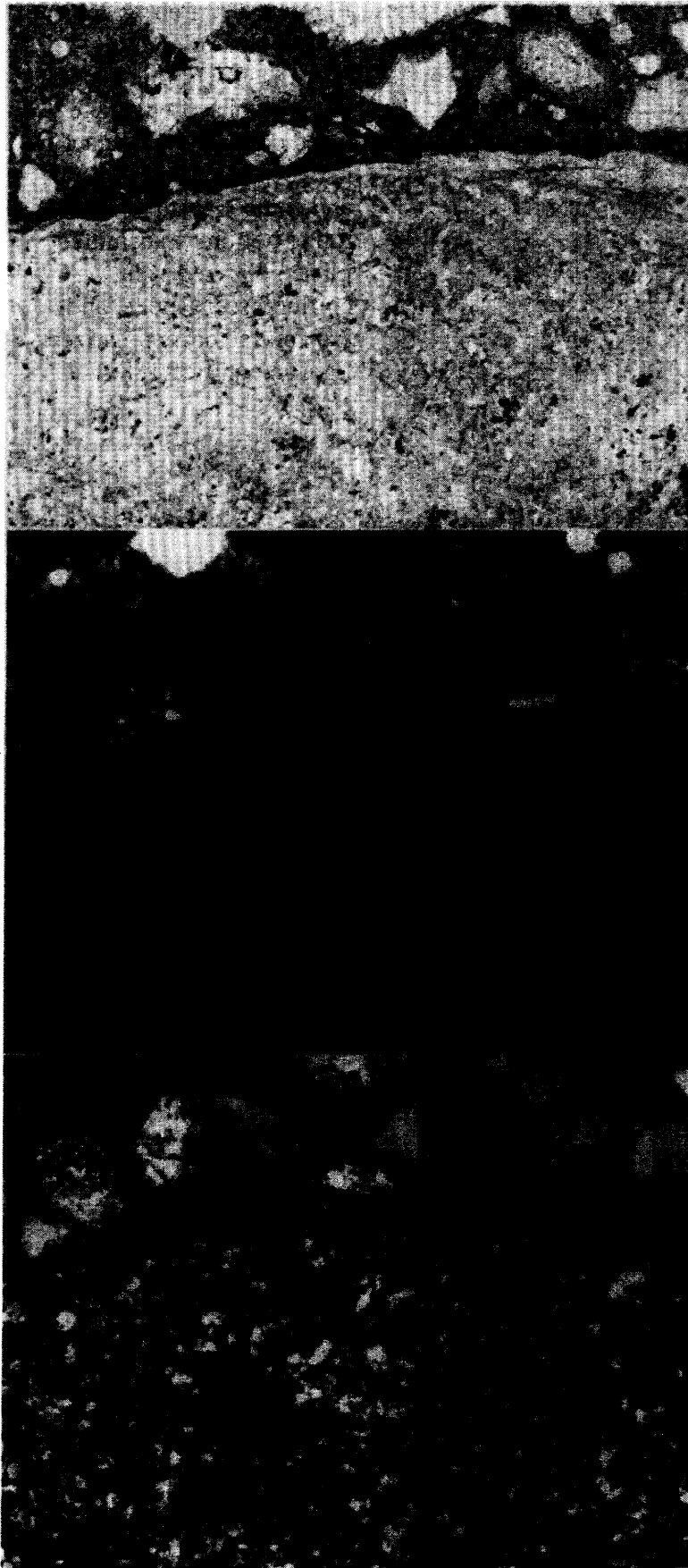


Figure 3-66. Petrographic micrograph of core CA-058-141-001E, thin-section micrographs of ASR gel deposit in crack along felsic volcanic aggregate. The same deposit was analyzed with the SEM to collect quantitative chemical information about the gel. From top to bottom: transmitted plane polarized light, epifluorescent mode, and transmitted cross polarized light (magnified 48x).

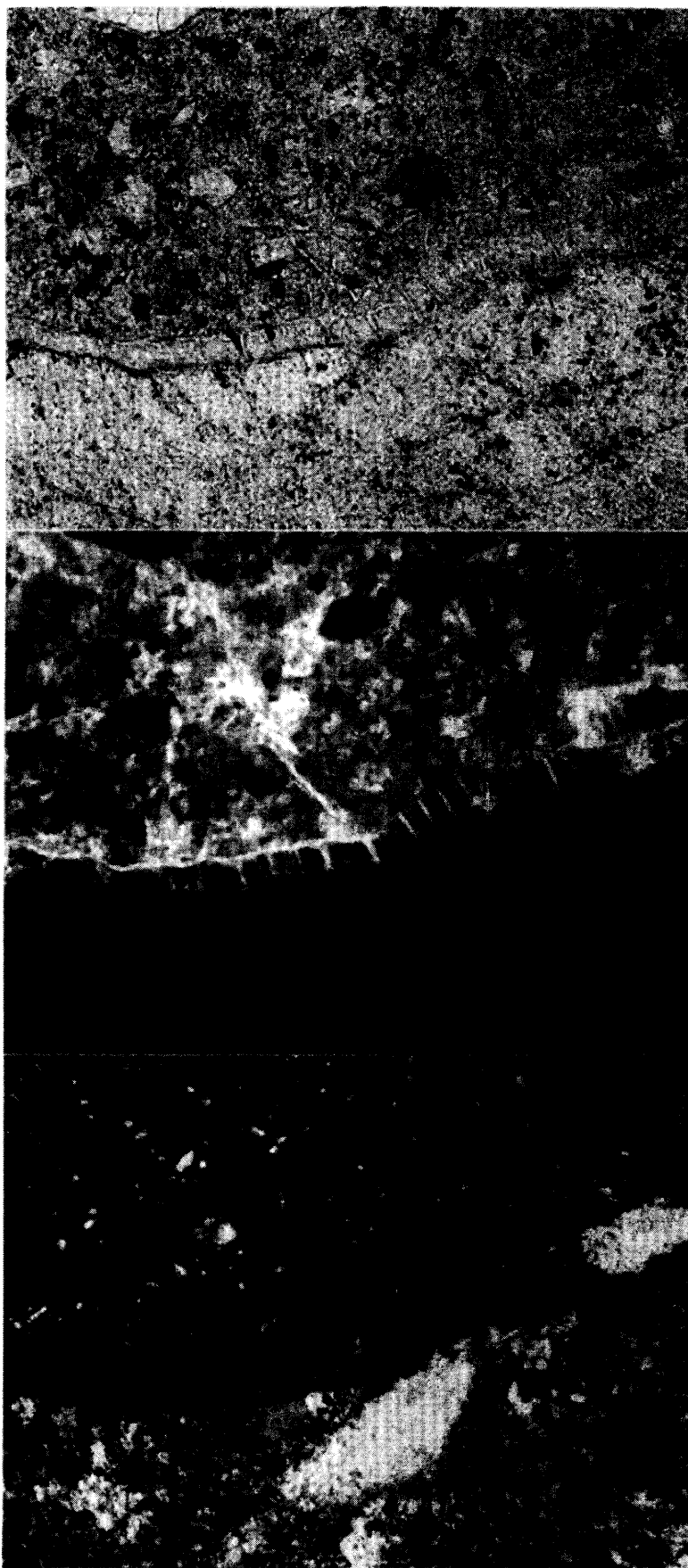
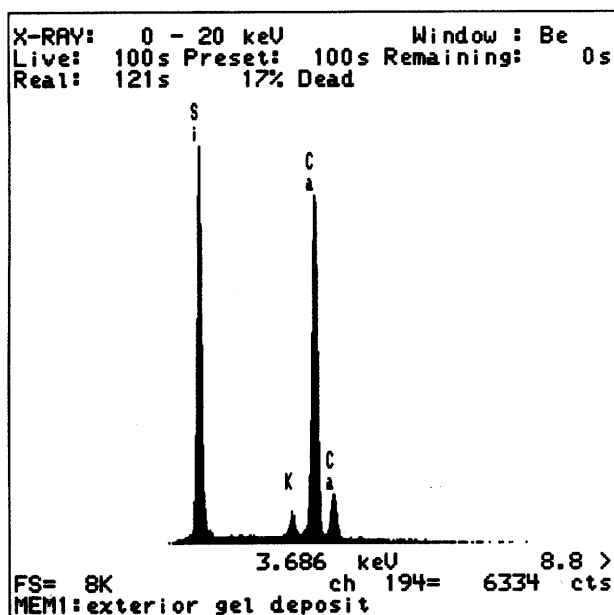
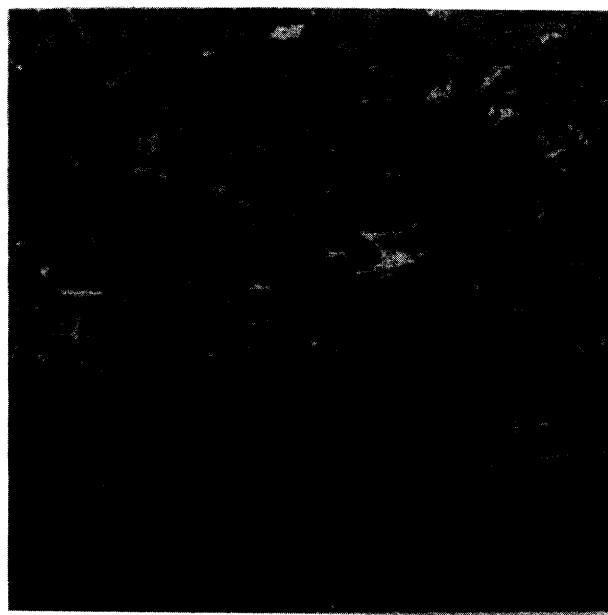


Figure 3-67. Petrographic micrograph of core CA-058-141-001E, thin-section micrographs of ettringite filled crack along contact between coarse aggregate and cement paste. From top to bottom: transmitted plane polarized light, epifluorescent mode, and transmitted cross polarized light (magnified 188x).



(a) Typical spectrum from ASR gel adjacent to volcanic aggregate pictured in (b).



(b) BSE image of ettringite filling a crack along the contact between a coarse aggregate and the cement paste.

Figure 3-68. SEM spectra and micrograph from CA-058-141.

Table 3-28. Summary of 12 analyses of ASR gel deposit shown in figure 3-68.

Element	Average Wt%	Standard Deviation %
Na	0.5	0.3
Mg	0.6	2.3
Al	0.2	0.5
Si	20.4	1.6
S	0.0	0.0
Cl	0.0	0.1
K	0.8	0.6
Ca	28.8	6.0
Ti	0.0	0.0
Mn	0.0	0.0
Fe	0.0	0.1
O	Not Measured	
H	Not Measured	
sum	51.2	

Interpretation and Diagnosis

Having performed the described laboratory analyses and applied the diagnostic flow charts, shown in figures 3-69 through 3-73, two possible MRDs were identified in CA-058-141, including sulfate attack and ASR, with ASR being the dominant MRD. To finalize the diagnosis, the diagnostic tables were consulted. In this case, the diagnostic tables were being used as a review to ensure that no possible MRD was overlooked. The diagnostic features identified in the analysis processes are listed below in table 3-29 along with their associated MRD type and significance as related to this pavement. A brief discussion of each distress is given below:

ASR - In consulting the diagnostic tables, the only other possibility other than ASR is some form of sulfate attack. However, according to the construction records, Type II modified cement was specified, which should provide protection from the moderate sulfate exposure. As a result, ASR is the most likely cause. The reaction was extensive and clearly documented in the laboratory analysis.

External Sulfate Attack - The large amounts of ettringite present are significant but may be opportunistic. Given the fact that Type II cement was used and there was no evidence of ettringite formation within the paste, sulfate attack is ruled out. In general, without clear evidence of ettringite forming within the hardened paste, sulfate attack is unlikely.

Although many would argue that guidelines are not needed on such an "obvious" distress, the guidelines are useful because the analyst is not allowed to make a final judgment until all the data are in. In this case, construction records provided the final piece of data (i.e., the soil sulfate content) and without pulling all sources of data together, clues about other possible distresses may be missed.

Recommended Treatment/Rehabilitation Alternatives

Using the procedures presented in Guideline III in *Volume 2: Guidelines Description and Uses*, feasible treatment and rehabilitation alternatives were selected. The two most significant MRD mechanisms found were ASR and external sulfate attack. Because the two mechanisms are acting in concert, it is difficult to rate the severity of each independently. The distress is characterized by high severity map cracking over the entire pavement surface accompanied by exudates, spalling, and patching. The severity level would thus be assigned as high severity whether it is ASR or sulfate attack. As a result, feasible treatment/rehabilitation alternatives include:

- Rubblization/overlay.
- Recycling.
- Reconstruction.

If recycling is considered, precautions must be taken to avoid ASR and/or sulfate attack in the newly constructed pavement.

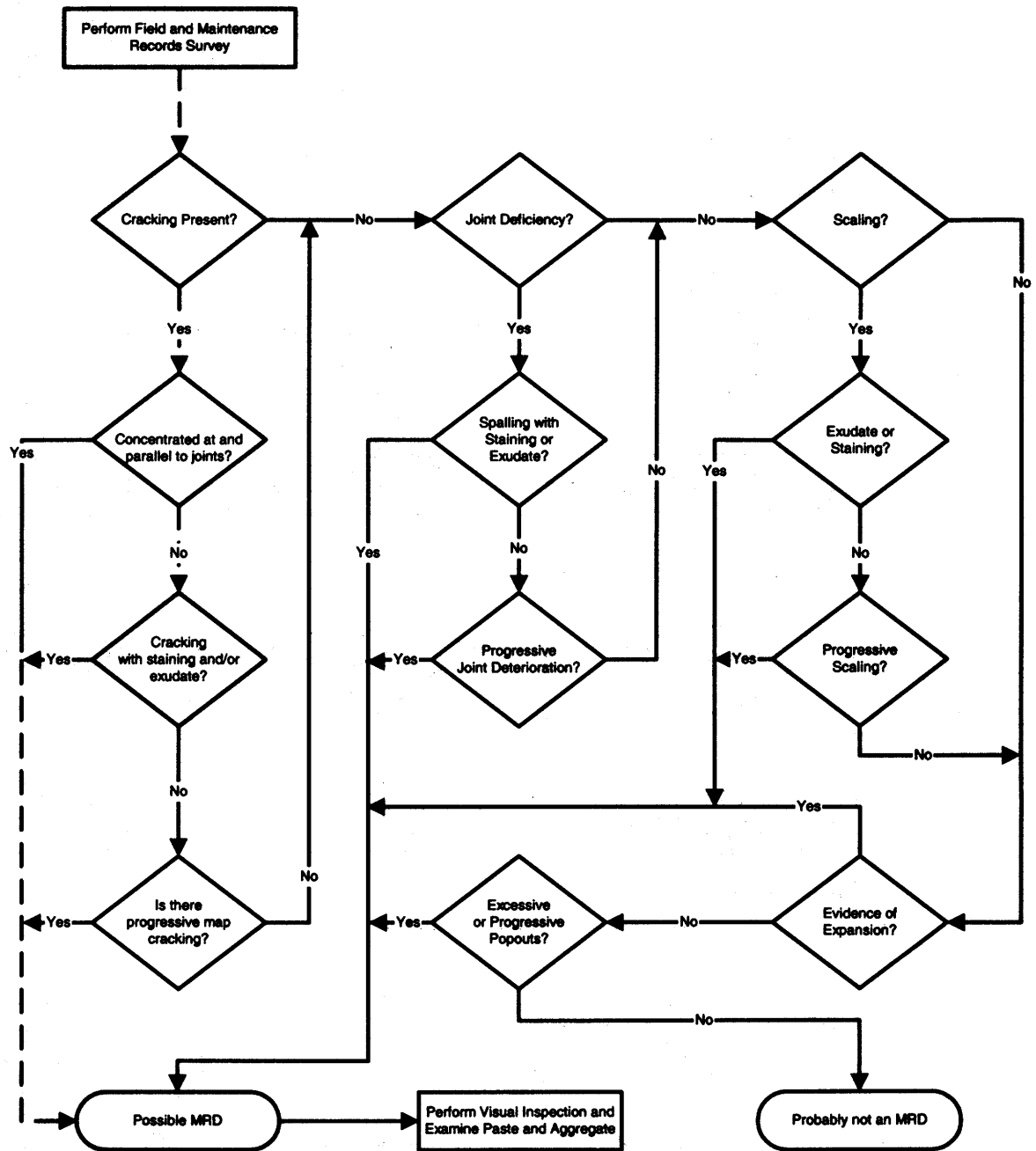


Figure 3-69. Flowchart for assessing the likelihood of MRD causing the observed distress in the pavement as applied to CA-058-141.

Possible Distress	Present		Additional Information
Error in Mix Proportioning	Yes	No	See Recommended Literature
Poor Placement	Yes	No	See Recommended Literature
Poor Finishing/Curing	Yes	No	See Recommended Literature
Poor Steel Placement	Yes	No	See Recommended Literature
Carbonation at Depths > 5-10 mm	Yes	No	See Recommended Literature

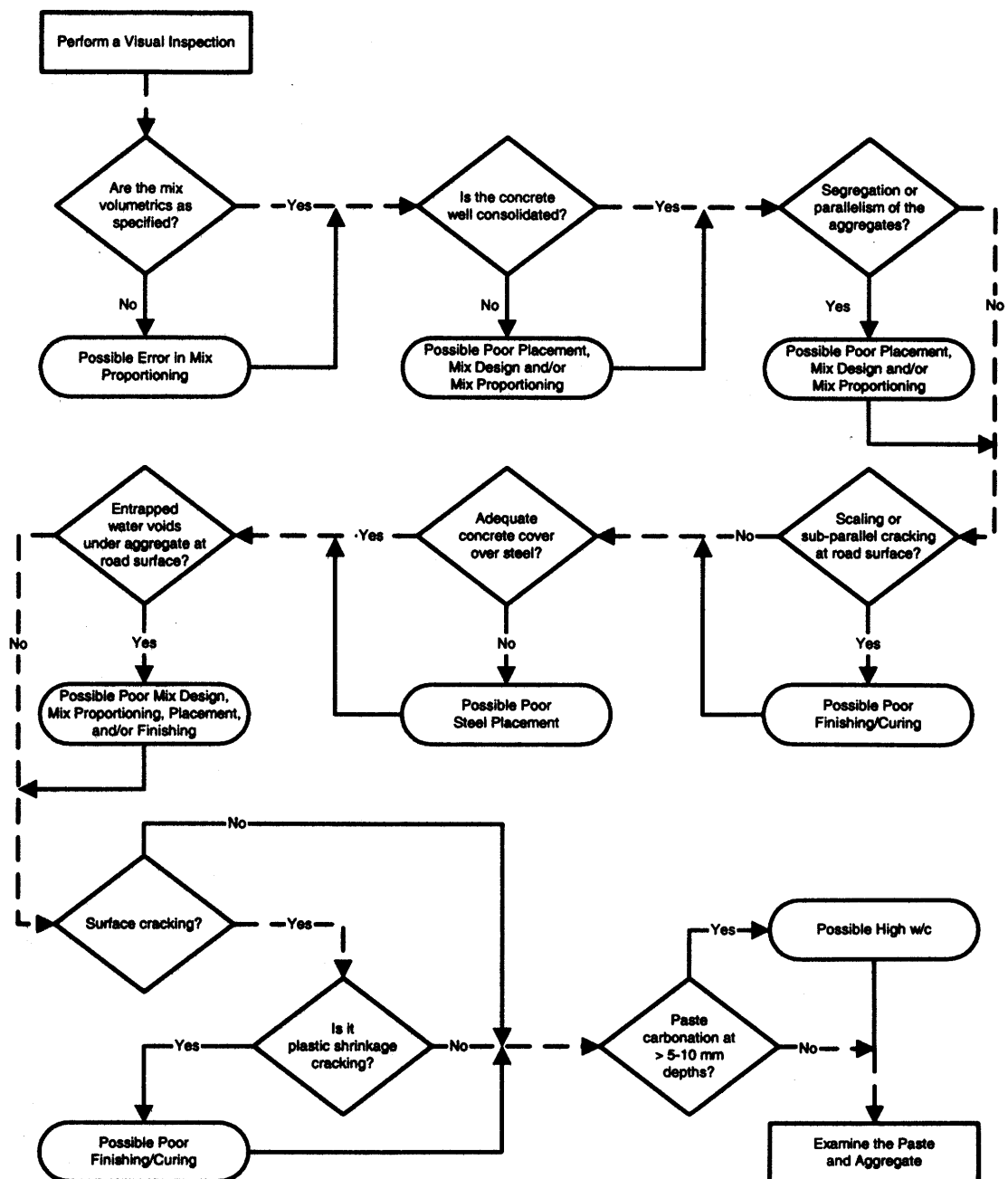


Figure 3-70. Flowchart for assessing general concrete properties based on visual examination as applied to CA-058-141.

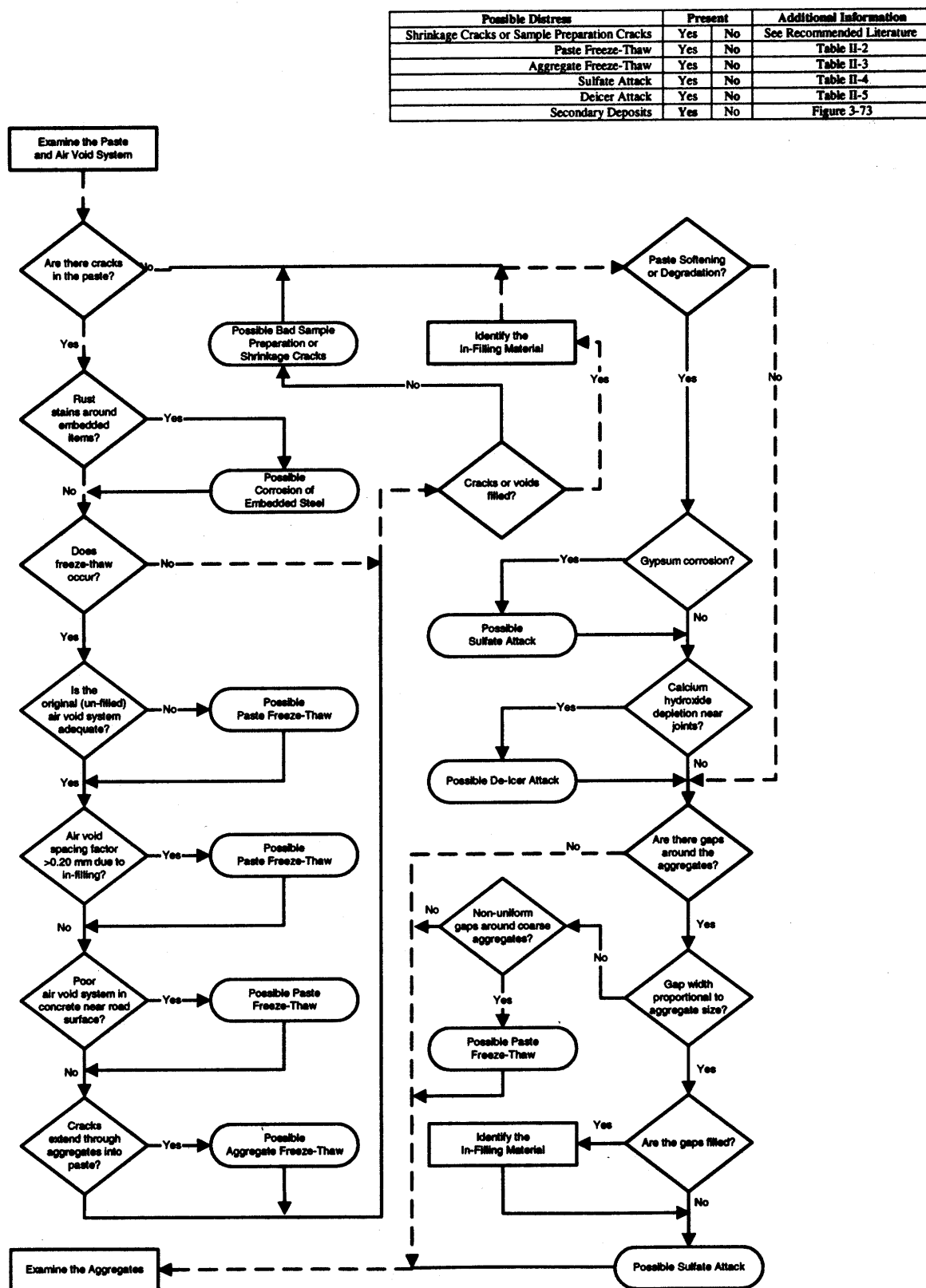


Figure 3-71. Flowchart for assessing the condition of the concrete paste as applied to CA-058-141.

Possible Distress	Present	Additional Information
Natural Cracking of Aggregate	Yes	See Recommended Literature
Sample Preparation Cracks	Yes	See Recommended Literature
Aggregate Freeze-Thaw	Yes	Table II-3
Natural Weathering of Aggregates	Yes	See Recommended Literature
Alkali-Silica Reaction	Yes	Table II-6
Alkali-Carbonate Reaction	Yes	Table II-7
Secondary Deposits	Yes	Figure 3-73

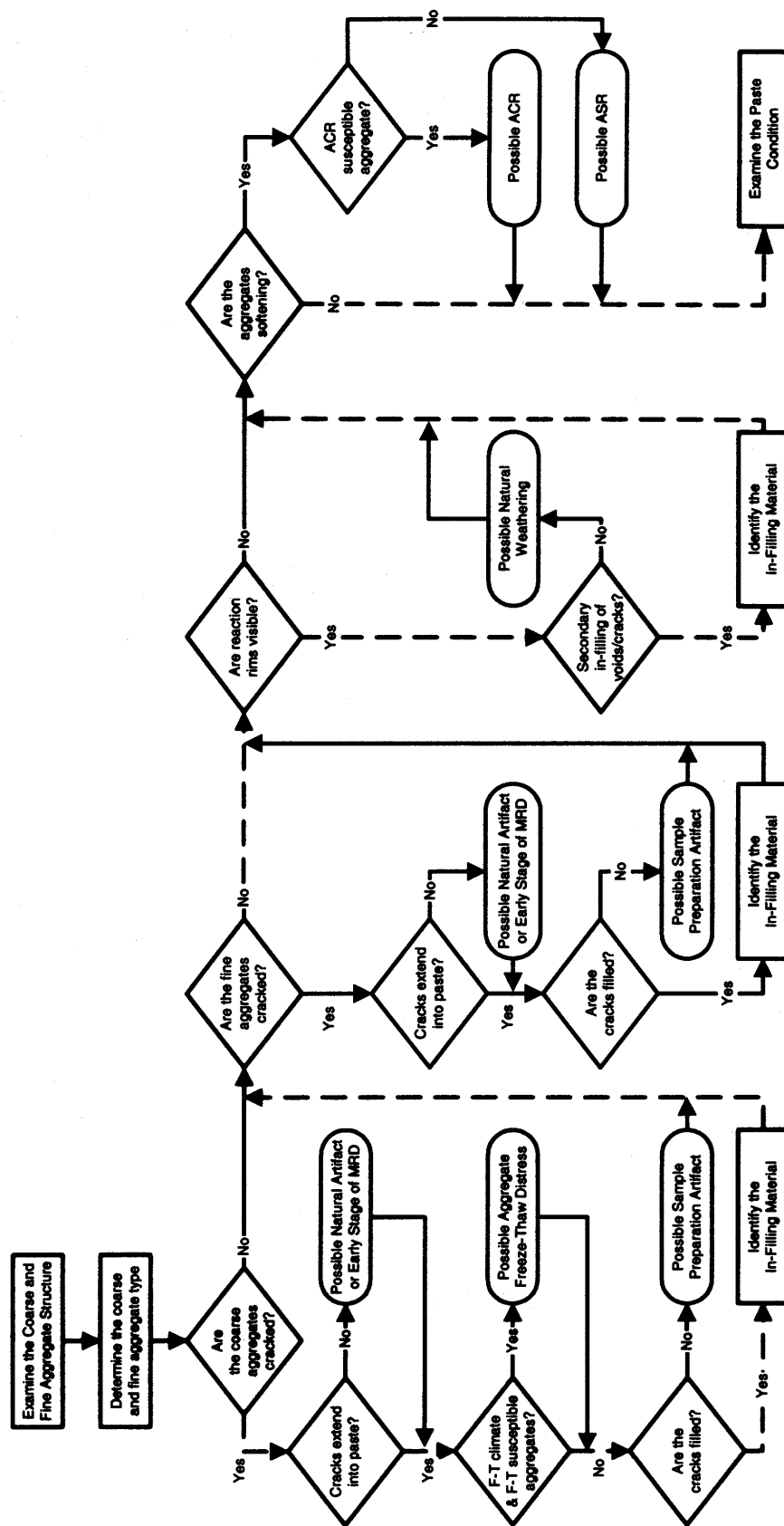


Figure 3-72. Flowchart for assessing the condition of the concrete aggregates as applied to CA-058-141.

Possible Distress	Present	Additional Information
Sulfate Attack	Yes	Table II-4
Deicer Attack	Yes	Table II-5
Alkali-Silica Reaction	Yes	Table II-6
Alkali-Carbonatic Reaction	Yes	Table II-7
Corrosion of Embedded Steel	Yes	Table II-1

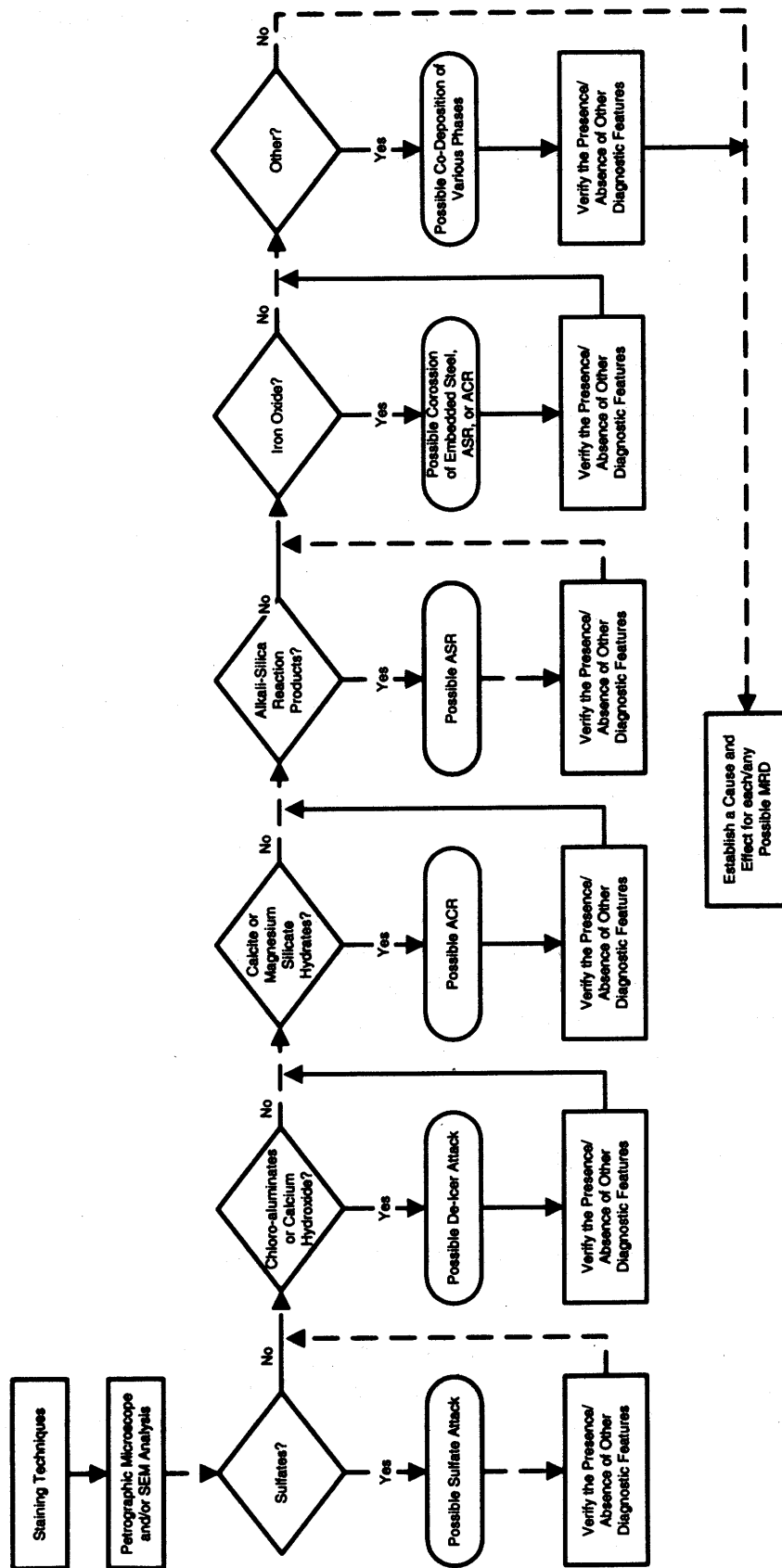


Figure 3-73. Flowchart for identifying infilling materials in cracks and voids as applied to CA-058-141.

Table 3-29. Diagnostic features identified along with their associated MRD type and significance as related to this pavement.

Diagnostic Feature	Method of Characterization	Associated with MRD Type	Significance
Map cracking without exudate		ASR	Medium
ASR reaction products in cracks and voids	Petrographic OM SEM		High
Reaction rims on aggregates	Petrographic OM SEM		Low
Microcracking radiating from reacted aggregates	Stereo OM Petrographic OM		Medium
Significant sulfate deposits in cracks and voids	Staining Stereo OM Petrographic OM SEM	Sulfate attack (both internal and external)	Low
External source of sulfur only	Construction records Chemistry lab analysis	External sulfate attack	Medium

Recommended Prevention Strategies

For the distresses noted, the best preventative strategy is to use a source of aggregate that is not ASR susceptible and a cement type and w/c combination that will not deteriorate under moderate sulfate conditions. Testing in accordance with the guidelines should show that the current aggregate source would be unacceptable without mitigation. Mitigation strategies for ASR include aggregate benefaction using the following strategies:

- Heavy media separation.
- Blending with non-susceptible aggregates.
- Washing.

If aggregate benefaction is not feasible or cost effective, other strategies can also be employed including:

- Reducing the total mixture alkalinity to less than 3 kg/m³.
- Using a blended cement containing a pozzolan or ground slag.
- Through supplementation or addition, use pozzolans or ground slag in the mixture.
- Add lithium nitrate.

Sulfate attack is typically mitigated by using a different cement (such as Type II or V), adding supplementary cementitious materials such as a pozzolan or ground slag, and/or reducing the w/c. For moderate sulfate conditions, Type II, IP(MS), or IS(MS) cement should be used, or a blend of Type I cement and a GGBFS or a pozzolan that has been determined by tests to give equivalent sulfate resistance. Further, a maximum w/c of 0.5 is recommended.

CHAPTER 3. SECONDARY CASE STUDIES

3.1 NEAR MOJAVE, CALIFORNIA (CA-014-011)

Project Description

The California DOT provided several candidate projects and this particular project was selected as a secondary site in the dry-nonfreeze region. The project is located on SR 14 near Mojave, California from MP 2 to 12 in both the northbound and southbound lanes. The project is situated on a four-lane divided highway.

The key design features of this project are presented in table 3-30. The pavement was built in 1972 and includes a 215-mm JPCP surface on a cement-treated base course. The subgrade is sandy material. The transverse joints are skewed and include a random joint spacing pattern of 3.7-4.0-5.8-5.5 m. No means of load transfer (other than aggregate interlock) is provided and neither the transverse or longitudinal joints have been sealed. Both shoulders are paved with an AC surface; the inside shoulder is 1.2 m wide and the outside shoulder is 2.4 m wide.

Table 3-30. Summary of design features for CA-014-011.

Category	Design Feature	Description
General Information	Project limits	MP 2.0 – 12.0
	Highway type	Divided
	Number of lanes	4
	Direction	Northbound/southbound
	Construction date	1972
	Cumulative ESALs	
Pavement Cross Section	Pavement type	JPCP
	PCC slab thickness	215 mm
	Base	CTB
	Subbase	
	Subgrade type	Sand
Transverse Joint	Joint spacing	3.7-4.0-5.8-5.5 m
	Joint skew	1:6
	Load transfer	None
	Sealant type	None
Longitudinal Joint	Load transfer	
	Sealant type	None
Outer Shoulder	Surface type	AC
	Width	2.4 m
Inner Shoulder	Surface type	AC
	Width	1.2 m
Climatic Conditions ¹	Region	Dry-nonfreeze
	Annual precipitation	305 mm
	Freezing index	0 °C-days

¹ Climatic data are for Los Angeles, California.

Distress Survey Results

Due to the similar performance observed throughout the project, only one section was selected for detailed survey. The section begins at milepost 11.0 and extends 150 m to the south. The section is located approximately at grade.

This section exhibits an array of distresses, as summarized in table 3-31. First, over one-half of the slabs contain corner breaks, one-third of which are medium severity. The corner breaks are all located at the acute angle formed at the intersection of a transverse joint and the longitudinal centerline joint. Nearly one-third of the slabs also contain transverse cracks and again many have progressed to medium-severity levels. Several longitudinal cracks are present but all are still low severity. Many of the cracks and corner breaks have been sealed with a hot-pour sealant using a band-aid configuration. Faulting is also problematic, averaging 5.1 mm and 4.0 mm at distances of 0.30 and 0.75 m from the outer slab edge, respectively. Finally, the entire surface area exhibits map cracking consisting of interconnecting transverse and longitudinal surface cracks (this distress is discussed in more detail in the next section of this report).

Table 3-31. Summary of pavement condition surveys for CA-014-011-001.

	Distress Type	Distress Measure	Severity Level			Comments
			Low	Moderate	High	
Cracking	Corner Breaks	number	12	6	0	
	Longitudinal Cracking	linear meters	8.5	0.0	0.0	
	Transverse Cracking	number of cracks	6	4	0	
		linear meters	17.8	14.8	0.0	
		percent of slabs	31			
Transverse Joints	Sealant		n/a			joints not sealed
	Spalling	number	1	2	0	
		linear meters	0.4	0.5	0.0	
	Faulting	millimeters	5.1			measured at 0.30 m
		millimeters	4.0			measured at 0.75 m
Long-Joints	Width	millimeters	5.8			
	Sealant		n/a			joints not sealed
	Spalling	linear meters	0.0	0.0	0.0	
	Shoulder Dropoff	millimeters	18.2			
Surface Conditions	Map Cracking	number of slabs	32			all slabs
		square meters	561.0			entire area
	Scaling	number of slabs	0			
		square meters	0.0			
	Polished Aggregate	square meters	0.0			
	Popouts	number/sq. meter	0.0			
Other	Blowups	number	0			
	Flexible Patches	number	0	0	0	
		square meters	0.0	0.0	0.0	
	Rigid Patches	number	0	0	0	
		square meters	0.0	0.0	0.0	
	Pumping/Bleeding	number	0			
		linear meters	0.0			

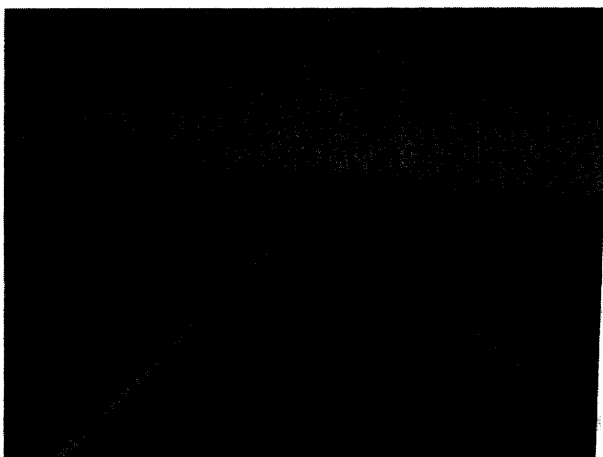
MRD Field Characterization

A more detailed evaluation of the potential MRDs was conducted during the visual surveys. The key characteristics of these distresses are summarized in table 3-32. Although such an evaluation cannot be used to provide a definite diagnosis, it can provide useful information in conjunction with the laboratory investigation.

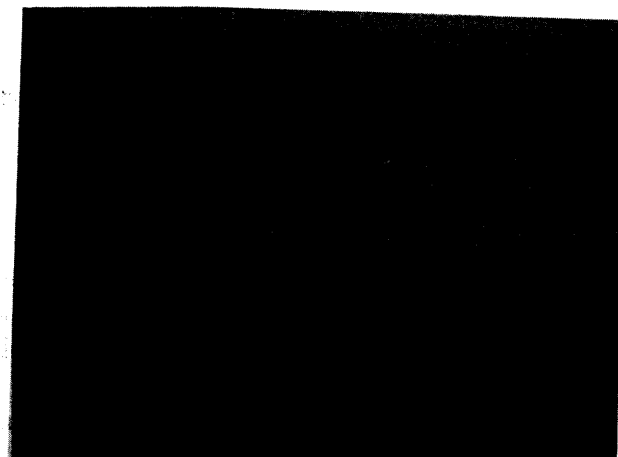
The potential MRD is characterized by map cracking over the entire pavement surface. These cracks, made up of multiple interconnecting surface cracks, form a honeycomb pattern on the pavement surface. The cracks are generally hairline cracks but are more visible in the wheel paths because they are slightly more open. No staining or exudate was observed within or surrounding the cracks and joints. Figure 3-74 shows the typical site conditions.

Table 3-32. Summary of MRD characterization for CA-014-011.

Description		Section 001	Comments
Cracking	Location	Entire slab	More prevalent in wheel paths
	Orientation/shape	Honeycomb	
	Extent	Entire slab	
	Crack size	Hairline	
Staining	Location	None	
	Color	n/a	
Exudate	Present	None	
	Color	n/a	
	Extent	n/a	
Scaling	Location	None	
	Area of surface	n/a	
	Depth	n/a	
Vibrator Trails	Visible	None	
	Discolored	n/a	
	Distressed	n/a	
	Change in texture	n/a	



(a) Section overview



(b) Close up of observed map cracking

Figure 3-74. Typical conditions at CA-014-011.

Laboratory Analysis

Core selection/Visual Inspection

Through visual examination, the aggregate type was determined to be granitic crushed gravel. The fine aggregate was the same rock type as the coarse aggregate. In examining all pavements in this study, the flowchart for assessing the likelihood of MRD (figure II-14 in Guideline II) was used to determine if the distress is most likely an MRD. For the previous sites, this flowchart always determined that an MRD was probable and it wasn't discussed. For this site, figure II-14 yielded the answer of probably not an MRD. Although a map cracking pattern was observed on the pavement surface, as shown in figures 3-74(b) and 3-75, it was thought to be shrinkage cracks, given the nature of the cracks, the slow progression of the distress, and the age of the pavement (28 years). However, to be confident of our visual assessment, it was decided to examine core E in the laboratory since a definitive assessment of a possible MRD cannot be performed without examining the concrete with a stereo optical microscope.

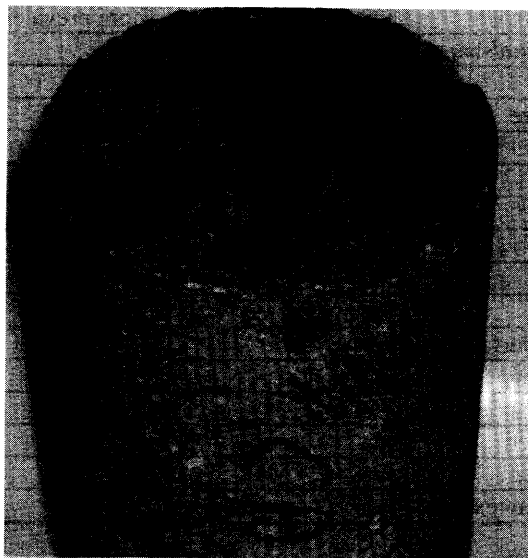


Figure 3-75. Map cracking pattern on core CA-014-011-001E, emphasized by wetting down the surface.

Stereo Optical Microscopy

The stereo optical microscope was used to examine the cracking and trace its path back into the specimen. The surface cracks pass through the paste, some go around aggregates, and some go through aggregates. Cracks are wide and irregular in cross-section near pavement surface, but narrow as the crack descends into the pavement. To image these diagnostic features, a conventional flatbed scanner hooked to a PC was used. The flatbed scanner is a convenient way to get an image that, when scanned in at high resolution (e.g., 1200-2400), can be zoomed digitally and viewed magnified on the computer monitor. This is a fast and easy way of documenting polished slabs.

In figure 3-76, a crack is seen that runs the length of the image. It starts wide at the top and narrows as it goes deeper into the concrete, jogging around one large aggregate grain. That portion of the crack is typical of plastic shrinkage, wide and irregular at the pavement surface, where the paste was soft and cracked preferentially. The rest of the crack is more typical of drying shrinkage where much larger stresses are applied to the aggregates as the paste hardens with time. Stresses build to the point where the crack already started at the surface propagates through an aggregate and continues. Figure 3-77 is a normal scan of the same specimen. Some darkened rims are evident on the coarse aggregate, which is typical of ASR.

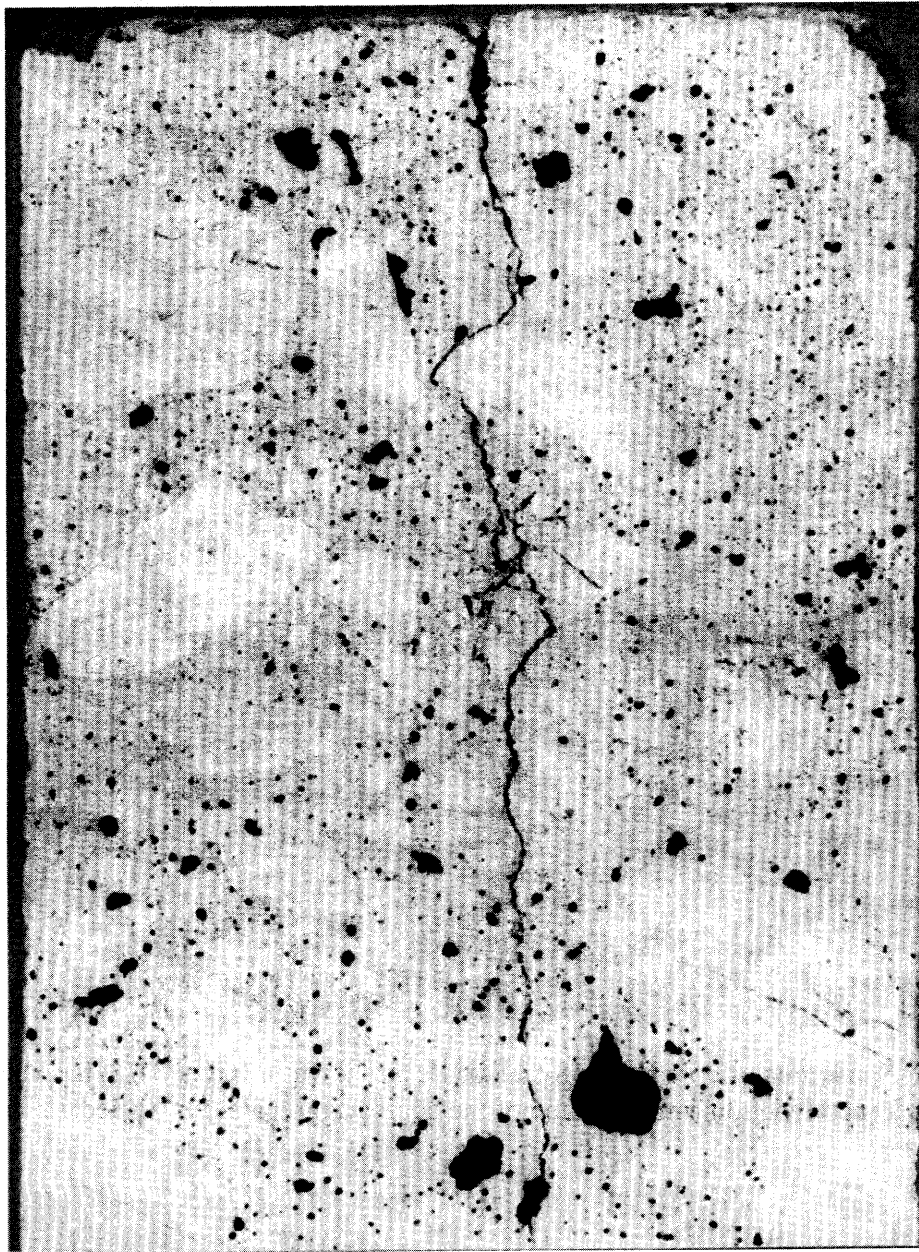


Figure 3-76. Inverse image of polished cross section of core CA-014-011-001E, through pavement, after painting the surface black and pressing white powder into the voids and cracks (magnified 1.5x).

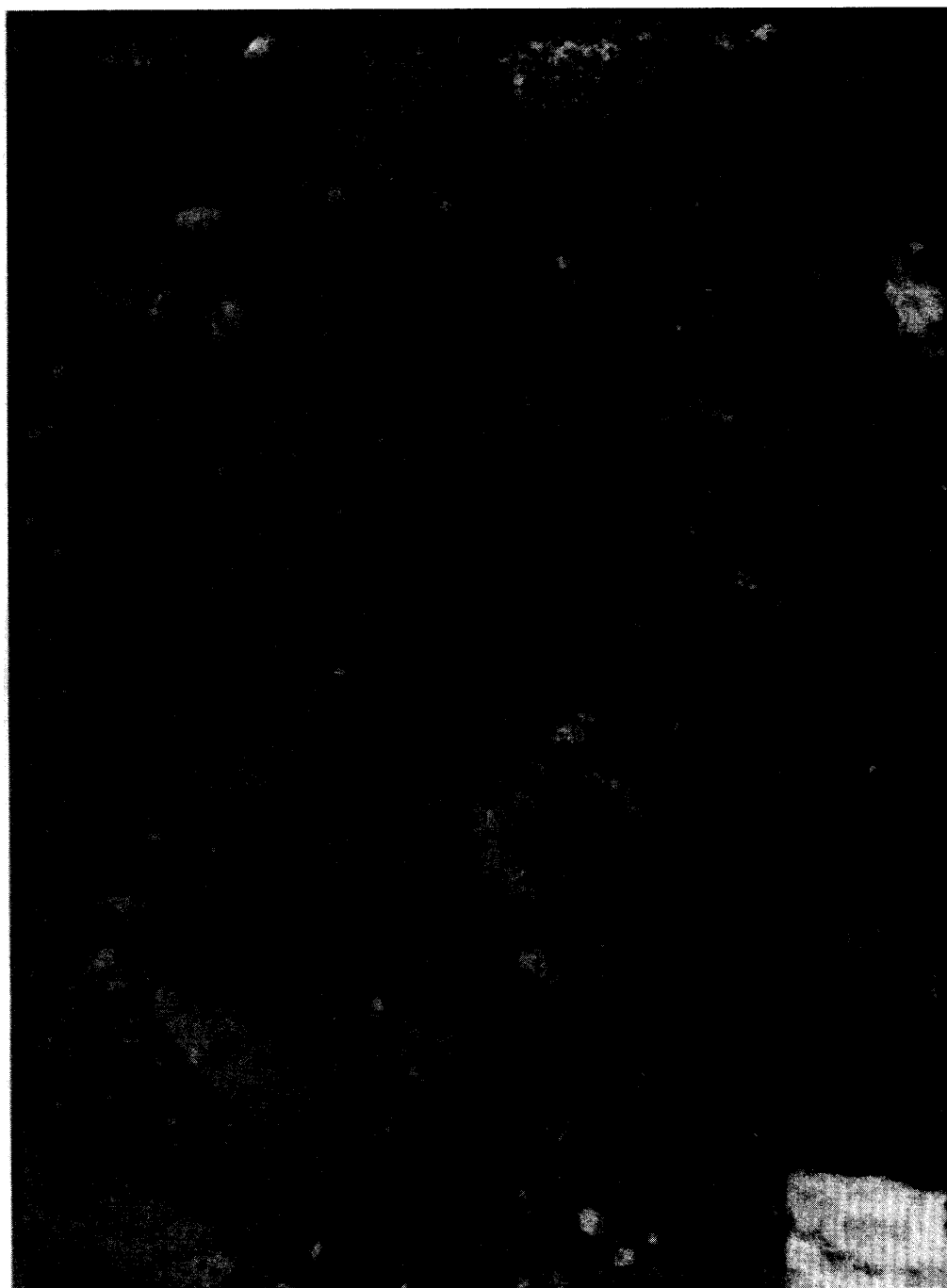


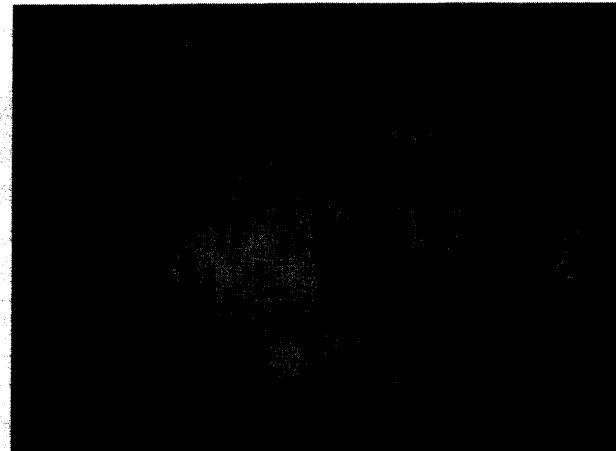
Figure 3-77. Same area of core CA-058-011-001E as shown in figure 3-78, included to show darkened reaction rims on some of the coarse aggregate (magnified 1.5x).

Staining Tests

The sodium cobaltinitrite and barium chloride/potassium permanganate stains were applied and both were positive meaning ASR reaction products and sulfate minerals were present in the concrete. Micrographs showing ASR reactive particles and ettringite inclusions are shown below in figure 3-78. Also the phenolphthalein stain was used to determine the depth of carbonation. This slab was scanned and is shown in figure 3-79. Note the areas of deeper carbonation in the vicinity of the plastic shrinkage crack, indicating the increased permeability of the cracked surface.



(a) Yellow sodium cobaltinitrite stain for ASR gel in cracks associated with granitic coarse aggregate



(b) Ettringite filled air voids that have picked up the purple to pink stain from the solution of barium chloride and potassium permanganate

Figure 3-78. Results of staining test applied to core CA-058-011-001E.

Interpretation and Diagnosis

This site provides an excellent case for demonstrating the value of the guidelines. First, through the rigorous field inspection, it was decided that an MRD was likely not the cause of the observed distress. The logic for this conclusion is shown in figure 3-80. But it was believed that laboratory work should be conducted to verify this conclusion. As discussed in Guideline II, to reach a diagnosis, the concrete must be observed using stereo microscopy. Because of this examination, the true nature of the surface cracking was documented, confirming the field evaluation. In addition, it was determined that there were diagnostic features of MRD, specifically ASR reaction products. Mild infilling of air voids and cracks with ettringite was also observed but not considered significant.

Having performed the necessary laboratory analyses and applying the diagnostic flowcharts, no possible MRDs were identified in CA-058-011. To finalize the diagnosis, the diagnostic tables were consulted. From the tables only two possible distresses were identified, including ASR and sulfate attack. The diagnostic features identified in the analysis processes are listed below in table 3-33 along with their associated MRD type and significance as related to this pavement. A brief discussion follows of each possible MRD identified in the laboratory analysis:



Figure 3-79. Phenolphthalein stained polished slab, showing carbonation along plastic shrinkage crack (magnified 1.5x).

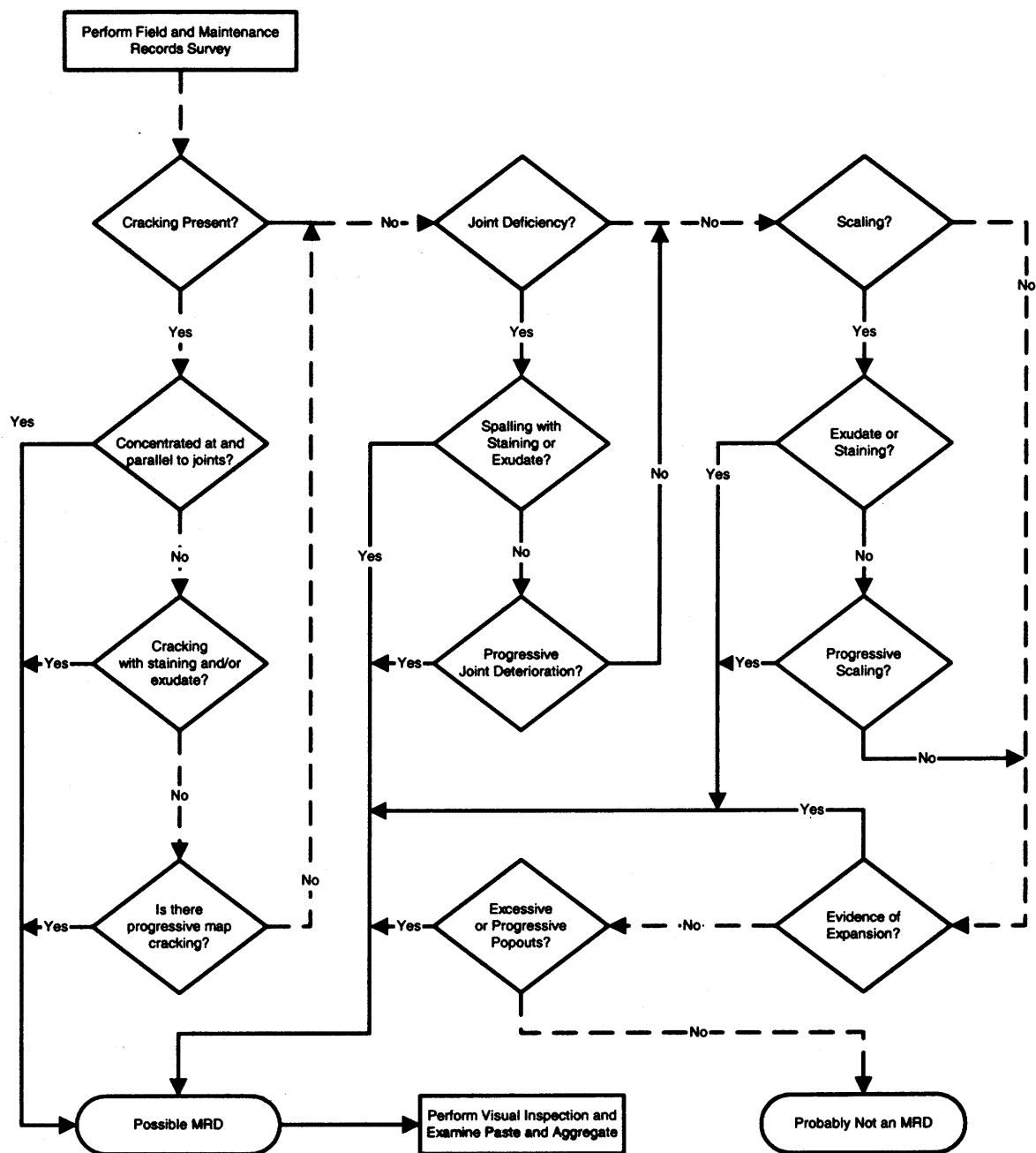


Figure 3-80. Flowchart for assessing the likelihood of MRD causing the observed distress in the pavement as applied to CA-014-011.

ASR - ASR is certainly occurring in this pavement, but at this time there is little to no distress resulting from ASR. Additionally, there are no cracks associated with the ASR reaction products found in this concrete. These reaction products are filling adjacent voids and cracks within the aggregate. It is thus concluded that the ASR is not currently deleterious and is not a major contributor to the distress of this pavement at this time. Monitoring the pavement condition over time will demonstrate whether this distress is progressive, possibly helping engineers in planning maintenance schedules if the ASR does become deleterious.

Sulfate Attack - This is highly unlikely as the only signs of sulfate attack was some moderate infilling of air voids, perfectly normal in good quality concrete. Also, this pavement was constructed using Type II modified cement that helps to prevent sulfate attack at a moderate exposure level. Sulfate attack is not a major contributor to the distress of this pavement at this time.

In summary, applying the guidelines as proposed provided information for engineers that can help establish a maintenance program for this pavement, thereby extending its life. Specifically, shrinkage cracks propagating with time and applied load are the most probable cause of the distress. As the concrete becomes more permeable as a result of the cracking, opportunistic MRDs occur such as ASR. Some mitigation of ASR may be appropriate.

Table 3-33. Diagnostic features identified along with their associated MRD type and significance as related to CA-014-001.

Diagnostic Feature	Method of Characterization	Associated with MRD Type	Significance
Map cracking without exudate	Visual Stereo OM	ASR	Low
ASR reaction products in voids	Visual Staining Stereo OM		Low
Reaction rims on aggregates	Visual Stereo OM		Low
Some sulfate deposits in cracks and voids	Visual Stereo OM	Sulfate attack (both internal and external)	Low

3.2 SR 2 NEAR IOWA-NEBRASKA BORDER (IA-002-002)

Project Description

This project is located on SR 2 in Iowa near the Nebraska border; the closest city to the project site is Nebraska City, Nebraska. The Iowa DOT indicated that the pavement surface had a slight map cracking pattern over about 60 percent of the pavement area. This project was thus selected as a secondary test site in the wet-freeze climatic region. This area receives approximately 760 mm of precipitation per year and has a freezing index of 580 °C-days.

The project, located in both the eastbound and westbound lanes from MP 2.09 to 3.59, is situated on a four-lane divided highway. The project was constructed in 1986. The pavement cross section includes a 240-mm JPCP and a 150-mm granular base course. The transverse joints are

skewed at a 1:6 ratio, spaced at 6.1-m intervals, and contain 32-mm dowel bars for load transfer. The longitudinal and transverse joints are both sealed with a hot-pour sealant. The inside and outside shoulders, which are surfaced with AC, are 3.0 and 1.2 m wide, respectively. Specific design features for the project are summarized in table 3-34.

Table 3-34. Summary of design features for IA-002-002.

Category	Design Feature	Description
General Information	Project limits	MP 2.09 – 3.59
	Highway type	Divided
	Number of lanes	4
	Direction	Eastbound/westbound
	Construction date	1986
	Cumulative ESALs	> 2,500,000
Pavement Cross Section	Pavement type	JPCP
	PCC slab thickness	240 mm
	Base	150-mm granular
	Subbase	
	Subgrade type	Glacial clay
Transverse Joint	Joint spacing	6.1 m
	Joint skew	1:6
	Load transfer	32-mm dowels
	Sealant type	Hot-pour
Longitudinal Joint	Load transfer	
	Sealant type	Hot-pour
Outer Shoulder	Surface type	AC
	Width	3.0 m
Inner Shoulder	Surface type	AC
	Width	1.2 m
Climatic Conditions ¹	Region	Wet-nonfreeze
	Annual precipitation	760 mm
	Freezing index	580°C-days

¹ Climatic data are for Omaha, Nebraska.

Distress Survey Results

Two sections were selected for survey within this project, both of which are located in the westbound, outer traffic lane. Section 001 begins at Station 1513+60 and Section 002 begins at Station 1495+00. Both sections are located approximately at grade.

The performance of each section is summarized in tables 3-35 and 3-36. It is observed from these tables that both sections are performing similarly. Section 001 contains two transverse cracks—one low severity and one medium severity—and Section 002 contains only one low-severity transverse crack. Short longitudinal cracks, which appear to be more than surface cracks, are also present throughout both sections. These cracks are generally confined to the wheel paths. Spalling is exhibited on a few transverse joints but is limited to low severity. The ride quality is not affected by the faulting.

MRD Field Characterization

A characterization of potential MRD was conducted in the field to assist in the diagnosis of the type and cause of the distress. The potential MRD on both sections is the presence of short longitudinal cracks throughout the sections. These cracks are generally confined to the wheel paths and in many cases initiate at a transverse joint. There is some slight staining, which is brownish-gray in appearance, around transverse joints and in the wheel paths. There is no exudate observed at the cracks. Table 3-37 provides a summary of the MRD characteristics for this project. Figure 3-81(a) shows staining along longitudinal cracks and at the transverse joints. Figure 3-81(b) shows closeup views of the hairline cracks. Additional site conditions are shown in figure 3-82.

Laboratory Analysis

Core Selection/Visual Inspection

The distresses observed at both sections were similar, and appeared to be concentrated at the joints. Core A was selected from Section 001 for analysis. Core A exhibited hairline cracking at the pavement surface, and a large crack near the base running parallel to the subbase contact. Figure 3-83 shows a polished slab from core A. Other than the visible cracks, the concrete seemed in good condition. The coarse aggregate consisted of a blend of a quarried limestone and pink granite.

Stereo Optical Microscopy

The most striking feature of the concrete was the abundance of small, entrained air voids, as shown in figure 3-84. Although the concrete did contain a large percentage of air, the specific surface and spacing factors were within reasonable values. A summary of the Modified Point Count is included in table 3-38. There was moderate infilling of the void structure by secondary ettringite. Some isolated alkali-silica gel deposits were observed with some of the fine aggregate particles. The gel deposits were found filling air voids near the reactive particles, and were not associated with any cracking. The coarse aggregates were intact, and did not appear to be reactive.

Table 3-35. Summary of pavement condition surveys for IA-002-002-001.

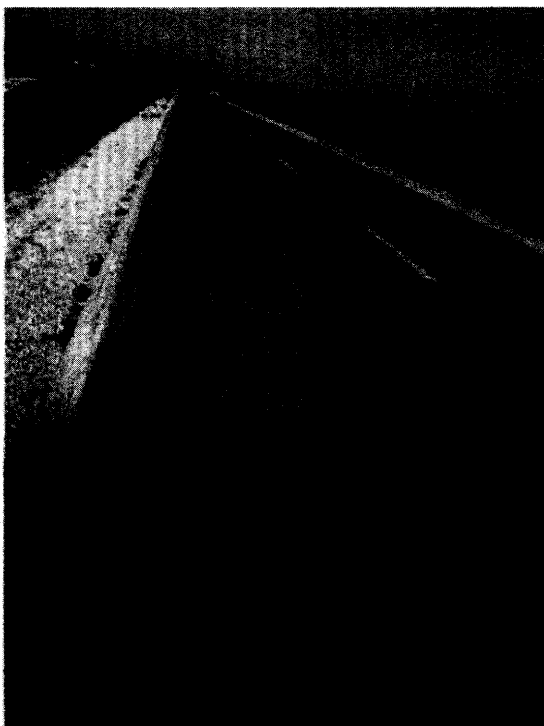
	Distress Type	Distress Measure	Severity Level			Comments
			Low	Moderate	High	
Cracking	Corner Breaks	number	0	0	0	
	Longitudinal Cracking	linear meters	14.0	0.0	0.0	
	Transverse Cracking	number of cracks	1	1	0	
		linear meters	0.2	3.7	0.0	
		percent of slabs	8			
Transverse Joints	Sealant		good condition			hot-pour sealant
	Spalling	number	5	0	0	
		linear meters	1.5	0.0	0.0	
	Faulting	millimeters	1.1			measured at 0.30 m
		millimeters	0.8			measured at 0.75 m
	Width	millimeters	10.5			
Long Joints	Sealant		good condition			hot-pour sealant
	Spalling	linear meters	0.0	0.0	0.0	
	Shoulder Dropoff	millimeters	26.8			
Surface Conditions	Map Cracking	number of slabs	0			
		square meters	0.0			
	Scaling	number of slabs	0			
		square meters	0.0			
	Polished Aggregate	square meters	0.0			
	Popouts	number/sq. meter	0.0			
Other	Blowups	number	0			
	Flexible Patches	number	0	0	0	
		square meters	0.0	0.0	0.0	
	Rigid Patches	number	0	0	0	
		square meters	0.0	0.0	0.0	
	Pumping/Bleeding	number	0			
		linear meters	0.0			

Table 3-36. Summary of pavement condition surveys for IA-002-002-002.

	Distress Type	Distress Measure	Severity Level			Comments
			Low	Moderate	High	
Cracking	Corner Breaks	number	0	0	0	
	Longitudinal Cracking	linear meters	3.0	0.0	0.0	
	Transverse Cracking	number of cracks	1	0	0	
		linear meters	1.5	0.0	0.0	
		percent of slabs	4			
Transverse Joints	Sealant		good condition			hot-pour sealant
	Spalling	number	1	0	0	
		linear meters	0.3	0.0	0.0	
	Faulting	millimeters	1.0			measured at 0.30 m
		millimeters	0.8			measured at 0.75 m
	Width	millimeters	10.5			
Long. Joints	Sealant		good condition			hot-pour sealant
	Spalling	linear meters	0.0	0.0	0.0	
	Shoulder Dropoff	millimeters	22.4			
	Map Cracking	number of slabs	0			
Surface Conditions		square meters	0.0			
	Scaling	number of slabs	0			
		square meters	0.0			
	Polished Aggregate	square meters	0.0			
	Popouts	number/sq. meter	0.0			
	Blowups	number	0			
Other	Flexible Patches	number	0	0	0	
		square meters	0.0	0.0	0.0	
	Rigid Patches	number	0	0	0	
		square meters	0.0	0.0	0.0	
	Pumping/Bleeding	number	0			
		linear meters	0.0			

Table 3-37. Summary of MRD characterization for IA-002-002.

Description		Section 001	Section 002	Comments
Cracking	Location	Wheel paths	Wheel paths	Most cracks initiate at joints
	Orientation/shape	Parallel to longitudinal joint	Parallel to longitudinal joints	
	Extent	Wheel paths	Wheel paths	
	Crack size	Hairline	Hairline	
Staining	Location	Joints/wheel paths	Joints/wheel paths	
	Color	Brownish-gray	Brownish-gray	
Exudate	Present	None	None	
	Color	n/a	n/a	
	Extent	n/a	n/a	
Scaling	Location	None	None	
	Area of surface	n/a	n/a	
	Depth	n/a	n/a	
Vibrator Trails	Visible	None	None	
	Discolored	n/a	n/a	
	Distressed	n/a	n/a	
	Change in texture	n/a	n/a	



(a) Staining along longitudinal cracks



(b) Staining along transverse joints

Figure 3-81. Site conditions at IA-002-002.



(a)



(b)

Figure 3-82. Closeup view of longitudinal hairline cracks.



Figure 3-83. Polished slab from core IA-002-002-001A. The irregular surface along the left-hand side of the core is a cross-sectional view of the transverse joint texture.

Table 3-38. Air-void characteristics of core IA-002-002-001A as determined by ASTM C457.

Core	Original		Existing	
	Air Content (vol. %)	Spacing Factor (mm)	Air Content (vol. %)	Spacing Factor (mm)
Site 1 Core C	8.73	0.213	8.59	0.216

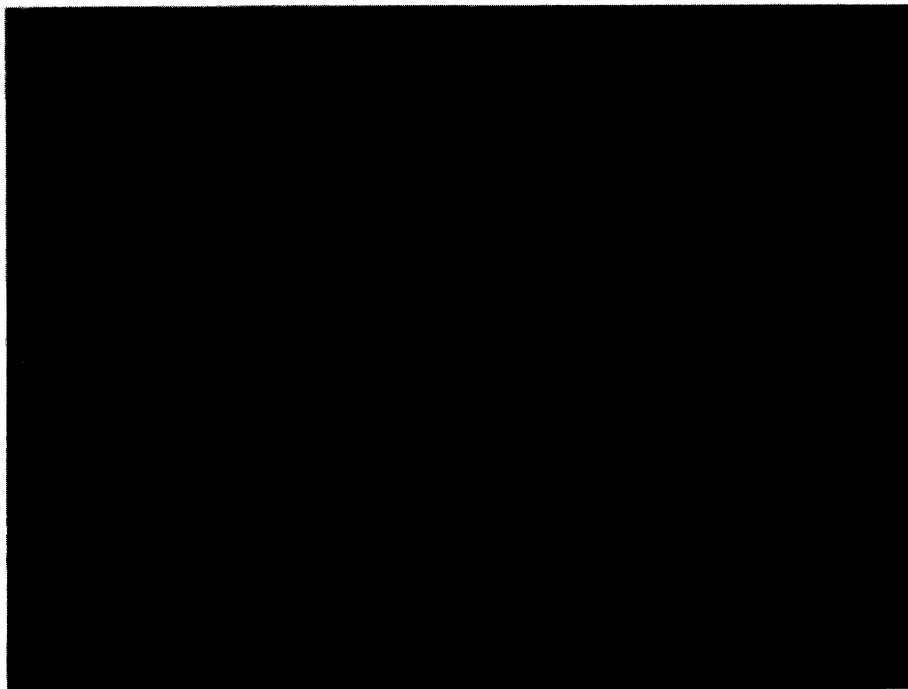


Figure 3-84. Stereo micrograph showing air void structure of IA-002-002-001A, magnified 7.5x.

Petrographic Optical Microscopy

Areas observed to contain reactive fine aggregate particles were prepared in thin section. Figure 3-85 shows a reactive particle that has undergone dissolution, cracking, and the reaction product has filled some neighboring air voids. The reactive particles, which appear to be volcanic in origin with phenocrysts in a very fine matrix, are likely to have originated from much further west, and been brought to the area by the Missouri River. The air-void structure has experienced limited infilling by secondary ettringite.

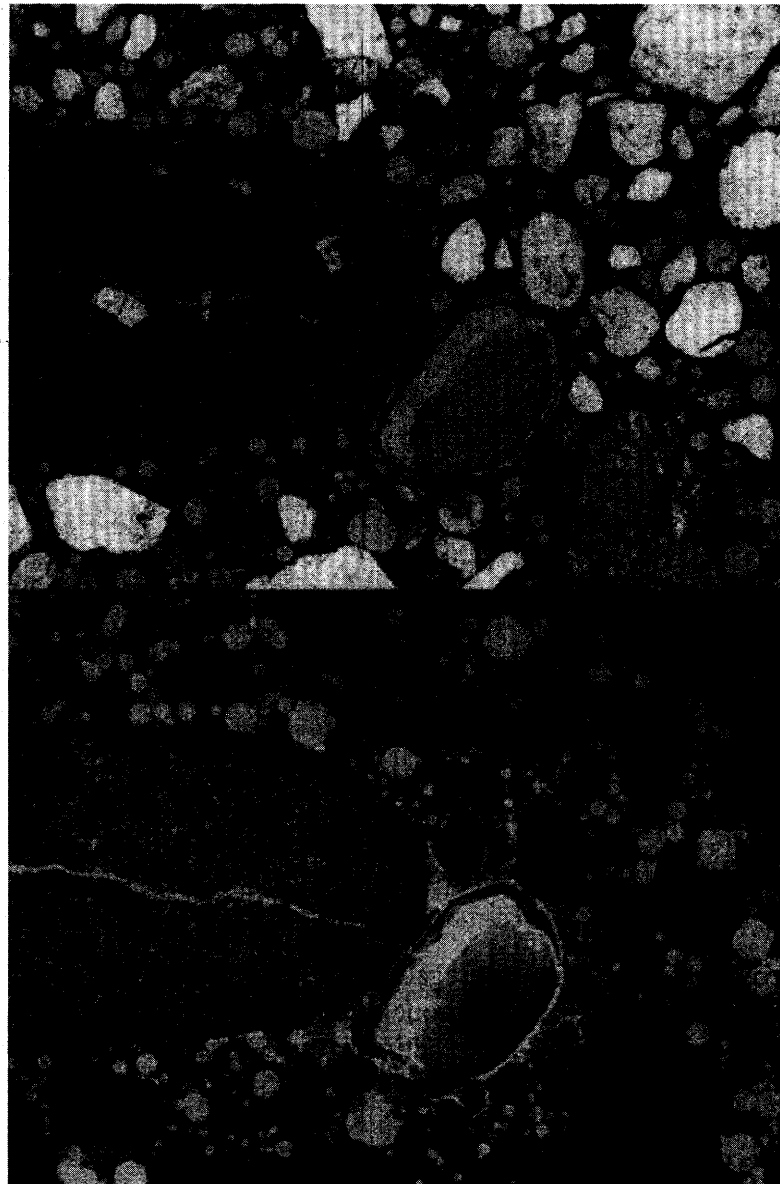


Figure 3-85. Reactive fine aggregate particle with alkali-silica gel filled air voids as viewed in thin section. Top image is transmitted plane polarized light, bottom image is in epifluorescent mode, magnified 20x.

Interpretation and Diagnosis

Although the concrete exhibits signs of distress such as hairline longitudinal cracking with staining in addition to staining at the transverse joints, it is still performing well. Some ASR was present in the fine aggregate, although it did not seem to be associated with any cracking. The air-void content was unusually high, over 8 percent, with an abundance of small-entrained air voids that were sometimes coalesced into dense groupings.

Having performed the described laboratory analyses and applied the diagnostic flowcharts, as shown in figures 3-86 through 3-90, three possible MRDs were identified in IA-002-002, including paste freeze-thaw, ASR and sulfate attack with none being dominant or extensive. To

finalize the diagnosis, the diagnostic tables were consulted. The diagnostic features identified in the analysis processes are listed below in table 3-39 along with their associated MRD type and significance as related to this pavement. A brief discussion of each distress is given below.

ASR – The ASR occurring in this pavement was not extensive and did not seem to be related to any of the observed cracking. As a result, ASR is not considered to be a major cause of the observed MRD. This does not rule out ASR in its early stages as being present.

Paste Freeze-Thaw – The only diagnostic feature of paste freeze-thaw present was the marginal air-void system in terms of the measured Powers spacing factor. This is considered to be a diagnostic feature of low significance given the fact that no other diagnostic feature of paste freeze-thaw was seen. As a result, paste freeze-thaw is not considered to be a major cause of the observed distress.

Sulfate Attack – The only diagnostic feature of sulfate attack was ettringite infilling in entrained air voids. This was considered a low significance diagnostic feature for a variety of reasons. First, ettringite deposits by themselves are not diagnostic of sulfate attack. Second, the amount of infilling was limited, not extensive. Finally, no other diagnostic feature of sulfate attack was observed. Therefore, sulfate attack is ruled out as a major cause of the observed distress.

In summary, the exact nature of the observed distress is not known. The unusual air-void structure may be a contributor but the exact mechanism could not be discerned from this analysis. It is noted that the concrete had a very fine coarse aggregate grading, which may also be a contributing factor but, again, no evidence of a specific mechanism for the observed distress was seen related to this gradation. The guidelines do help rule out the obvious types of MRD but in the end, this is an example of a pavement that cannot be absolutely diagnosed using the developed guidelines.

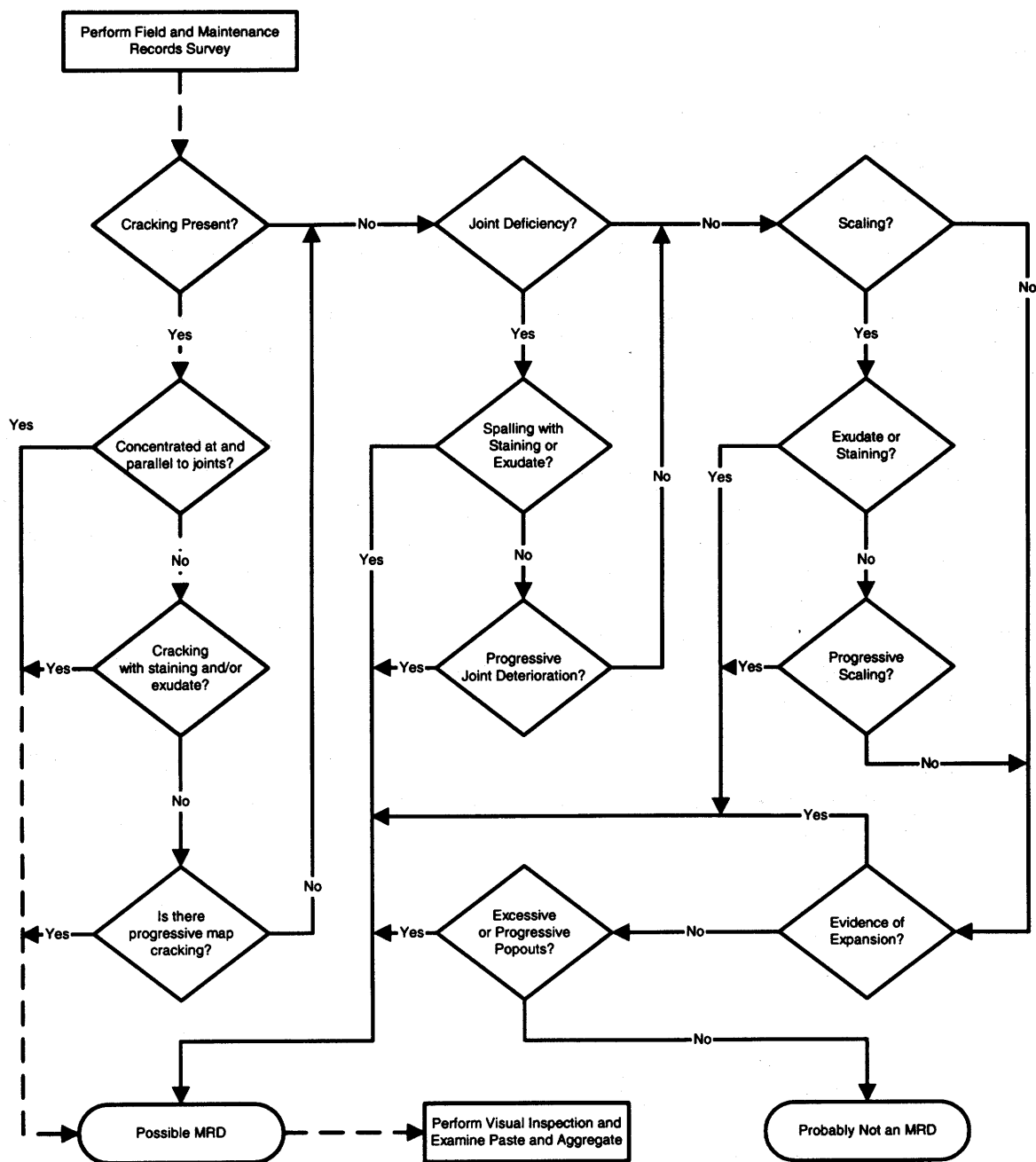


Figure 3-86. Flowchart for assessing the likelihood of MRD causing the observed distress in the pavement as applied to IA-002-002.

Possible Distress	Present		Additional Information
Error in Mix Proportioning	Yes	No	See Recommended Literature
Poor Placement	Yes	No	See Recommended Literature
Poor Finishing/Curing	Yes	No	See Recommended Literature
Poor Steel Placement	Yes	No	See Recommended Literature
Carbonation at Depths > 5-10 mm	Yes	No	See Recommended Literature

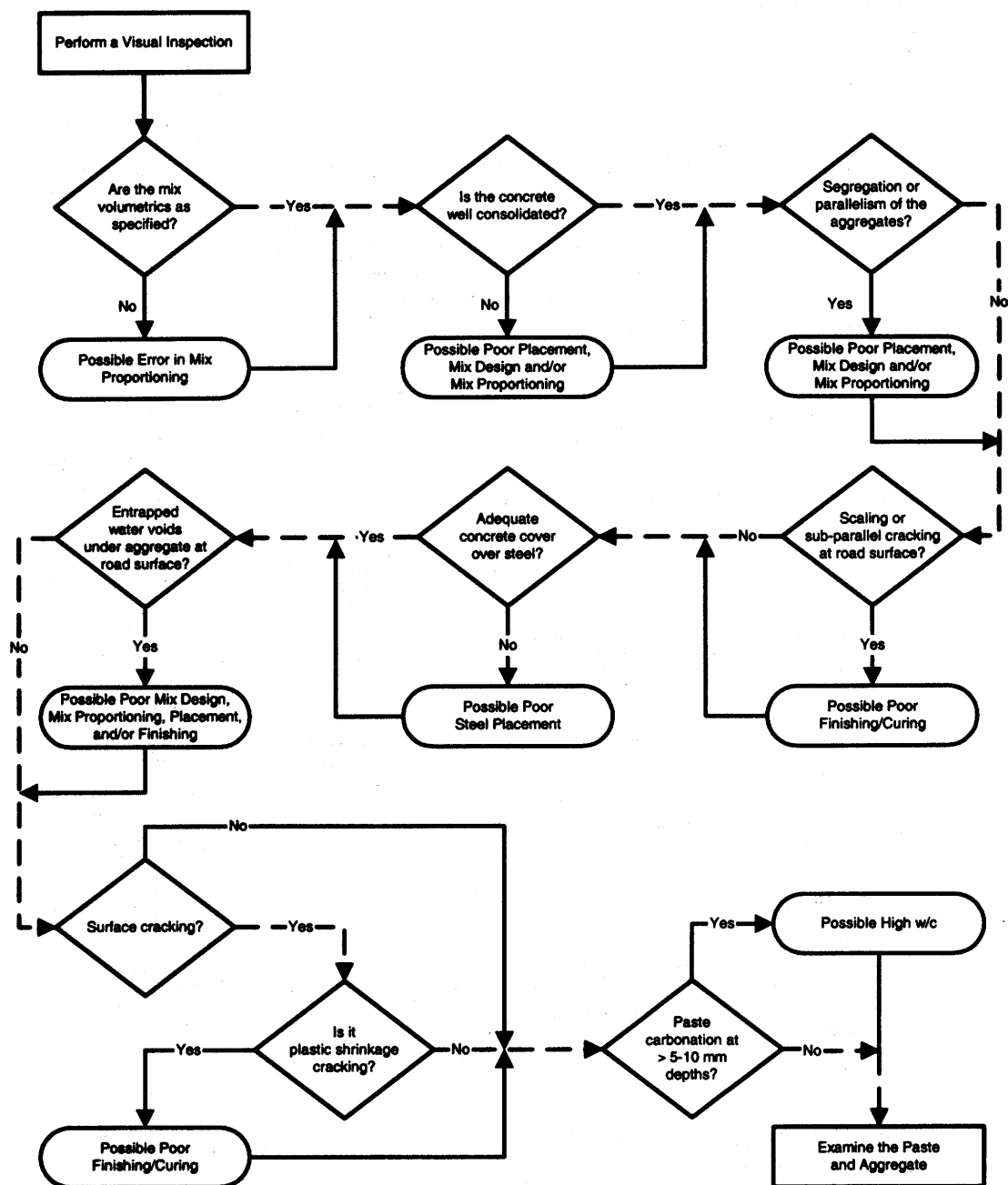


Figure 3-87. Flowchart for assessing general concrete properties based on visual examination as applied to IA-002-002.

Possible Distress	Present		Additional Information
Shrinkage Cracks or Sample Preparation Cracks	Yes	No	See Recommended Literature
Paste Freeze-Thaw	Yes	No	Table II-2
Aggregate Freeze-Thaw	Yes	No	Table II-3
Sulfate Attack	Yes	No	Table II-4
Deicer Attack	Yes	No	Table II-5
Secondary Deposits	Yes	No	Figure 3-90

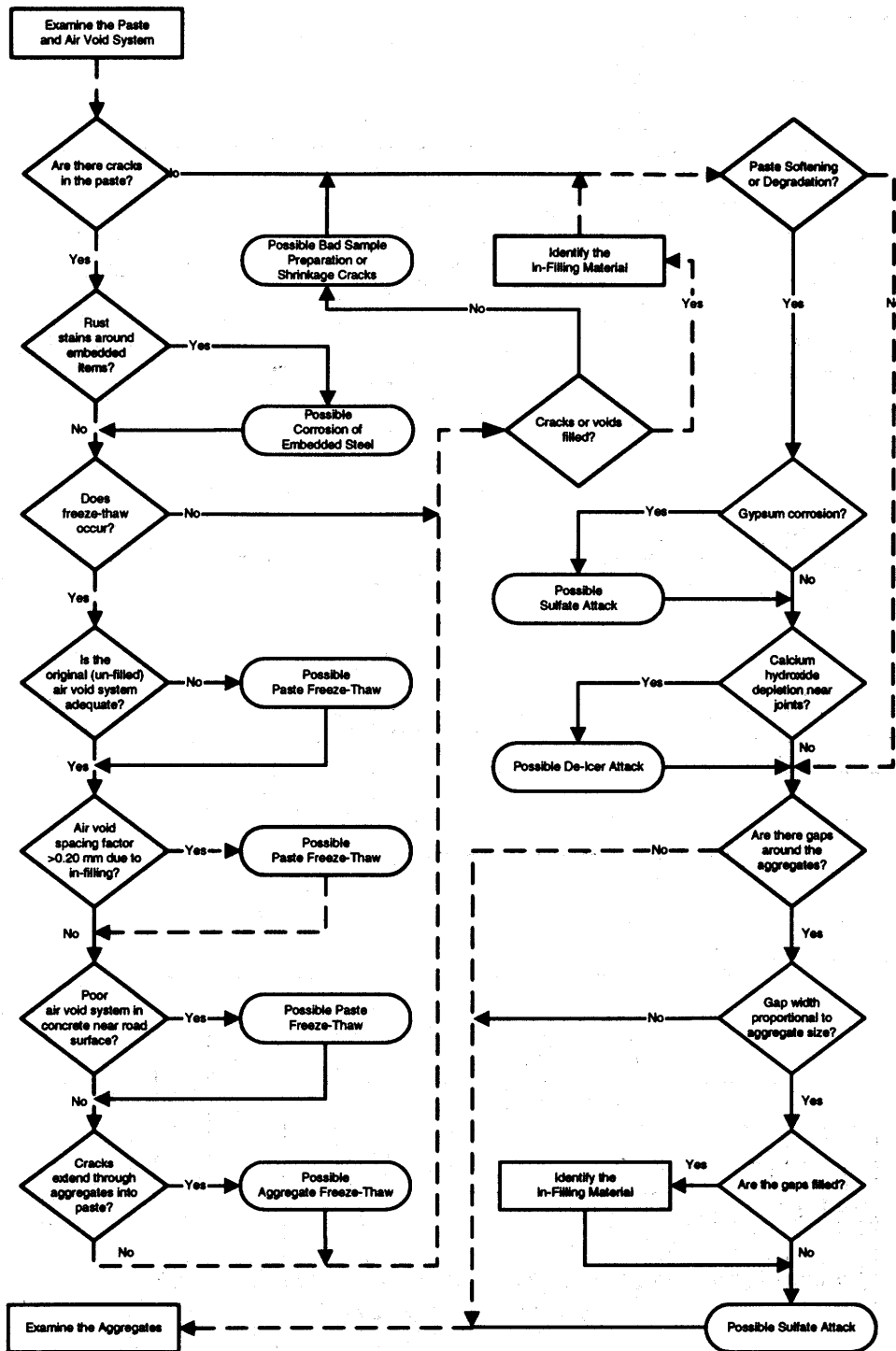


Figure 3-88. Flowchart for assessing the condition of the concrete paste as applied to IA-002-002.

Possible Distress	Present	Additional Information
Natural Cracking of Aggregate	Yes	See Recommended Literature
Sample Preparation Cracks	Yes	See Recommended Literature
Aggregate Freeze-Thaw	Yes	Table II-3
Natural Weathering of Aggregates	Yes	See Recommended Literature
Alkali-Silica Reaction	Yes	Table II-6
Alkali-Carbonate Reaction	Yes	Table II-7
Secondary Deposits	Yes	Figure 3-90

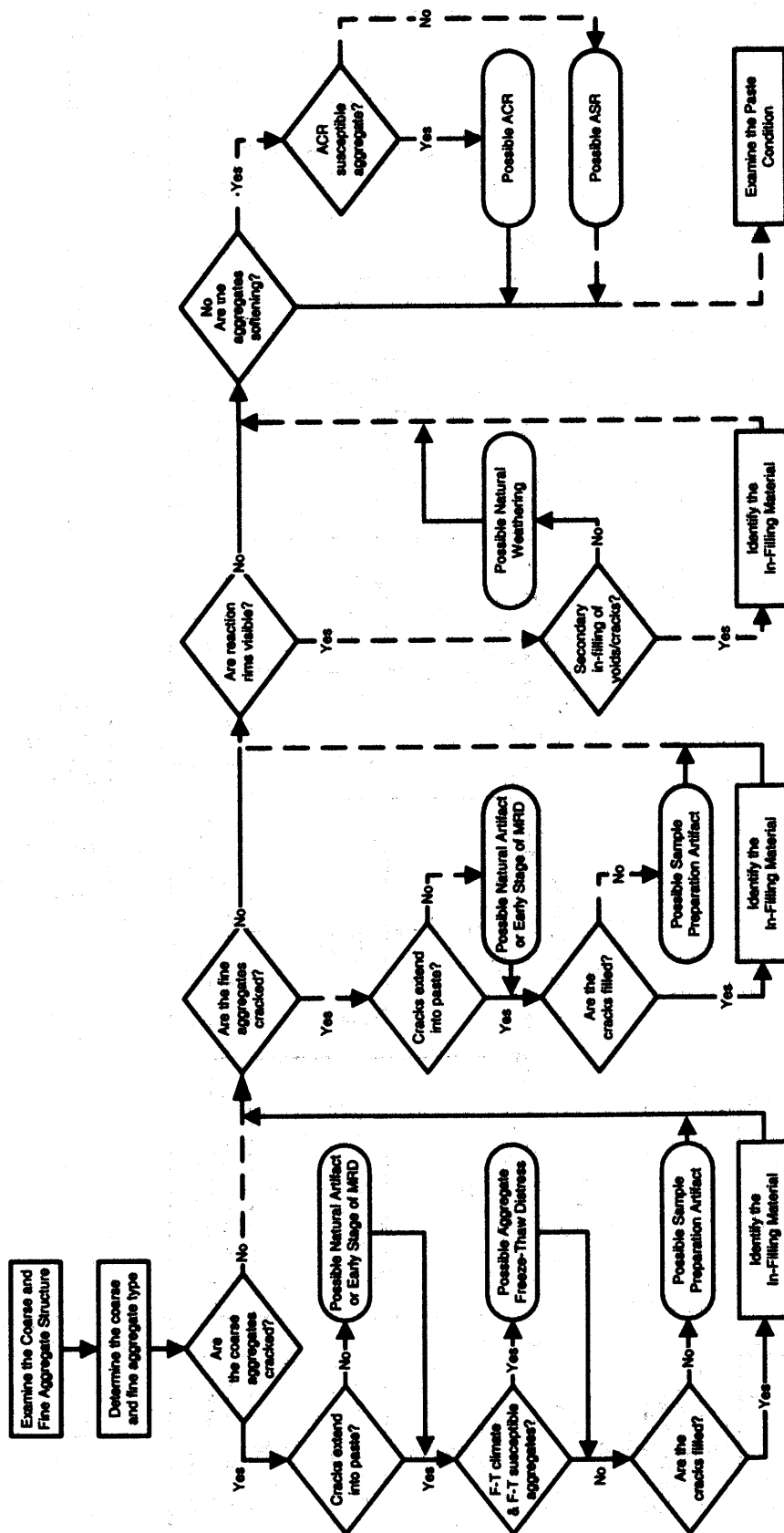


Figure 3-89. Flowchart for assessing the condition of the concrete aggregates as applied to IA-002-002.

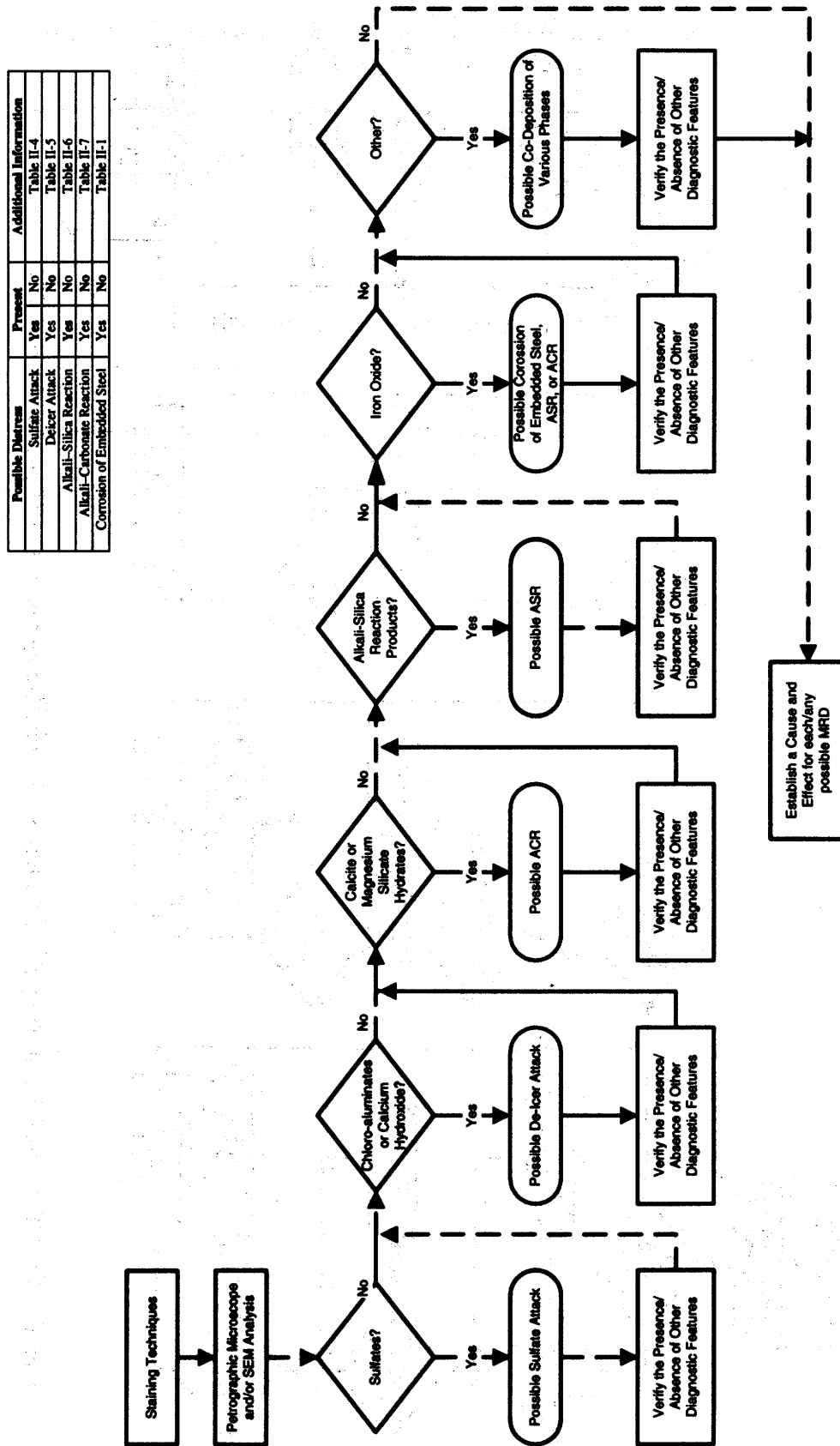


Figure 3-90. Flowchart for identifying infilling materials in cracks and voids as applied to IA-002-002.

Table 3-39. Diagnostic features identified along with their associated MRD type and significance as related to this pavement.

Diagnostic Feature	Method of Characterization	Associated with MRD Type	Significance
ASR reaction products in voids	Petrographic OM SEM	ASR	Low
Significant sulfate deposits in cracks and voids	Staining Stereo OM Petrographic OM SEM	Sulfate attack (both internal and external)	Low
Inadequate air-void system	Stereo OM	Paste freeze-thaw	Low

1. The first part of the document is a letter from the President of the United States to the Congress, dated January 3, 1862. It is a very important document, as it contains the President's views on the state of the Union and the progress of the war.

2. The second part of the document is a report from the Secretary of the War Department, dated January 10, 1862. It contains a detailed account of the military operations of the Army during the year 1861.

3. The third part of the document is a report from the Secretary of the Navy Department, dated January 15, 1862. It contains a detailed account of the naval operations of the Navy during the year 1861.

4. The fourth part of the document is a report from the Secretary of the Department of the Interior, dated January 20, 1862. It contains a detailed account of the operations of the Department during the year 1861.

5. The fifth part of the document is a report from the Secretary of the Department of the Treasury, dated January 25, 1862. It contains a detailed account of the operations of the Department during the year 1861.

6. The sixth part of the document is a report from the Secretary of the Department of the State, dated January 30, 1862. It contains a detailed account of the operations of the Department during the year 1861.

7. The seventh part of the document is a report from the Secretary of the Department of the War, dated February 5, 1862. It contains a detailed account of the operations of the Department during the year 1861.

8. The eighth part of the document is a report from the Secretary of the Department of the Navy, dated February 10, 1862. It contains a detailed account of the operations of the Department during the year 1861.

9. The ninth part of the document is a report from the Secretary of the Department of the Interior, dated February 15, 1862. It contains a detailed account of the operations of the Department during the year 1861.

10. The tenth part of the document is a report from the Secretary of the Department of the Treasury, dated February 20, 1862. It contains a detailed account of the operations of the Department during the year 1861.

11. The eleventh part of the document is a report from the Secretary of the Department of the State, dated February 25, 1862. It contains a detailed account of the operations of the Department during the year 1861.

12. The twelfth part of the document is a report from the Secretary of the Department of the War, dated March 1, 1862. It contains a detailed account of the operations of the Department during the year 1861.

13. The thirteenth part of the document is a report from the Secretary of the Department of the Navy, dated March 5, 1862. It contains a detailed account of the operations of the Department during the year 1861.

14. The fourteenth part of the document is a report from the Secretary of the Department of the Interior, dated March 10, 1862. It contains a detailed account of the operations of the Department during the year 1861.

15. The fifteenth part of the document is a report from the Secretary of the Department of the Treasury, dated March 15, 1862. It contains a detailed account of the operations of the Department during the year 1861.

16. The sixteenth part of the document is a report from the Secretary of the Department of the State, dated March 20, 1862. It contains a detailed account of the operations of the Department during the year 1861.

17. The seventeenth part of the document is a report from the Secretary of the Department of the War, dated March 25, 1862. It contains a detailed account of the operations of the Department during the year 1861.

18. The eighteenth part of the document is a report from the Secretary of the Department of the Navy, dated March 30, 1862. It contains a detailed account of the operations of the Department during the year 1861.

19. The nineteenth part of the document is a report from the Secretary of the Department of the Interior, dated April 5, 1862. It contains a detailed account of the operations of the Department during the year 1861.

20. The twentieth part of the document is a report from the Secretary of the Department of the Treasury, dated April 10, 1862. It contains a detailed account of the operations of the Department during the year 1861.

CHAPTER 4. CONCLUSIONS

This volume of the final report, *Volume 3: Case Studies*, has presented six case studies in which the developed guidelines were applied. In the primary case studies, the guidelines were found to be very useful in directing and organizing the laboratory analysis and in interpreting the data with the purpose of making a diagnosis. One of the two secondary case studies was used to illustrate how the guidelines functioned when analyzing a pavement section that turned out not to have an MRD at work. The other secondary case study presented an example when the guidelines were unable to be used to draw meaningful conclusions.

A major conclusion of this effort is that, when diagnosing a MRD using laboratory methods, data acquisition and interpretation must be performed simultaneously. As the data from a first set of tests are analyzed, new questions are posed requiring interpretation of that first set of data before a second set of analyses can be applied. Then, additional analyses are performed, often using different techniques, and the process is repeated. After the new results are interpreted, a new battery of tests may be required. As the laboratory/interpretation procedure continues, a diagnosis begins to form and the analyst must use caution not to stop at the first MRD identified. Final diagnosis comes after all necessary laboratory tests are completed and the results are summarized. The developed guidelines provide a systematic way of approaching this problem.

The diagnostic flowcharts frame the questions that should be asked about the concrete, and the laboratory methods recommended in the guidelines provide the means of answering those questions. How the analyst performs the work required for each analysis is up to the individual. In general, the work tends to be done following the process shown in figure II-1 in the second guideline where specific techniques are applied in sequence and each technique allows the analyst to progress incrementally through the flowcharts, answering a few more questions each time. How far the analyst proceeds through figure II-1 before completing all five diagnostic flowcharts varies. In general, all cases of MRD analyzed require visual inspection and stereo optical microscopy and most progress to the level of needing petrographic optical microscopy and/or SEM analysis. As a result of applying the diagnostic flowcharts, a number of possible MRDs can be identified. Then, referring to the diagnostic tables, the list of diagnostic features identified in the laboratory can be compared to common diagnostic features for the various MRD types. All diagnostic features listed are rarely all present at one time for a given MRD. The analyst has to weight the significance of each diagnostic feature relative to the magnitude, extent, and nature of the observed MRD. It is this last step that results in final diagnosis and requires objectivity and sound data to perform.

CHAPTER 5. REFERENCES

- American Concrete Institute (ACI) (1992). "Guide to Durable Concrete." *ACI Manual of Concrete Practice—Part 1*. ACI 201.2R-92. American Concrete Institute, Farmington Hills, MI.
- Elsen, J., et al. (1995). "Determination of the w/c Ratio of Hardened Cement Paste and Concrete Samples on Thin Sections Using Automated Image Analysis Techniques." *Cement and Concrete Research*. pp. 827-834.
- Gerold, B. T. (2000). *Estimation of Water-Cement Ratios Using Fluorescent Petrography and Extreme Value Distributions*. Thesis for a degree of Masters of Science in Civil Engineering. Michigan Technological University, Houghton, MI. 78 pp.
- Jakobsen, U.H., V. Johansen, and N. Thaulow (1995). "Estimating the Capillary Porosity of Cement Paste by Fluorescence Microscopy and Image Analysis." *Materials Research Society Symposium Proceedings*. Vol 370. pp. 227-236.
- Jakobsen, U.H., V. Johansen, and N. Thaulow (1997). "Optical Microscopy – A Primary Tool in Concrete Examination." *Proceedings: 19th International Conference on Cement Microscopy*. Cincinnati, OH. April 27 - May 1. pp. 275-286.
- Mayfield, B. (1990). "The Quantitative Evaluation of the Water/Cement Ratio Using Fluorescence Microscopy." *Magazine of Concrete Research*. Vol 42. No. 150. pp. 45-49.
- Neville, A. (1999). "How Useful is the Water-Cement Ratio?" *Concrete International*. Volume 21, No. 9. September. pp. 69-70.
- Spry, P.G., G. Gan, R.D. Cody, and A.M. Cody (1996). "The Formation of Rims on Dolomite Aggregate in Iowa Highway Concrete." *1996 Semisesquicentennial Transportation Conference Proceedings*. Transportation Research Board, Washington, DC.
- Stark, D., B. Morgan, P. Okamoto, and S. Diamond (1993). *Eliminating or Minimizing Alkali-Silica Reactivity*. SHRP-C-343. Strategic Highway Research Program, Washington, DC.
- Walker, H. N. (1992). *Petrographic Methods of Examining Hardened Concrete: A Petrographic Manual*. Report No. FHWA/VA-R14. Virginia Transportation Research Council, Charlottesville, VA.

